Experimental and Numerical Studies of Hydrodynamic Interaction of Two Bodies in Waves

by

©Ming Liu

A Thesis submitted to the School of Graduate Studies
in partial fulfillment of the requirements for
the degree of Master of Engineering

Faculty of Engineering and Applied Science

Memorial University of Newfoundland

May 2016

St. John's Newfoundland Canada

Abstract

This thesis focuses on experimental and numerical studies of the hydrodynamic interaction between two vessels in close proximity in waves. In the model tests, two identical box-like models with round corners were used. Regular waves with the same wave steepness and different wave frequencies were generated. Six degrees of freedom body motions and wave elevations between bodies were measured in a head sea condition. Three initial gap widths were examined. In the numerical computations, a panel-free method based seakeeping program, MAPS0, and a panel method based program, WAMIT, were used for the prediction of body motions and wave elevations. The computed body motions and wave elevations were compared with experimental data.

Acknowledgments

The past three years as a Master student in Memorial University of Newfoundland was indeed a meaningful and memorable journey for me in terms of both academic growth and personality maturity. I would not have completed this journey without the help of countless people over this period.

First and most importantly, I would like to express my sincere gratitude to my supervisor, Dr. Wei Qiu. I thank him for offering me the opportunity to pursue my Master study in Memorial University from the very beginning, and provide me with the strongest academic, technical, financial support for my study as always. Whenever I met with problems, he can always understand my circumstances and guide me through the difficulties.

I am extremely grateful to Dr. Heather Peng for her understanding and patient guidance and advice in real life when I am facing troubles. I would like to acknowledge the laboratory technologist, Mr. Trevor Clark, who provided steady help in the laboratory setting part of my research, and my experiment partners, Quan Zhou, Min Zhang and Kalene Hines, with whom I overcame countless difficulties in the experiment process. Without their participation, I would not have the real field data to do my analysis. A big thank you goes out to students in our research group who accompanied me in life and gave me advice in research, especially Peng Wen and Md. Shahriar Nizam.

I would also thank the financial support by Natural Science and Engineering Research

Council (NSERC).

Lastly, and far from the least, I would like to thank my parents, and my wife, Yamei Yu, for their continuous love, understanding, encouragement and support. Thank all the people who kindly provided me help and support throughout my entire life.

Table of Contents

Abstract **ii**

Table of Contents **vii**

List of Tables **ix**

List of Figures **xiv**

1 Introduction **1**

1.1 Background 1

1.2 Literature Review 2

1.2.1 Numerical Studies 2

1.2.2 Experimental Studies 7

1.3 Objectives 9

1.4 Thesis Outline 10

2 Model Test Preparations **11**

2.1 Ship Model 12

2.2 Mooring System 16

2.3 Motion Capture Instrument 18

2.3.1 Qualisys Motion Capture System 18

2.3.2 MotionPak 20
2.3.3 Wave Probes 21
2.4 Ship Model Ballasting 22
2.5 Inclining Test 24
2.6 Swing Test 26
2.7 Decay Test 26
2.8 Summary 29

3 Model Tests **30**
3.1 Regular Wave Calibration 30
3.2 Single Body Model Test 32
3.2.1 Set-Up 32
3.2.2 Instrument Calibration 34
3.2.3 Test Cases 38
3.2.4 Data Acquisition and Analysis 38
3.3 Two-Body Model Tests 39
3.3.1 Set-Up 39
3.3.2 Test Cases 41
3.3.3 Data Acquisition and Analysis 41
3.4 Summary 41

4 Numerical Simulation **44**
4.1 Theoretical Formulation of Frequency-Domain Computation Based on the Panel-Free Method 44
4.2 MAPS0 Simulation 47
4.2.1 Geometry Representation 47
4.2.2 Simulation Cases 48

5 Results and Validation Studies **52**

5.1 Tank Wall Effect and Mooring Line Effect 52

5.2 Single Body Case 60

5.2.1 Experimental Data 60

5.2.2 Comparison Results 62

5.3 Two-Body Cases 64

5.3.1 Experimental Data 64

5.3.2 Comparison Results 80

5.3.2.1 Comparison Results of MAPS0, WAMIT and Experimental Data 80

5.3.2.2 Comparison Results of Different Gap Widths 91

5.4 Comparison Results of Single Body/Two-body Cases 94

6 Conclusions and Recommendations **99**

6.1 Conclusions 99

6.2 Recommandations 100

Bibliography **101**

Appendices **106**

A Theory of Inclining Test **107**

B Theory and Procedure of Swing Test **109**

C Theory of Decay Test **114**

D Experimental Data of Roll Motion in Two-Body Cases **116**

List of Tables

2.1 Model and Ship Particulars 14

2.2 Wave Probe Locations in Single Body Test 21

2.3 Wave Probe Locations in Two-Body Test 21

2.4 Procedure of Weight Movement 25

3.1 Wave Information in Model Scale 31

3.2 Wave Information in Full Scale 31

3.3 Location of Model and Wave Probes in Single Body Test 34

3.4 Location of Models and Wave Probes in Two-Body Tests 40

3.5 Test Cases of Two-Body Model Tests 42

4.1 Single Body Simulation Cases 49

4.2 Two-Body Simulation Cases 49

5.1 Body motion data in single body case 62

5.2 Motion data of model 1 in two-body case, round 1, gap width 0.4 m . 71

5.3 Motion data of model 2 in two-body case, round 1, gap width 0.4 m . 71

5.4 Wave elevation data in two-body case, round 1, gap width 0.4 m . . . 72

5.5 Motion data of model 1 in two-body case, round 2, gap width 0.4 m . 72

5.6 Motion data of model 2 in two-body case, round 2, gap width 0.4 m . 73

5.7 Wave elevation data in two-body case, round 2, gap width 0.4 m . . . 73

5.8 Motion data of model 1 in two-body case, round 1, gap width 0.45 m 74
5.9 Motion data of model 2 in two-body case, round 1, gap width 0.45 m 74
5.10 Wave elevation data in two-body case, round 1, gap width 0.45 m . . 75
5.11 Motion data of model 1 in two-body case, round 2, gap width 0.45 m 75
5.12 Motion data of model 2 in two-body case, round 2, gap width 0.45 m 76
5.13 Wave elevation data in two-body case, round 2, gap width 0.45 m . . 76
5.14 Motion data of model 1 in two-body case, round 1, gap width 0.55 m 77
5.15 Motion data of model 2 in two-body case, round 1, gap width 0.55 m 77
5.16 Wave elevation data in two-body case, round 1, gap width 0.55 m . . 78
5.17 Motion data of model 1 in two-body case, round 2, gap width 0.55 m 78
5.18 Motion data of model 2 in two-body case, round 2, gap width 0.55 m 79
5.19 Wave elevation data in two-body case, round 2, gap width 0.55 m . . 79

D.1 Roll motion data of two models in two-body case, gap width 0.4 m . 117
D.2 Roll motion data of two models in two-body case, gap width 0.45 m . 117
D.3 Roll motion data of two models in two-body case, gap width 0.55 m . 118

List of Figures

2.1 Towing tank 11
2.2 Model draft 13
2.3 Ship model 13
2.4 Mooring system 17
2.5 Model end of soft restraint lines 17
2.6 Post end of soft restraint lines 18
2.7 Oqus cameras 19
2.8 Tracking markers 19
2.9 QTM user interface 20
2.10 Upstream wave probe 22
2.11 Trim tank 23
2.12 Ballasting weight distribution for Model 1 24
2.13 Inclining test 25
2.14 Free decay test time series of Model 1 27
2.15 Free decay test time series of Model 2 28
2.16 Moored decay test time series of Model 1 28

3.1 Wave calibration results 32
3.2 Layout of single body model test 33
3.3 Single body model test set-up 33

3.4 Tank coordinate system 34
3.5 Qualisys calibration results 35
3.6 Wave probe 1 calibration results 36
3.7 Wave probe 2 calibration results 36
3.8 Wave probe 3 calibration results 37
3.9 Wave probe 4 calibration results 37
3.10 Wave probe 5 calibration results 37
3.11 Layout of two-body model tests 39
3.12 Two-body model tests set-up 40

4.1 Coordinate system of MAPS0 (Qiu et al., 2014) 45
4.2 NURBS Surface of Model 1 48
4.3 Convergence study of wave elevation at wave probe 3 (gap 0.55m) . . 49
4.4 Convergence study of surge RAOs for two-body (gap 0.55m) cases . . 50
4.5 Convergence study of heave RAOs for two-body (gap 0.55m) cases . . 50
4.6 Convergence study of pitch RAOs for two-body (gap 0.55m) cases . . 51

5.1 Tank wall effect on surge 53
5.2 Tank wall effect on sway 53
5.3 Tank wall effect on heave 54
5.4 Tank wall effect on roll 54
5.5 Tank wall effect on pitch 55
5.6 Tank wall effect on yaw 55
5.7 Tank wall effect on wave elevation at wave probe 4 56
5.8 Mooring line effect on surge 56
5.9 Mooring line effect on sway 57
5.10 Mooring line effect on heave 57

5.11 Mooring line effect on roll 58
5.12 Mooring line effect on pitch 58
5.13 Mooring line effect on yaw 59
5.14 Mooring line effect on wave elevation at wave probe 4 59
5.15 Single body surge time series and FFT analysis results (0.81 Hz) . . . 61
5.16 Single body heave time series and FFT analysis results (0.81 Hz) . . . 61
5.17 Single body surge RAO 63
5.18 Single body heave RAO 63
5.19 Single body pitch RAO 64
5.20 Two-body surge time series and FFT analysis results (wave frequency 0.68 Hz, gap width 0.4 m) 65
5.21 Two-body sway time series and FFT analysis results (wave frequency 0.68 Hz, gap width 0.4 m) 66
5.22 Two-body heave time series and FFT analysis results (wave frequency 0.68 Hz, gap width 0.4 m) 66
5.23 Two-body roll time series and FFT analysis results (wave frequency 0.68 Hz, gap width 0.4 m) 67
5.24 Two-body pitch time series and FFT analysis results (wave frequency 0.68 Hz, gap width 0.4 m) 67
5.25 Two-body yaw time series and FFT analysis results (wave frequency 0.68 Hz, gap width 0.4 m) 68
5.26 Two-body wave elevation time series and FFT analysis results at WP1 (wave frequency 0.68 Hz, gap width 0.4 m) 68
5.27 Two-body wave elevation time series and FFT analysis results at WP3 (wave frequency 0.68 Hz, gap width 0.4 m) 69

5.28 Two-body wave elevation time series and FFT analysis results at WP4 (wave frequency 0.68 Hz, gap width 0.4 m) 69
5.29 Two-body wave elevation time series and FFT analysis results at WP5 (wave frequency 0.68 Hz, gap width 0.4 m) 70
5.30 Surge RAO of body 1 in two-body case, gap width 0.4m 81
5.31 Sway RAO of body 1 in two-body case, gap width 0.4m 81
5.32 Heave RAO of body 1 in two-body case, gap width 0.4m 82
5.33 Pitch RAO of body 1 in two-body case, gap width 0.4m 82
5.34 Wave elevation at wave probe 3 in two-body case, gap width 0.4m . . 83
5.35 Wave elevation at wave probe 4 in two-body case, gap width 0.4m . . 83
5.36 Wave elevation at wave probe 5 in two-body case, gap width 0.4m . . 84
5.37 Surge RAO of body 1 in two-body case, gap width 0.45m 84
5.38 Sway RAO of body 1 in two-body case, gap width 0.45m 85
5.39 Heave RAO of body 1 in two-body case, gap width 0.45m 85
5.40 Pitch RAO of body 1 in two-body case, gap width 0.45m 86
5.41 Wave elevation at wave probe 3 in two-body case, gap width 0.45m . 86
5.42 Wave elevation at wave probe 4 in two-body case, gap width 0.45m . 87
5.43 Wave elevation at wave probe 5 in two-body case, gap width 0.45m . 87
5.44 Surge RAO of body 1 in two-body case, gap width 0.55m 88
5.45 Sway RAO of body 1 in two-body case, gap width 0.55m 88
5.46 Heave RAO of body 1 in two-body case, gap width 0.55m 89
5.47 Pitch RAO of body 1 in two-body case, gap width 0.55m 89
5.48 Wave elevation at wave probe 3 in two-body case, gap width 0.55m . 90
5.49 Wave elevation at wave probe 4 in two-body case, gap width 0.55m . 90
5.50 Wave elevation at wave probe 5 in two-body case, gap width 0.55m . 91
5.51 Wave elevation at wave probe 3 with 3 gap widths 92

5.52 Wave elevation at wave probe 4 with 3 gap widths 93
5.53 Wave elevation at wave probe 5 with 3 gap widths 93
5.54 Surge RAOs of single body and two-body (gap 0.4m) cases 94
5.55 Heave RAOs of single body and two-body (gap 0.4m) cases 95
5.56 Pitch RAOs of single body and two-body (gap 0.4m) cases 95
5.57 Surge RAOs of single body and two-body (gap 0.45m) cases 96
5.58 Heave RAOs of single body and two-body (gap 0.45m) cases 96
5.59 Pitch RAOs of single body and two-body (gap 0.45m) cases 97
5.60 Surge RAOs of single body and two-body (gap 0.55m) cases 97
5.61 Heave RAOs of single body and two-body (gap 0.55m) cases 98
5.62 Pitch RAOs of single body and two-body (gap 0.55m) cases 98

A.1 Metacentric height 107

B.1 Swing frame 109
B.2 Variables in swing test 110

D.1 Roll RAO of body 1 in two-body case, gap width 0.4m 118
D.2 Roll RAO of body 1 in two-body case, gap width 0.45m 119
D.3 Roll RAO of body 1 in two-body case, gap width 0.55m 119

List of Symbols

A_{xx}	Added moment of inertia
B_{xx}	Added damping coefficient
G	Green function
$\overline{GM_T}$	Transverse metacentric height
I_T	Moment of the water plane
I_{xx}	Roll moment of inertia
K'	Effective stiffness of the restraint spring
M'	Added mass
$OXYZ$	Global coordinate system
$o_i x_i y_i z_i$	Body fixed coordinate system of body i
P	Field point in the domain of interest
Q	Source point on the body surface
S_b	Mean wetted surface
β	Incident wave angle
ζ	Damping ratio in roll motion
θ	Roll angle
σ	Source strength on body surface
ϕ	Velocity potential
ω_{roll}	Natural frequency of roll motion

∇	Volume of displacement

Chapter 1

Introduction

1.1 Background

When two vessels are in close proximity, a large resonant free surface elevation can occur in the gap. This resonant gap phenomenon can lead to large motion of the vessels and cause unsafe offshore operations. A lot of research has been conducted in this area. Most of the linear potential-flow based seakeeping programs over-predict the free surface elevation between the vessels, which brings problems in the design of fenders and hawsers (Qiu et al., 2014).

To overcome this problem, Huijsmans et al. (2001) developed the lid technique to suppress the unrealistic values of low-frequency forces. In this method, the free surface in the gap is replaced by a flexible plate. Newman (2003) modelled the free surface with a generalized mode technique. Chen (2004) proposed a linear damping term to modify the free surface boundary condition in the gap.

However, these methods require input of the artificial damping factors, which are determined from experimental data. That means these methods are inadequate to give reasonable predictions without providing the experimental data beforehand, which

makes it impractical to apply them to design and analysis. Thus, experimental data is desired to provide the damping contribution due to viscous flow in the study of multi-body interaction problem (Zhou et al., 2015).

1.2 Literature Review

It has been so many years since researchers began to study the multi-body interaction in waves problem. Kodan (1984) presented evidence that an interaction effect exists between two adjacent floating bodies. Significant differences of wave force and vessel motions were found between the adjacent body case and the single body case. The study was performed with both strip theory analysis and model tests. After that, the problem of multi-body interaction in waves was continued to be studied by many researchers with various numerical methods and experimental methods.

1.2.1 Numerical Studies

Many researchers have investigated the multi-body interaction in waves problem based on the potential-flow theory in the frequency domain by using lower-order and high-order panel methods.

Miao et al. (2001) presented a theoretical approach for computing the wave interaction of twin caissons with a small gap in between. Twin caissons with rectangular sections and cylindrical sections were studied and body forces were simulated with potential flow theory. Strong hydrodynamic interaction between twin caissons was observed at certain wave frequencies, which was discovered as narrow open channel resonant phenomena. The sharp peak force at resonant wave frequency was said to be 10 times greater than that in single body case. The resonant wave number was proved to be around $kL = n\pi(n = 1, 2, 3, \cdots \infty)$, where k is the wave number and L is the gap

length.

Pauw et al. (2007) compared the numerical analysis results with measured data of two side-by-side LNG carriers in head seas. A panel method code was employed in the numerical analysis, in which a flexible damping lid was added in the gap region. Different gap widths were studied in an attempt to obtain rationale for predicting suitable damping factors. In the conclusion, no unique damping factor value was found to fully cover all the measured cases. Also, the damping factor was shown to have the greatest effect on the second-order drift force.

Cheetham et al. (2007) used AQWA, a seakeeping program based on potential flow theory, to compute the hydrodynamic interaction between multiple floating bodies. Kodan model (Kodan, 1984) case and a trimaran model with forward speed case were simulated. An external damping lid was applied in the simulation and the results were validated by experiment data.

Bunnick et al. (2009) performed a numerical simulation to compare to the model tests results of two side-by-side LNG carriers in head seas. In the numerical simulation based on potential flow method, a damping lid was used and it was also extended to the surface inside the vessel, not just the free surface gap. From the comparison results with experimental data, it was proved that the damping lid method worked better than the rigid lid method.

Molin et al. (2009) used a linear potential-flow code DIODORE to analyze two side-by-side fixed barges and compared the results with the experimental data. A set of massless plates were added to the gap between the barges. A quadratic damping force was determined and applied to the massless plates. For determining the quadratic damping force, a drag coefficient $C_D = 0.5$ was used, which led to good agreement with measured data. It was recommended that an investigation of freely floating ships be performed in the future work.

Zhang et al. (2013) used a potential-flow software HYDROSTAR to conduct numerical calculations of the hydrodynamic interactions of two bodies. Different gap distances, relative sizes and the arbitrary relative angles were examined. From the results of different cases, it was shown that the resonance phenomenon became more dominant than the shielding effect when the gap distances were reduced. For cases of different relative angles, it can be seen from the results that sway and heave response were sensitive in head sea. For parallel arrangement, larger motion responses occurred when the size of the barges became smaller.

Clauss et al. (2013) conducted frequency domain numerical simulations to investigate the gap effects between side-by-side LNGs. In the simulation, a damping lid was added to adapt the free surface elevation in the gap. A potential theory based program WAMIT was used to examine the wave propagation.

Xu et al. (2013) also used WAMIT in their research to calculate the second-order mean drift force and moment on three side-by-side barges during float-over operation. Simulation results were validated by model tests and it indicated that satisfactory numerical predictions could be obtained by adding viscous damping corrections.

Kashiwagi and Shi (2010) investigated the pressure distribution for multiple bodies in close proximity. The integral equation of the diffraction potential was solved by using Higher-Order Boundary Element Method (HOBEM). The results suggested that a smaller separation distance between bodies would lead to a larger deviation of the pressure distribution.

Hong et al. (2013) performed an investigation on the gap resonance phenomenon between the bodies in close proximity. Two numerical methods, a nine-node discontinuous higher order boundary element method (9dHOBEM) and a constant boundary element method based on the boundary matching formulation (BM-CBEM), were used in his research. The simulation results indicated that using BM-CBEM combined

with the free surface damping, or using 9dHOBEM combined with a tuned value of the wetted surface damping parameter, could largely reduce the over-predicted first-order hydrodynamic coefficients and precisely estimate the time-mean drift forces of two side-by-side floating structures.

Besides the researches in frequency domain, efforts have been made to investigate the multi-body interaction problem in the time domain.

Xiang and Faltinsen (2011) used 3D Rankine source method to solve the linear loads and motions of two tankers paralleled in calm and deep water in lightering operation. A numerical solution was developed in time domain and validated by comparing with existing analytical, numerical and model test results.

Zhu et al. (2008) computed the problem of two side-by-side floating structures with a time domain method based on potential-flow theory. In the computation, two side-by-side box-shaped hulls with a narrow gap in between were fixed in space. Body forces due to incoming waves and diffracted waves were simulated. Results of this time domain analysis showed good agreement for the narrow gap resonant phenomena with the frequency domain analysis.

Numerical methods based on non-linear potential-flow theory, such as the finite element method, have also been developed and used to solve the multi-body interaction problem.

Wang et al. (2011) studied 2D resonant waves in the gap between two floating structures based on fully non-linear potential theory. To analyze the fully non-linear resonant oscillations of the liquid in the gap, a higher-order finite element method was applied. By comparing the second-order time domain results with corresponding fully non-linear results, it can be concluded that the wave amplitude in the gap and the wave loads on the structures might be overestimated with the second-order theory.

Ma et al. (2013) applied the fully non-linear potential theory to investigate the 2D

resonant waves in the gap between two floating barges. Quasi Arbitrary Lagrangian-Eulerian Finite Element Method (QALEFEM) was used in the analysis to compute the free surface elevations and the forces acting on barges. The results showed that higher-order non-linear models were recommended to be used in computing such cases. Reynolds Averaged Navier–Stokes (RANS) equations have also been attempted to be solved in order to determine the viscous effect in multi-body interaction problems.

Lu et al. (2010a) applied both potential flow theory and viscous fluid theory to study the problem of two identical bodies and three identical bodies in close proximity. In the viscous flow model, no artificial damping force was considered and a three-step finite element solver was employed. The free surface in the gap region was captured with the CLEAR-VOF method. Computation results of each model were compared with experimental results. Comparison results showed that both potential and viscous models performed well for predicting frequencies outside the resonance band. For the predictions around resonant frequencies, the potential flow model over-predicts the wave height and the viscous flow model still agreed well with measured values.

Lu et al. (2010b) applied artificial damping to the free surface to improve the predictions with the potential flow method. With comparison, a damping coefficient $\mu = 0.4$ was found out. With this damping coefficient, the predictions of potential flow model showed good agreement with the viscous flow results and measured values for two-body cases and for both gaps in three-body cases.

Lu et al. (2011) extended their study by investigating the effects of gap width, body draft, body width and number of bodies of multi-bodies at close proximity. Both a viscous model and a potential flow model (damped and undamped) were used in the study. It was found that as the gap width increases, the resonant frequency decreases. Increasing the draft of the bodies results in lower resonant frequencies, while resonant wave heights become larger. A reduction in beam of the downstream body was found

to increase the resonant frequency and decrease the resonant wave height.

Lu and Chen (2012) performed CFD computations to examine the energy dissipation around resonant frequencies between two bodies. The computation results showed that the energy dissipation was relatively constant over frequencies near the resonant frequency. It is also indicated that the over-predicted resonant wave elevation could be reduced by using the dissipation coefficient to assimilate the friction force.

Zou and Larsson (2013) used a steady-state RANS solver to compute the interactions of two side-by-side ships in shallow water during a lightering operation. The computation results were compared with experimental data and a good agreement was found between measured and computed wave heights, which suggested that the predicted pressure distribution on the free surface was appropriate.

1.2.2 Experimental Studies

Molin et al. (2002) performed an experiment to investigate wave propagation in a narrow channel between a barge-like structure and a wall. Free surface elevation, flow velocity and wave length in the gap were measured in the experiment and drag coefficients were then derived. It was verified that the gap natural frequency was in agreement with the theory presented in Molin (2001).

McTaggart et al. (2003) conducted the model tests of two semi-captive ship models in waves. In the tests, a supply ship model and a frigate model were in close-proximity and with forward speeds. Different forward speeds, wave headings and longitudinal separations were tested. Three-dimensional ship motion (Heave, Roll and Pitch) and three-dimensional retraining forces (Surge, Sway and Yaw) were measured. A numerical frequency domain code was also developed to predict the ship motions and restraining forces. Through comparison, the experimental and numerical results were in good agreement with each other and showed that the presence of a larger

vessel could significantly influence the motion of a smaller vessel in waves. The wall interference effects during experiments were also discussed and it should be taken into account in the future works.

Cho et al. (2011) carried out experimental studies of side-by-side moored FSRU and LNGC including sloshing effect. Body motions and drift forces were measured in the tests. Different filling level of LNG cargo tank in FSRU and LNGC were tested and the sloshing effect caused by different filling level was studied. The effect of gap flow was also investigated. A conclusion was given that the sway motion, sway drift force and gap flow were influenced by sloshing in head sea even when the sloshing was weak.

Kim et al. (2012) performed a series of model tests to investigate the effect of the heading control on the offloading operability of side-by-side moored vessels, LNGC and LNG FPSO (FLNG). Hawser tensions, fender loads, and relative motions between two vessels were measured in the tests. Two different heading angles were tested, which includes the heading angles aligned with swell, and between swell and wind wave. For better comparison, the loading conditions of the FLNG and LNGC were chosen to have a similar roll natural period. From the model test results, it can be proved that the heading control improves the offloading operability in the multi-directional environments.

Smith (2014) conducted the model tests of two side-by-side ships in regular waves. Two initial gap widths were examined. Four wave headings, 90 degrees, 60 degrees, 30 degrees and 0 degree, were studied. The free surface elevation in the gap and six degrees of freedom body motions were recorded.

Besides reviewing the existing model tests of multi-body interaction in waves problem, ITTC-recommended procedures and guidelines were also studied for conducting the model tests.

ITTC-recommended procedures and guidelines of ocean engineering analysis proce-

dure for model tests in regular waves (ITTC, 2002) introduced the requirements for Fourier analysis and parameters in the tests. For Fourier analysis, the determination of interval, number of analyzed cycles, fundamental period, start and end points, and signal filtering were discussed and recommendations were given. In the recommendations of test parameters, details of the requirements were provided for model dimensions, tank dimensions, wave calibration, test duration, measuring equipment, restraint method, wave information, wave probe location and number of repeat runs. ITTC-recommended procedures and guidelines of floating offshore platform experiments (ITTC, 2005) presented the requirements for the calibration of environment and instrument. Guidelines were also introduced about data collection and analysis. The positioning of model in the tank during the test was especially emphasised.

1.3 Objectives

This study was to perform experimental tests to investigate the problem of two-body interaction in waves and obtain the benchmark data of body motions and free surface elevations in the gap. Numerical simulations with frequency domain potential-flow programs were also conducted and the numerical results were validated with the experimental data. The main tasks include:

- To design and manufacture the ship models and soft mooring system used in the model tests.
- To determine the appropriate test matrix, including wave conditions and initial gap widths.
- To perform the model tests for single body and two-body cases in designed wave and gap condition. Repetitions of the tests also needs to be conducted.

- To perform numerical simulations with frequency domain potential-flow programs.
- To validate and analyze the obtained data.

1.4 Thesis Outline

This thesis presents the experimental and numerical studies of hydrodynamic interactions of two bodies in waves.

- Chapter 1 provides the background of multi-body interaction problem in waves, reviews previous work on numerical simulations with frequency/time domain potential-flow theory and CFD methods, and experimental tests.
- Chapter 2 introduces the model test preparations with details. This chapter includes the design of ship models and soft mooring system, the operation of motion capture instrument and the procedure of ship model ballasting, inclining test, swing test and decay test.
- Chapter 3 presents the process of model tests. Regular wave calibrations are introduced first. The details of model tests for single body/two-body cases are also described.
- Chapter 4 describes the numerical simulation with frequency domain potential-flow programs, MAPS0 and WAMIT. The theoretical formulations of the numerical method are provided based on the panel-free method.
- Chapter 5 provides the experimental and numerical results, and the validation and analysis of the obtained data.
- Chapter 6 concludes the work and provides recommendations for future research.

Chapter 2

Model Test Preparations

Model tests were conducted at the towing tank of the Ocean Engineering Research Center at Memorial University from March to May of 2014. Model test preparations, including design and manufacture of ship model, design of soft mooring system, the installation of motion capture facilities and a series of pre-tests are described below.

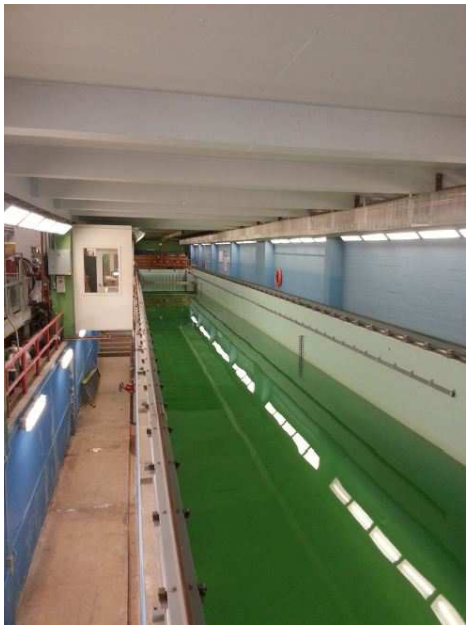

Figure 2.1: Towing tank

Refer to Figure 2.1, a 58 m long towing tank with a width of 4.5 m and depth of 3.04

m was used for the model tests. The water depth in the model tests was set as 1.80 m. Regular waves were generated by a wave maker during the tests, with a frequency range from 3.92 to 7.16 rad/s.

2.1 Ship Model

Two FPSO-like models with simplified body shape were used for this test program. Main particulars of several real FPSOs were reviewed to determine the model particulars (Li et al., 2003). The model length/breadth ratio was designed as 5.0 and the breadth/draft ratio of 4.0. The depth/draft ratio was 3.0, which was determined to be sufficiently large to avoid green water on deck.

Refer to Figures 2.2 and 2.3, the body shape of the ship model was simplified to be box-like. The bow/stern and bilge shapes were simplified with smooth circle arcs. The main part of the model was built with normal foam (30 kg/m^3 of density). To increase the longitudinal strength of the ship model, the foam used on ship bottom was high-density foam (RenShape 440, 545 kg/m^3 of density) with a steel bar longitudinally placed inside. Three sections (the midship section and the sections off the midship located 0.5 m towards fore and aft) were reinforced with the high-density foam to ensure the transverse strength of the ship models. The body surface was covered by 3 mm-thick fiber glass to make it waterproof. The body surface was painted black to avoid light reflection in the motion measurement process with the Qualisys motion capture system. Waterline, midsection line and center line were marked on the body surface. Four small screws were attached on the bow and stern for fixing the mooring lines.

Main particulars of the ship models are shown in Table 2.1.

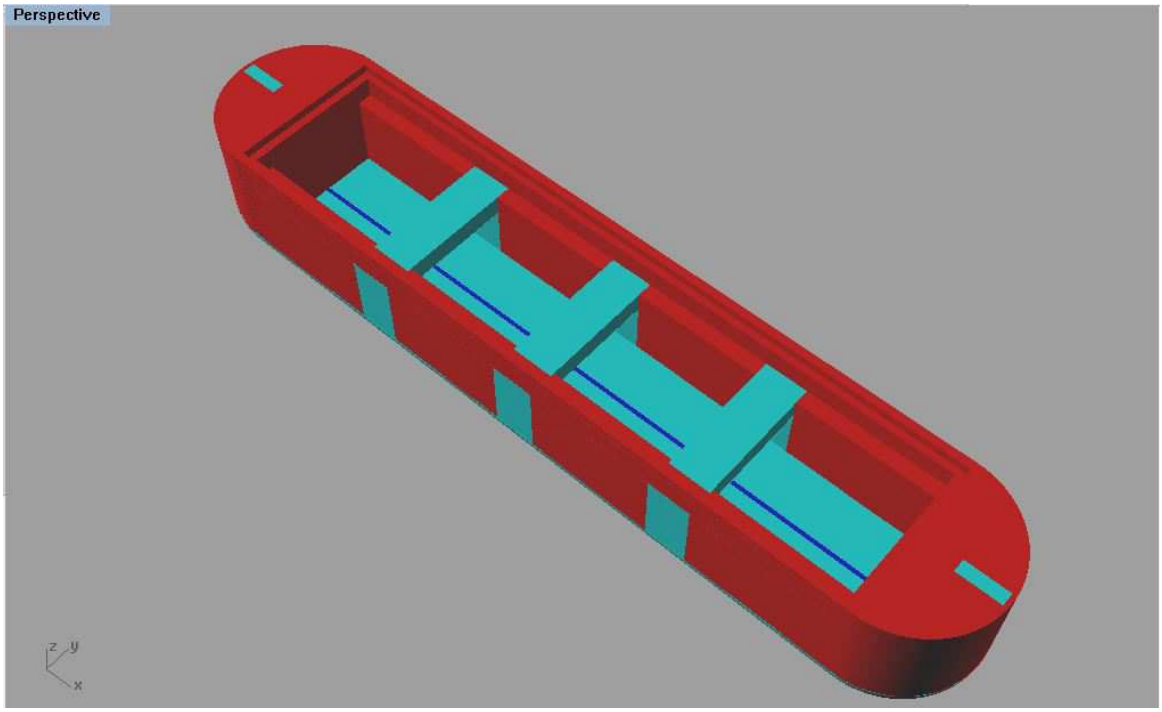

Figure 2.2: Model draft

Figure 2.3: Ship model

Table 2.1: Model and Ship Particulars

	Full scale ship	Ship model 1	Ship model 2
Length overall (m)	120	1.997	1.998
Breadth (m)	24	0.397	0.397
Depth (m)	18	0.301	0.300
Draft at midship (m)	6	0.103	0.104
Initial trim angle ($^\circ$)	0	0.01	0.02
Displacement (kg)	$1.642E7$	76.6	76.6
KG (m)	7.2	0.133	0.130
LCG, fwd of midship (m)	0	0.000	0.000
C_B	0.928	0.938	0.929
Roll moment of inertia (kgm^2)	$1.159E9$	1.46	1.46
Pitch moment of inertia (kgm^2)	$1.478E10$	20.43	19.67

The center of gravity position, roll and pitch moments of inertia were determined from the real FPSO particulars. In the model hull design, calculations were needed to ensure the center of gravity position as well as roll and pitch moment of inertia can be achieved in the ballasting process, which means there should be enough space and proper positions to put the ballast weights in ship hull model.

The weight of each model hull was estimated as 35 kg since the volume and density of the materials used were known. Using the software Rhinoceros, the volume of the submerged body part was determined as 0.0742 m^3, from which the displacement of the ballasted model is 74.2 kg. Thus, 39.2 kg ballast weight should be distributed in each model. By calculation, the center of gravity of the empty model was 0.072 m above the bottom. Based on the model design, the center of gravity of the ballasted model was 0.12 m above the bottom. The center of gravity of the ballast weights

should be 0.163 m above the bottom, which can be easily achieved.

Similarly, the roll and pitch moments of inertia of the model were checked in the design process. Roll moment of inertia was more significant and needed to be checked with higher priority. The roll moment of inertia is related to the model's roll motion natural frequency. In our model test, the roll motion natural frequency was determined as 5.5 rad/s, which was in the middle of the targeted wave frequency range [3.92, 7.16] rad/s. The relation between roll natural frequency and roll moment of inertia was shown in the following equation:

$$\omega_{roll}^2 = \frac{\Delta \overline{GM_T}}{I_{xx} + I'_{xx}} \tag{2.1}$$

where Δ is force, $\overline{GM_T}$ is transverse metacentric height, I'_{xx} is added roll moment of inertia. The relationship between I_{xx} and I'_{xx} could be obtained from the empirical formula $I'_{xx} = 0.25 I_{xx}$ for typical ships. As the models in the project were box-shaped, it was assumed that $I'_{xx} = 0.3 I_{xx}$ in the calculation. Thus, roll moment of inertia could be determined once $\overline{GM_T}$ was known. From Rhinoceros, center of buoyancy position could be found. Then $\overline{GM_T}$ could be calculated with the following equations.

$$\overline{GM_T} = KB + BM - KG \tag{2.2}$$

$$BM = \frac{I_T}{\nabla} \tag{2.3}$$

where ∇ is volume of displacement, I_T is the moment of the water plane. The calculated I_{xx} of the ballasted model was 1.48 kgm^2. As the model roll moment of inertia was 0.91 kgm^2, all ballast weights should contribute 0.57 kgm^2 roll moment of inertia, which was achievable.

When the center of gravity of the model as well as the roll and pitch moments of

inertia were checked, the ship model was ready to be manufactured.

2.2 Mooring System

The mooring design is also an essential element of the project. A well designed mooring system must prevent excessive drift motions of the bodies as well as not influencing the first-order body motions.

According to ITTC recommended procedures and guidelines 7.5-02-07-03.1 (Floating Offshore Platform Experiments) (ITTC, 2005), the model should be positioned at the test location by using mooring lines. The restraint lines should be soft and elastic that allow motion but are able to restrain excessive drifting. The natural frequency of the restraint system was designed to be one order of magnitude smaller than the lowest wave frequency and the model's natural frequency.

The stiffness of the restraint springs is determined by Equation 2.4.

$$\sqrt{\frac{K'}{M+M'}} \leqslant \frac{\omega_{min}}{10} \tag{2.4}$$

where K' is the effective stiffness of the restraint springs, M is the mass of the ship model, M' is the added mass of the ship model, ω_{min} is the lowest wave frequency used in the model test.

In our model test, M is 74.2 kg and ω_{min} is 3.92 rad/s. The relationship between M and M' was determined with preliminary numerical simulation conducted by potential flow codes and it was found that M' was very close to M in the simulated case. Assuming M' equals to M, the effective stiffness of the restraint springs should be less than 22.8 N/m.

Eventually, the stiffness of the restraint springs used in the model test was determined as 3.5 N/m. For each ship model, 4 restraint springs were applied on it, as shown in

Figure 2.4. The angle between the two restraint springs on bow/stern was about 45 degrees. In the tests, each restraint mooring line consisted of one spring and two soft nylon fishing lines, as shown in Figures 2.5 and 2.6.

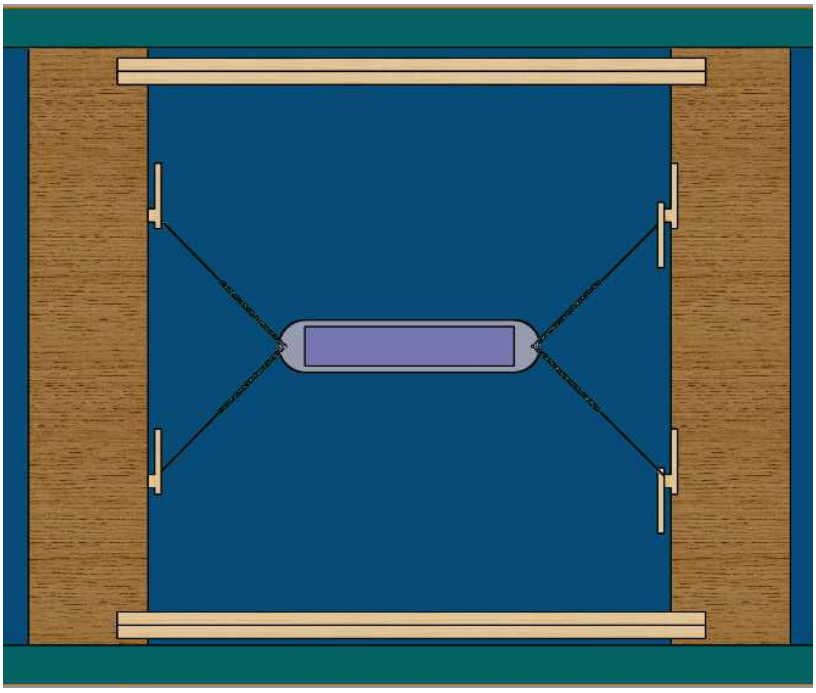

Figure 2.4: Mooring system

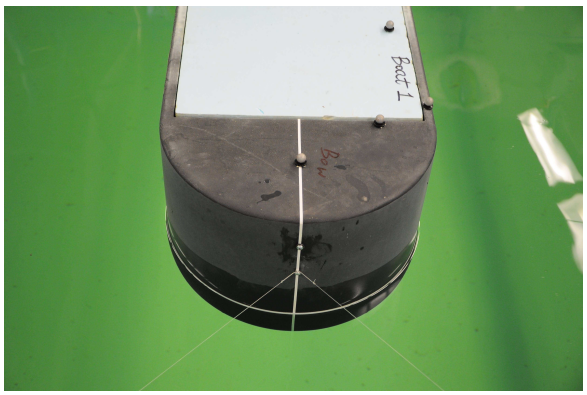

Figure 2.5: Model end of soft restraint lines

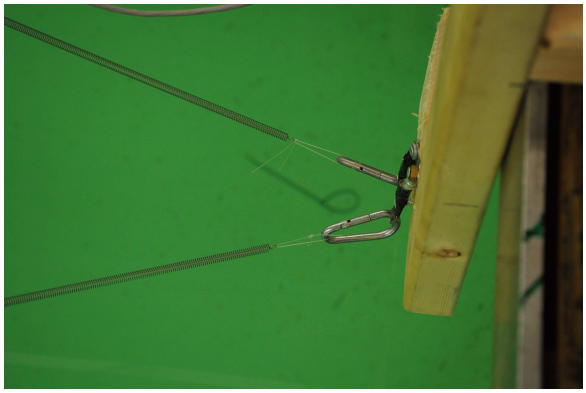

Figure 2.6: Post end of soft restraint lines

2.3 Motion Capture Instrument

Qualisys and MotionPak were used in the model tests to measure the motion of ship model. Wave elevation was measured by wave probes and analyzed by LabVIEW.

2.3.1 Qualisys Motion Capture System

The Qualisys motion capture system can capture the body motion with optical measurement hardware and analyze the body motion in 6 degree of freedom with Qualisys Track Manager software (Qualisys, 2013).

Refer to the Figures 2.7 and 2.8, the Qualisys optical hardware includes 3 Oqus cameras. 15 tracking markers were attached on the deck of each body. When the tracking markers moved with the bodies, the cameras captured and recorded the motions of these tracking markers. Motion data captured were later analyzed by Qualisys Track Manager. Calibration of the Qualisys system was conducted before use.

Qualisys Track Manager is a Windows-based data acquisition software. It has an interface that allows the user to perform 2D , 3D and 6D motion capture. During the capture, real time 2D, 3D and 6D camera information is displayed instantly. The

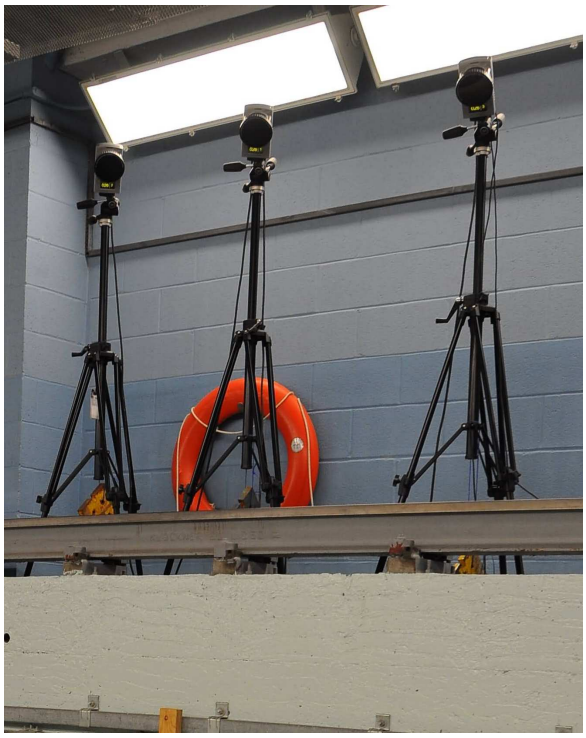

Figure 2.7: Oqus cameras

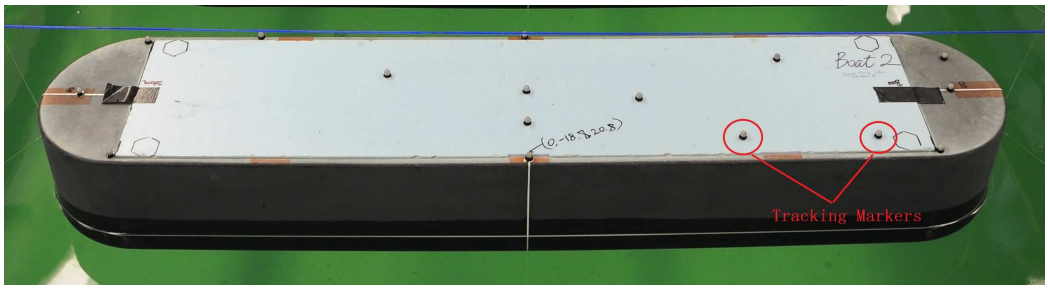

Figure 2.8: Tracking markers

individual 2D camera data is quickly processed and converted into 3D or 6D data by advanced algorithms. The data can be exported with several formats and can be analyzed by commonly used software, such as MatLAB.

In the motion data analysis process, a standard right-handed body fixed coordinate system was established. The origin of the coordinate system was set at the center of gravity. The z-axis is positive upwards. The positive direction of x-axis is from stern to bow. The positive direction of y-axis is from starboard to port.

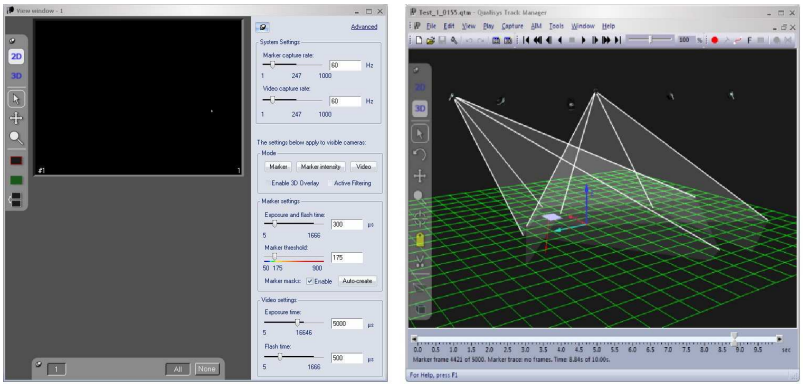

Figure 2.9: QTM user interface

2.3.2 MotionPak

MotionPak was also employed in the model test to capture the body motion. The body motion data acquired by MotionPak was compared with the data from Qualisys Motion Capture System to ensure the body motion data acquired are correct.

When MotionPak was installed inside the ship model at the center of the initial water plane, it records the roll, pitch and yaw motion of the ship model. The motion data acquired was sent to a laptop with wireless signals. Time series of body motions were then obtained with a software program by analyzing the data received.

2.3.3 Wave Probes

Wave probes were placed upstream and downstream of the ship model in all test cases and also placed in the gap in two-body model test cases. The data acquired by wave probes was simultaneously analyzed with LabVIEW on a desktop.

In the right handed tank (earth) coordinate system with the origin at the geometric center of the tank on the water surface and the x-axis along the tank wall positive towards the wave maker, the locations of the wave probes in single body test and two-body test are listed in Tables 2.2 and 2.3.

Table 2.2: Wave Probe Locations in Single Body Test

Facility	Location in tank coordinate system
	unit: (m, m, m)
Wave Probe 1 - upstream	(29.2, 0, 0)
Wave Probe 2 - downstream	(-7.5, 0, 0)
Wave Probe 3	(18.0, 0, 0)
Wave Probe 4	(2.2, 0, 0)
Wave Probe 5	(-1.8, 0, 0)

Table 2.3: Wave Probe Locations in Two-Body Test

Facility	Location in tank coordinate system
	unit: (m, m, m)
Wave Probe 1 - upstream	(29.2, 0, 0)
Wave Probe 2 - downstream	(-7.5, 0, 0)
Wave Probe 3 - in gap	(0.5, 0, 0)
Wave Probe 4 - in gap	(0, 0, 0)
Wave Probe 5 - in gap	(-0.5, 0, 0)

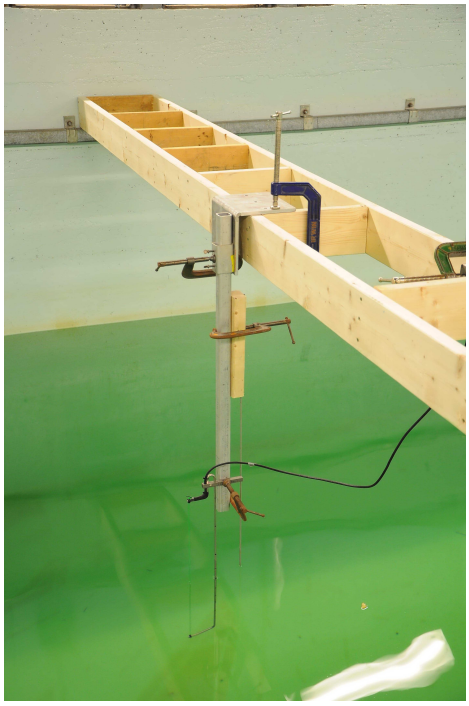

Figure 2.10: Upstream wave probe

2.4 Ship Model Ballasting

The models were ballasted after the ship models were manufactured. The ship model ballasting was conducted in the Trim Tank at the Ocean Engineering Research Center. The Trim Tank was 3.7 meter long, 1.0 meter wide and the water depth was 0.5 meter. Each model used in the model tests was ballasted by following the same procedure. The target mass was known based on the model design. In order to determine the mass of the ballast weights, the bare hull model was weighed and its mass was subtracted from the target mass. Once the mass of the ballast weight was determined, multiple ballast weights were selected so when added together would achieve the determined the mass of the ballast weight. Ballast weights were selected such that their mass was as close as possible to the calculated value. The bare hull model was placed in the Trim Tank and the ballast weights were added to the interior of the ship model.

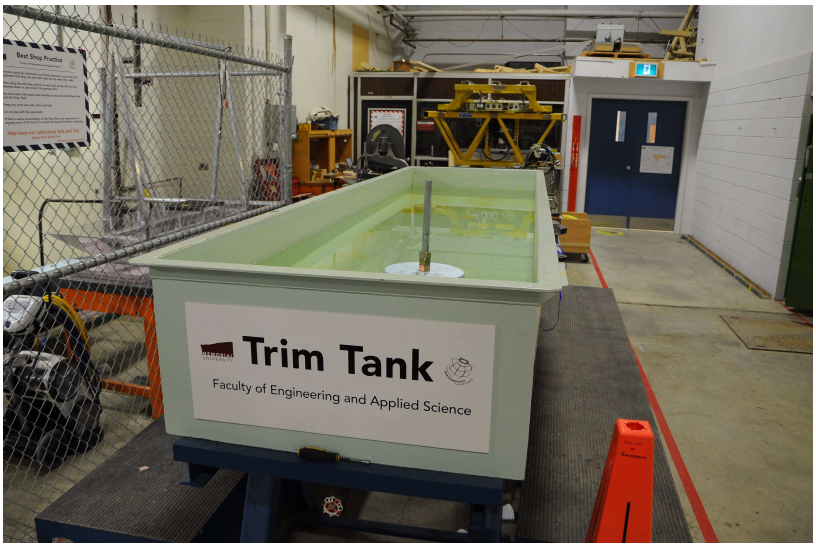

Figure 2.11: Trim tank

The ballast weights were added such that the model would be on an even keel with no heel or trim and the design waterline would correspond with the water surface. An inclinometer was placed on the model during this process to ensure that there was no heel or trim angle. Once this was achieved, all weights were numbered, their direction indicated and their placement outlined to allow quicker ballasting in the future. Inclining tests must be preformed to check that the vertical center of gravity matches that of the design. If the vertical center of gravity does not match within reasonable uncertainty, which was determined as 5 % in this project, the ballasting must be redone by placing the ballast weights at different heights in order to shift the vertical center of gravity.

Based on the design, the target mass of the ballasted ship model was 74.2 kg. Refer to Figure 2.12, Model 1 had a lightship mass of 40.0 kg and 36.6 kg of ballast weight was added for a total mass of 76.6 kg. Model 2 had a lightship mass of 39.6 kg and 37.0 kg of ballast weight was added for a total mass of 76.6 kg. Under these conditions, both ship models were at their design waterlines with negligible heel or trim angles. Both models were also reasonably close to the target mass (error within 5 %).

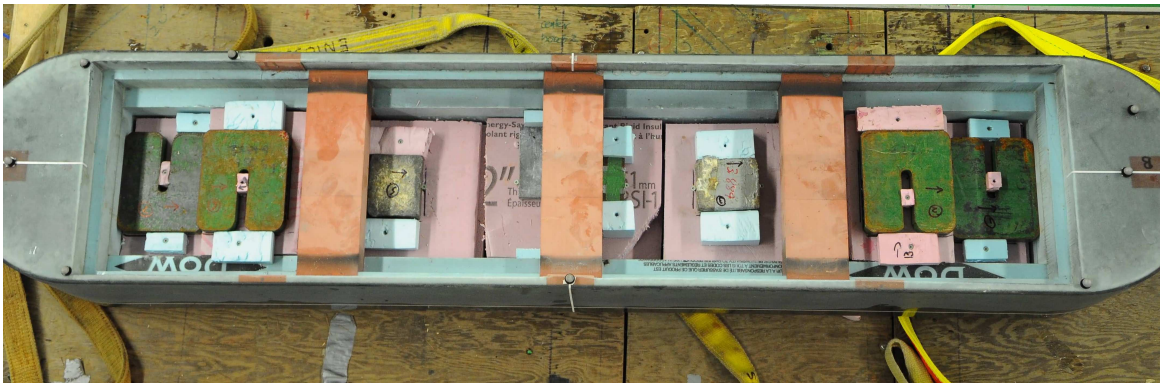

Figure 2.12: Ballasting weight distribution for Model 1

2.5 Inclining Test

The theory of the inclining test is presented in Appendix A.

In the inclining test, four weights (BW1, BW2, SW1, SW2) of equal weight were selected. Eight positions were outlined on the ship model, two on the port side aft of the midship, two on the port side forward the midship, two on the starboard side aft of the midship, and two on the starboard side forward the midship. These positions were chosen to be equidistant from the midship on both port and starboard as well we equidistant from the centerline for simplicity. The initial condition should have the weight distributed so that the ship model was sitting on an even keel with no roll angle. If the angle was not initially zero, this must be recorded and all other angles obtained from the test should be altered to extract the initial angle. The weights used for the test, when all on one side of the model, should create a roll angle between 2 and 4 degrees. Four weights were placed on the ship model in the positions shown in Figure 2.13 for the initial condition, with BW1 and BW2 placed on the bow side.

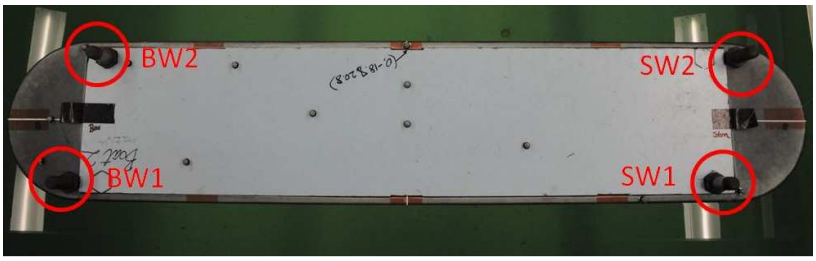

Figure 2.13: Inclining test

The procedure of the weight movement in inclining test was presented in Table 2.4.

Table 2.4: Procedure of Weight Movement

Step	Movement	Weight's Location	
		Port	Stbd
0		BW1, SW1	BW2, SW2
1	BW1 shift to Right	SW1	BW1, BW2, SW2
2	SW1 shift to Right		BW1, BW1, SW1, SW2
3	BW1 shift to Left	BW1	BW2, SW1, SW2
4	SW1 shift to Left	BW1, SW1	BW2, SW2
5	BW2 shift to Left	BW1, BW2, SW1	SW2
6	SW2 shift to Left	BW1, BW1, SW1, SW2	
7	BW2 shift to Right	BW1, SW1, SW2	BW2
8	SW2 shift to Right	BW1, SW1	BW2, SW2

The expected value for the vertical center of gravity based on the design was 0.13 m. After carrying out the inclining test on both models, the position of the ballast weights had to be changed and the inclining test done again as the vertical center of gravity found was not close enough to that of the design. Redoing the inclining tests resulted in a vertical center of gravity of 0.13 m for Model 1 and a vertical center of gravity of 0.133 m for Model 2.

2.6 Swing Test

The theory and procedure of the swing test are presented in Appendix B.

Based on the design, the expected vertical center of gravity was 0.13 m and the expected moments of inertia were 1.481 kgm^2 for roll and 18.55 kgm^2 for pitch. After carrying out the swing test for both models, Model 1 was found to have moments of inertia of 1.41 kgm^2 for roll and 19.35 kgm^2 for pitch. Model 2 was found to have moments of inertia of 1.39 kgm^2 for roll and 21.96 kgm^2 for pitch. The vertical center of gravity for Models 1 and 2 were 0.131 m and 0.132 m. Test results were reasonably close to the target values.

2.7 Decay Test

The theory of the decay test is presented in Appendix C.

The ballasted ship model was placed in the tank with its longitudinal axis parallel to the tank wall. It ensured that the reflections from the tank wall would have minimal effect of the experiment. An initial angle was given to the model. For roll decay, this was done by placing a weight on either the port or starboard side of the model at its midship. The weight was quickly removed and the motion of the model was recorded using an inertial sensor which could record the 6 degrees of freedom motions. An angle verses time series was obtained and analyzed to find the natural period and damping coefficient of the given model. A free decay test was done where the model was free floating in the body of water, and another decay test was done where the model was secured by mooring lines for comparison.

The damping calculated from the free decay test was 9.0% for Model 1 and 10.1% for Model 2. Only Model 1 was used for a moored decay test and the damping related to this test was calculated to be 9.1%.

From the comparison results of free decay test and moored decay test, it can be found that the damping factor increased from 9% to 9.1% by applying soft mooring lines to the model, which was very insignificant. It suggests that the soft restraint lines did not significantly affect the roll response characteristics.

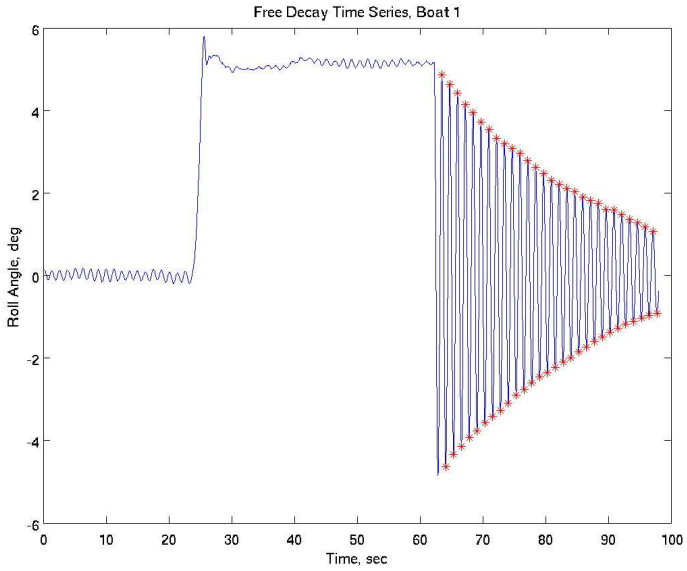

Figure 2.14: Free decay test time series of Model 1

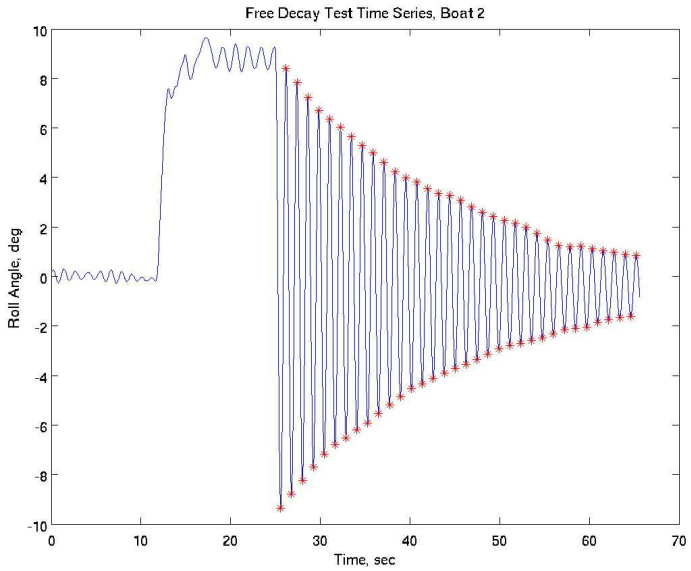

Figure 2.15: Free decay test time series of Model 2

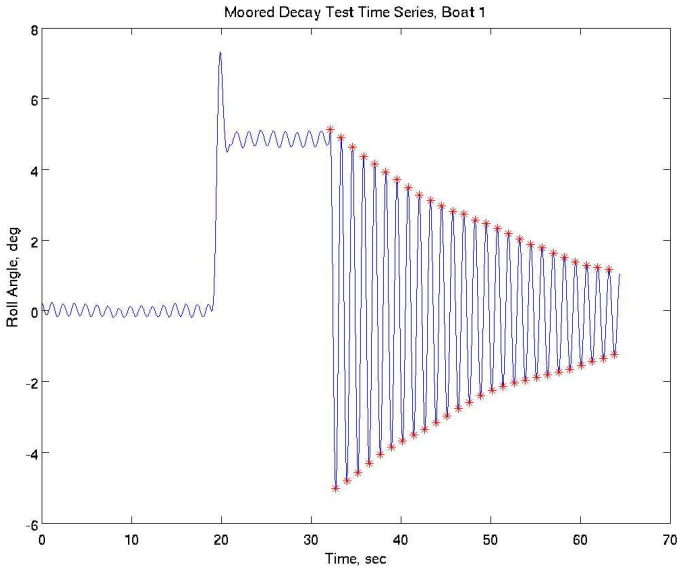

Figure 2.16: Moored decay test time series of Model 1

2.8 Summary

This chapter introduces the design of ship model and mooring system, the motion capture systems used in the test and the details of a series of pre-tests. After the ship model and mooring system were designed and manufactured, and a series of pre-tests were completed, the model tests for single body and two-body cases were ready to be carried out. The model masses, vertical center of gravities and roll/pitch moment of inertias were obtained from the pre-tests.

Chapter 3

Model Tests

Single body cases and two-body cases in regular waves in head seas were studied in the model tests.

3.1 Regular Wave Calibration

By referring to the wave information in full scale FPSO cases and considering the capability of the wave maker in the towing tank, the wave information in the model test was determined. The wave steepness was 1/30 for all cases. Wave information for both model scale and full scale was shown in Tables 3.1 and 3.2.

To ensure the wave frequency and wave height of the regular waves generated by the wave maker in the towing tank are as we desired in the table above, the calibration of the regular waves needs to be conducted.

In the calibration of the regular waves, the first thing to do was to ensure the water depth in the towing tank always remaining the same. It was achieved by daily check of water depth with a certain wave probe in the process of the model tests. Then, appropriate control commands of the wave maker were determined to generate the regular waves with the desired wave frequencies and wave heights. After that, four

Table 3.1: Wave Information in Model Scale

Case NO.	Wave length (m)	ω (rad/s)	f (Hz)	Wave height (mm)
1	1.2	7.16	1.14	40.00
2	1.27	6.97	1.11	42.21
3	1.4	6.63	1.06	46.67
4	1.6	6.20	0.99	53.33
5	1.72	5.98	0.95	57.33
6	1.8	5.85	0.93	60.00
7	1.92	5.66	0.90	64.00
8	2	5.55	0.88	66.67
9	2.2	5.29	0.84	73.33
10	2.4	5.06	0.81	80.00
11	2.6	4.87	0.77	86.67
12	2.8	4.69	0.75	93.33
13	3	4.53	0.72	100.00
14	3.2	4.39	0.70	106.67
15	3.4	4.25	0.68	113.33
16	3.6	4.13	0.66	120.00
17	3.8	4.02	0.64	126.67
18	4	3.92	0.62	133.33

Table 3.2: Wave Information in Full Scale

Case NO.	Wave length (m)	ω (rad/s)	f (Hz)	Wave height (m)
1	72	0.925	0.147	2.40
2	76	0.900	0.143	2.53
3	84	0.856	0.136	2.80
4	96	0.801	0.127	3.20
5	103.2	0.772	0.123	3.44
6	108	0.755	0.120	3.60
7	115.2	0.731	0.116	3.84
8	120	0.716	0.114	4.00
9	132	0.683	0.109	4.40
10	144	0.654	0.104	4.80
11	156	0.628	0.100	5.20
12	168	0.605	0.096	5.60
13	180	0.585	0.093	6.00
14	192	0.566	0.090	6.40
15	204	0.549	0.087	6.80
16	216	0.534	0.085	7.20
17	228	0.520	0.083	7.60
18	240	0.506	0.081	8.00

repetitions were conducted for regular wave calibration.

Figure 3.1 presents the calibration results of wave height. Measurement results of two wave probes in four repetition tests were compared. From the figure, it is indicated that the generated wave height was quite stable in the repetition tests and the regular waves can be applied in the model tests.

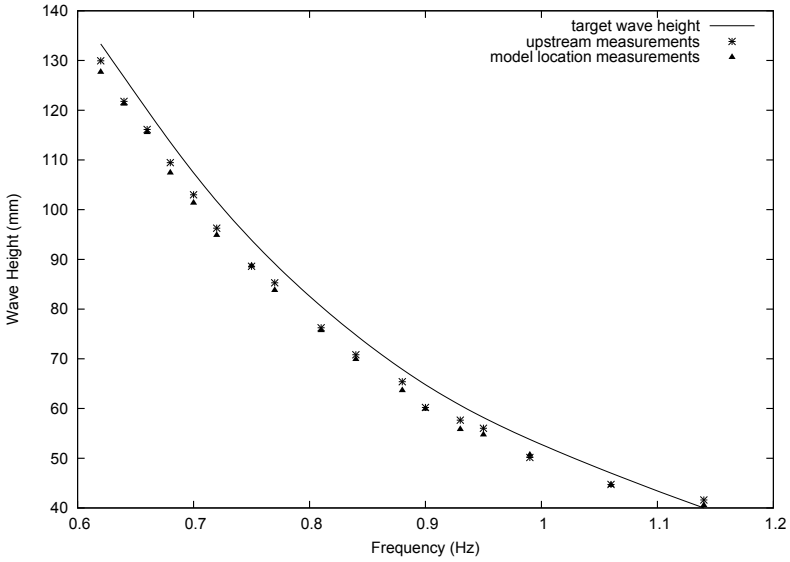

Figure 3.1: Wave calibration results

3.2 Single Body Model Test

3.2.1 Set-Up

In single body model test, the model was positioned in the middle of the tank (29.2 m from wave maker and 25.5 m from wave absorber), which was shown in Figure 3.2. The ship model was restrained by four soft mooring lines and the pre-tension of each soft mooring line was 1.8 N. The lines were tied up on the model 5 cm above the design water line in the longitudinal center plane. Each restraint line was fixed on a mooring post that was either placed on the operating deck or on the tank wall. As

confirmed in the roll decay tests, the soft restraint lines did not significantly affect the roll response characteristics.

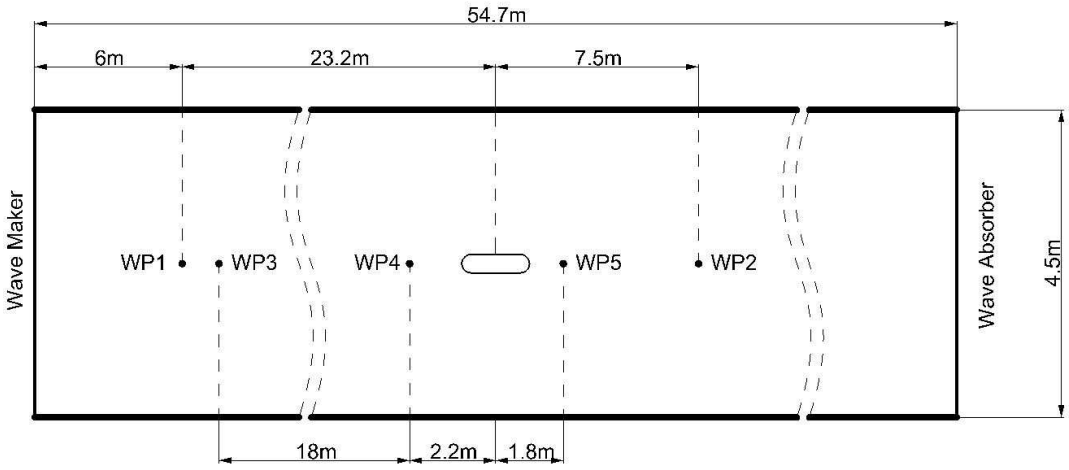

Figure 3.2: Layout of single body model test

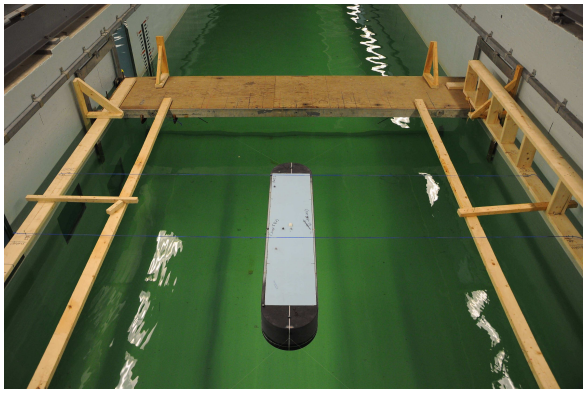

Figure 3.3: Single body model test set-up

The tank (earth) coordinate system is standard right handed, with the origin at the geometric center of the tank on the water surface. In the tank coordinate system, the x-axis is along the length of the tank (positive towards the wave maker), the y-axis across the tank and z-axis vertical (positive up). The model location in the tank and the locations of the specific instruments are referenced to the tank coordinate system.

Table 3.3 lists the location of the models and the wave probes in tank.

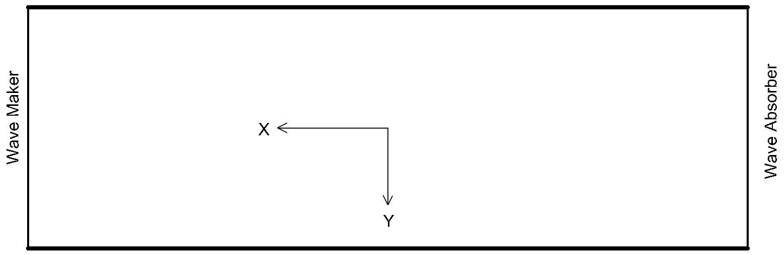

Figure 3.4: Tank coordinate system

Table 3.3: Location of Model and Wave Probes in Single Body Test

Facility	Location in tank coordinate system
	unit: (m, m, m)
Ship Model (CG)	(0.13, 0, 0)
Wave Probe 1 - upstream	(23.2, 0, 0)
Wave Probe 2 - downstream	(-7.5, 0, 0)
Wave Probe 3	(18.0, 0, 0)
Wave Probe 4	(2.2, 0, 0)
Wave Probe 5	(-1.8, 0, 0)

3.2.2 Instrument Calibration

Qualisys motion capture system was calibrated with its own software Qualisys Track Manager. The calibration was conducted before the model test and every two weeks in the model test process in order to ensure the quality of the motion measurements. In the calibration process, an *L*-shaped reference structure and a calibration wand, with tracking markers attached on both of them, were used. The *L*-shaped reference structure was placed where all cameras in the system can see all markers on it. Once it was placed, the desired coordinate system of the motion capture was obtained. The calibration wand was then moved inside the measurement volume in all three directions, which was to assure that all axes were properly scaled. The calibration algorithms would extract each camera's position and orientation by evaluating the

camera's view of the wand during the calibration. A higher calibration quality was anticipated with a longer period of calibration time.

In a good calibration result, the average residual of camera positions and the standard deviation of wand length calculated by Qualisys Track Manager should be acceptably small for the system to pass the calibration. Calibration results in this project were presented in Figure 3.5. In the figure, it is shown that the average residuals of camera positions and the standard deviations of wand length were smaller than 1 and 2, respectively, which were acceptable for the calibration.

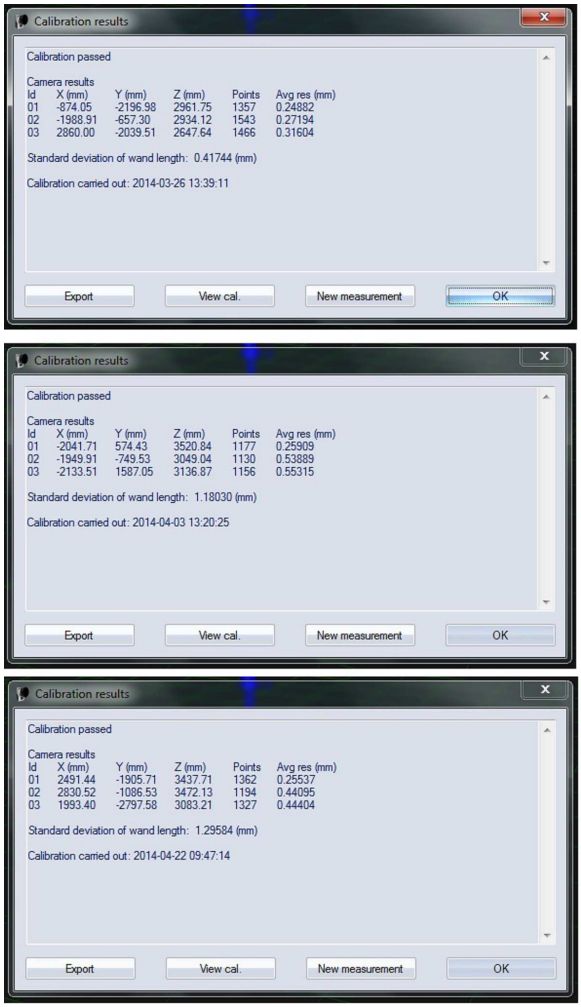

Figure 3.5: Qualisys calibration results

Wave probes were calibrated in calm water. In the calibration, the wave probes were submerged in calm water with 5 different designed depths. The outputs were analyzed and a linear relationship between water depth and wave probe output was anticipated. Calibration results were presented in Figures 3.6 to 3.10. From the figures, it can be found that the data points were linearly distributed, which indicates the wave probes performed very well in the measurement process.

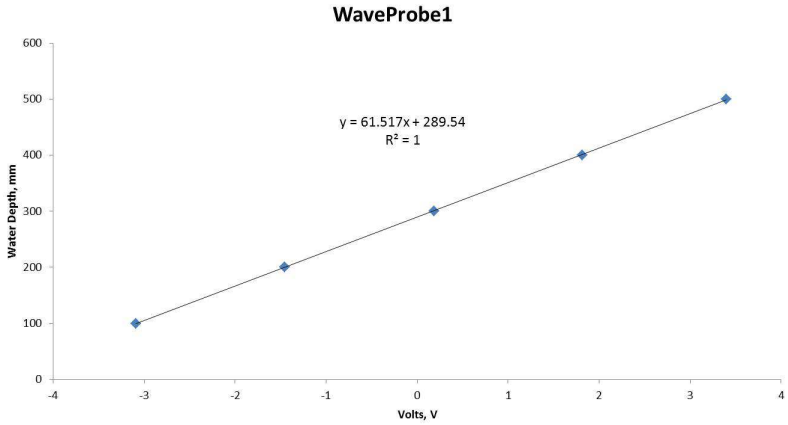

Figure 3.6: Wave probe 1 calibration results

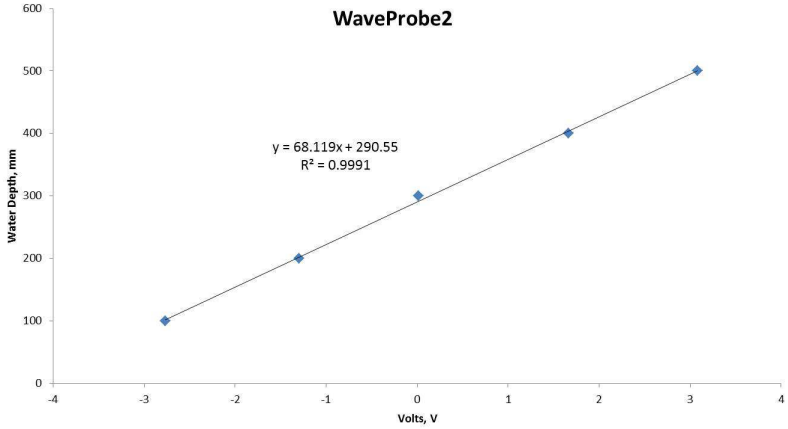

Figure 3.7: Wave probe 2 calibration results

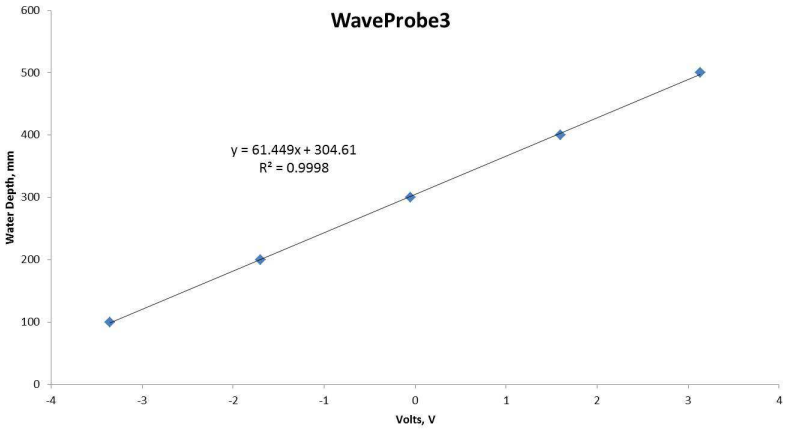

Figure 3.8: Wave probe 3 calibration results

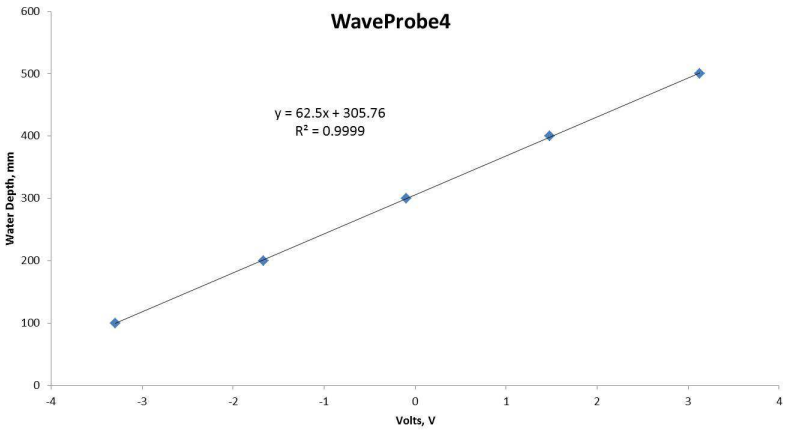

Figure 3.9: Wave probe 4 calibration results

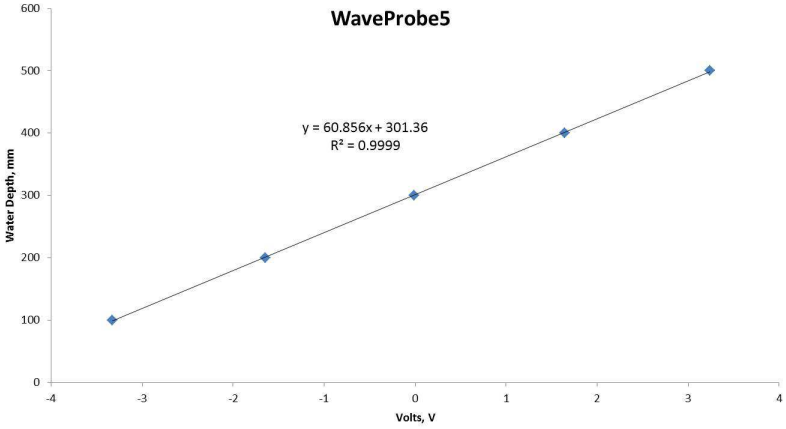

Figure 3.10: Wave probe 5 calibration results

A calm water test was carried out at the beginning of each day prior to the wave tests in order to determine the equilibrium status for model motions and wave elevation.

3.2.3 Test Cases

Eighteen cases with different incoming regular waves listed in Table 3.1 were tested in single body model test. As a result of the tight schedule and in order to save time for two-body model test, repeated tests cannot be conducted for all cases in single body model test. Repeated tests were only conducted for two high frequency cases, which are 0.90 and 0.95 Hz.

The run time for each case was 120 seconds.

3.2.4 Data Acquisition and Analysis

In the test process, Qualisys motion capture system acquired 6 degree of freedom body motion data. MotionPak system acquired 3 degree of freedom (roll, pitch yaw) body motion data. Wave probes acquired the free surface elevation data. Also, a JVC camcorder recorded the videos for all test runs.

Data analysis was completed by following ITTC recommended procedures and guidelines 7.5-02-07-03.2 (Analysis Procedure for Model Tests in Regular Wave) (ITTC, 2002). A spectra analysis was applied to model motions and wave elevation measurements throughout Fast Fourier Transform (FFT). Ship motion RAOs were calculated based on the ship motion data and incoming wave data.

3.3 Two-Body Model Tests

3.3.1 Set-Up

The tank preparation was similar to that of the single body tests. Two ship models were moored using soft restraints in the tank; however, each one was shifted off the center based on the gap requirement. Three wave probes were hung on an angle steel bar and placed in the centerline of the gap. Wave Probe 4 was in the middle of the gap; Wave Probe 3 and 5 were 0.5 m from Wave Probe 4 towards the bow and the stern, respectively. As there was a concern that the ship model would collide with the wave probes, three foams guards were also hung on the steel bar to protect the wave probes. The layout of two-body model tests was presented in Figure 3.11.

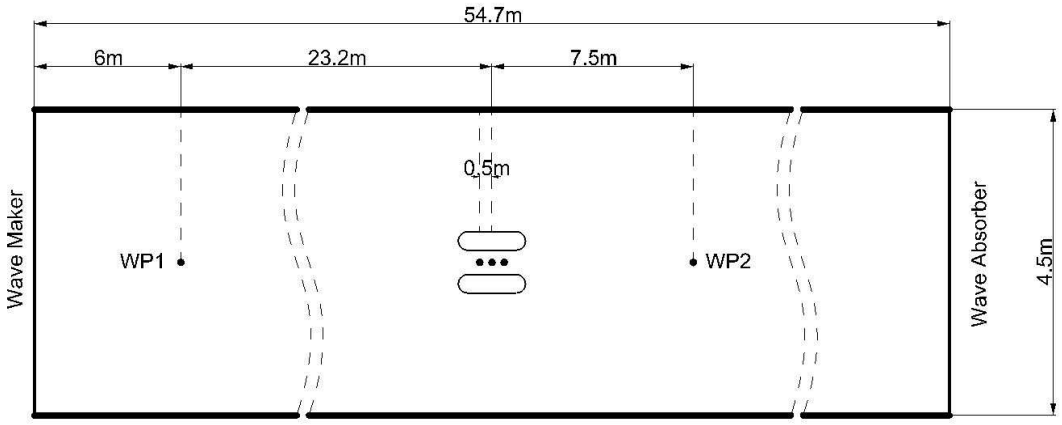

Figure 3.11: Layout of two-body model tests

Three different gap widths were tested in two-body model tests, which were 0.40 m, 0.45 m and 0.55 m, in model scale. One should note that those values refer to the gap widths when the models were stationary. The locations of the models for Gaps 1 to 3 and wave probes were listed in Table 3.4.

The calibration of Qualisys motion capture system and wave probes was same with

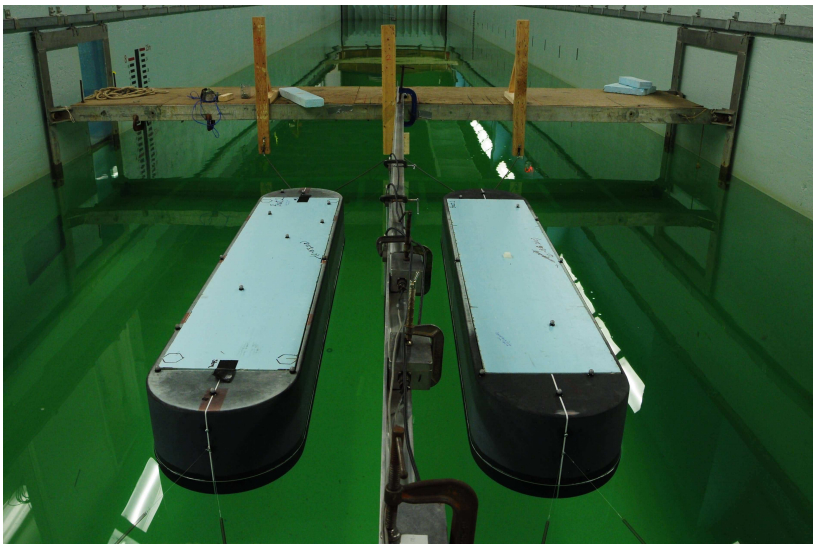

Figure 3.12: Two-body model tests set-up

Table 3.4: Location of Models and Wave Probes in Two-Body Tests

Facility	Location in tank coordinate system
	unit: (m, m, m)
Ship Model 1 (CG) for Gap 1	(0.13, 0.40, 0)
Ship Model 2 (CG) for Gap 1	(0.13, -0.40, 0)
Ship Model 1 (CG) for Gap 2	(0.13, 0.425, 0)
Ship Model 2 (CG) for Gap 2	(0.13, -0.425, 0)
Ship Model 1 (CG) for Gap 3	(0.13, 0.475, 0)
Ship Model 2 (CG) for Gap 3	(0.13, -0.475, 0)
Wave Probe 1 - upstream	(23.2, 0, 0)
Wave Probe 2 - downstream	(-7.5, 0, 0)
Wave Probe 3 - in gap	(0.5, 0, 0)
Wave Probe 4 - in gap	(0, 0, 0)
Wave Probe 5 - in gap	(-0.5, 0, 0)

that in single body test. A calm water test was also carried out at the beginning of each day prior to the wave tests in order to determine the equilibrium status for model motions and wave elevation.

3.3.2 Test Cases

Table 3.5 presents the test cases in two-body model tests. Two full test sets were carried out for each gap in two-body tests. Four frequencies were determined based on data analysis to conduct three more repeats. The frequencies were chosen where spike appeared or the RAOs were different from single body tests. The purpose of repeat tests was to confirm the measurements were correct by conducting uncertainty analysis.

The run time for each case was also 120 seconds.

3.3.3 Data Acquisition and Analysis

Data acquisition process in two-body model test was same as that in single body model test.

As only RAOs were being developed from the tests, the data analysis procedure was the same as employed by single body tests. Note that not only the motion responses but the wave elevations in gap were of interests during two-body model tests; therefore, the measurements from wave probes 3, 4 and 5 were also processed by the same analysis procedure.

3.4 Summary

This chapter presents the conduct of single body model test and two-body model tests in the towing tank. The details of regular wave calibration, model test set-up,

Table 3.5: Test Cases of Two-Body Model Tests

Case NO.	ω (rad/s)	f (Hz)	Wave height (mm)	Gap width (m)	Repetition
1	7.16	1.14	40.00	0.40	2
2	6.97	1.11	42.21	0.40	2
3	6.63	1.06	46.67	0.40	5
4	6.20	0.99	53.33	0.40	5
5	5.98	0.95	57.33	0.40	2
6	5.85	0.93	60.00	0.40	2
7	5.66	0.90	64.00	0.40	2
8	5.55	0.88	66.67	0.40	2
9	5.29	0.84	73.33	0.40	5
10	5.06	0.81	80.00	0.40	5
11	4.87	0.77	86.67	0.40	2
12	4.69	0.75	93.33	0.40	2
13	4.53	0.72	100.00	0.40	2
14	4.39	0.70	106.67	0.40	2
15	4.25	0.68	113.33	0.40	2
16	4.13	0.66	120.00	0.40	2
17	4.02	0.64	126.67	0.40	2
18	3.92	0.62	133.33	0.40	2
19	7.16	1.14	40.00	0.45	2
20	6.97	1.11	42.21	0.45	2
21	6.63	1.06	46.67	0.45	5
22	6.20	0.99	53.33	0.45	5
23	5.98	0.95	57.33	0.45	2
24	5.85	0.93	60.00	0.45	2
25	5.66	0.90	64.00	0.45	2
26	5.55	0.88	66.67	0.45	2
27	5.29	0.84	73.33	0.45	5
28	5.06	0.81	80.00	0.45	5
29	4.87	0.77	86.67	0.45	2
30	4.69	0.75	93.33	0.45	2
31	4.53	0.72	100.00	0.45	2
32	4.39	0.70	106.67	0.45	2
33	4.25	0.68	113.33	0.45	2
34	4.13	0.66	120.00	0.45	2
35	4.02	0.64	126.67	0.45	2
36	3.92	0.62	133.33	0.45	2
37	7.16	1.14	40.00	0.55	2
38	6.97	1.11	42.21	0.55	2
39	6.63	1.06	46.67	0.55	5
40	6.20	0.99	53.33	0.55	5
41	5.98	0.95	57.33	0.55	2
42	5.85	0.93	60.00	0.55	2
43	5.66	0.90	64.00	0.55	2
44	5.55	0.88	66.67	0.55	2
45	5.29	0.84	73.33	0.55	5
46	5.06	0.81	80.00	0.55	5
47	4.87	0.77	86.67	0.55	2
48	4.69	0.75	93.33	0.55	2
49	4.53	0.72	100.00	0.55	2
50	4.39	0.70	106.67	0.55	2
51	4.25	0.68	113.33	0.55	2
52	4.13	0.66	120.00	0.55	2
53	4.02	0.64	126.67	0.55	2
54	3.92	0.62	133.33	0.55	2

instrument calibration, experimental data acquisition and experimental data analysis were discussed. The experimental data obtained was to be compared with numerical simulation results in a later chapter.

Chapter 4

Numerical Simulation

In this thesis, a panel-free method based potential-flow programs, MAPS0, was used for the prediction of body motions and wave elevations. The computed body motions and wave elevations were compared with experimental data and the contribution of viscosity in predicting two bodies interaction was discussed. WAMIT was also used for comparison purpose.

4.1 Theoretical Formulation of Frequency-Domain Computation Based on the Panel-Free Method

Based on the work of Qiu et al. (2006), the panel-free method for frequency-domain analysis is summarized below.

As shown in Figure 4.1, two sets of right-handed coordinate systems are established in the computation. A global coordinate system, O-XYZ, is established first, in which the OXY plane coinciding with the undisturbed water surface and the Z-axis pointing vertically upward. The second set of coordinate systems, $o_i x_i y_i z_i$ are fixed on each body. In the body-fixed coordinate systems, the origin o_i is defined as the intersection

point of calm water surface, the longitudinal plane of symmetry, and the vertical plane passing through the mid section, where i represents for the ith body, i=1,N and N is the total number of bodies. The $o_i x_i y_i$ plane coincides with the undisturbed water surface, with positive x_i-axis pointing toward the bow and the y_i-axis to the port side. β is the incident wave angle relative to the x-axis.

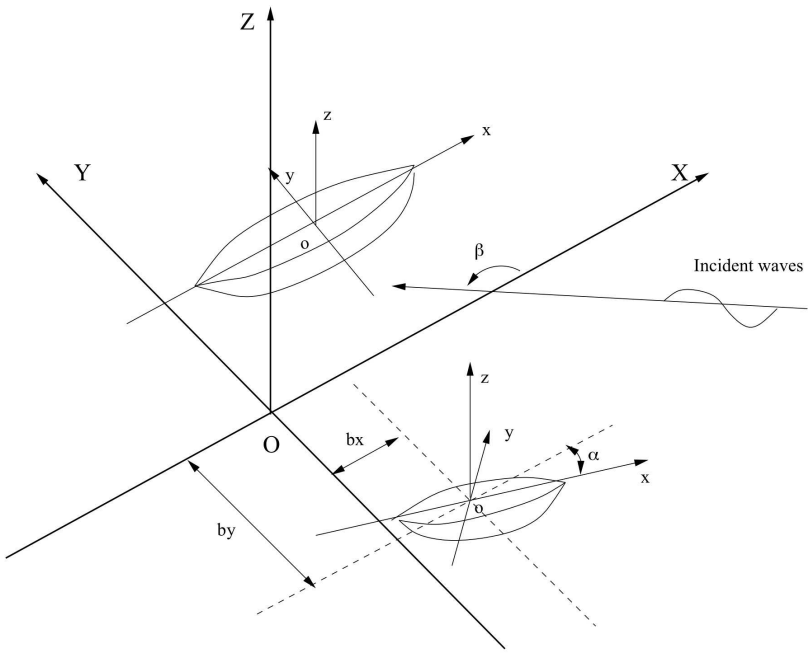

Figure 4.1: Coordinate system of MAPS0 (Qiu et al., 2014)

Assume that velocity potential at a field point $P(x, y, z)$ is time harmonic, the velocity potential can be expressed by $\phi(P)e^{-i\omega t}$. This velocity potential satisfies the Laplace equation and the linearized free-surface boundary condition on $z = 0$ and it can be decomposed as:

$$\phi(P) = \phi_R(P) + \phi_D(P) + \phi_I(P) \tag{4.1}$$

where ϕ_R, ϕ_D and ϕ_I are radiated, diffracted and incident wave velocity potentials, respectively. For each rigid body with six degrees of freedom, the radiation potential

is expressed as:

$$\phi_R(P) = -i\omega \sum_{k=1}^{6} \xi_k \phi_k \tag{4.2}$$

where ξ_k is the complex amplitude of the body motion in the kth mode. Introducing $\phi_7 = \phi_D$ and for a point P on the ith body surface, i.e. $P \in S_{b_i}$, the radiation and the diffraction potentials can be computed from the desingularized integral equation in terms of source strength as follows (Qiu et al., 2006) :

$$\begin{aligned}\phi_k(P) = &\int_{S_{b_i}} G_0(P,Q)\left[\sigma_k(Q) - \gamma(Q)\frac{\sigma_k(P)}{\gamma(P)}\right] dS \\ &+ \phi_0 \frac{\sigma_k(P)}{\gamma(P)} + \int_{\sum_{j=1,j\neq i}^{m} S_{b_j}} \sigma_k(Q) G_0(P,Q) dS \\ &+ \int_{\sum_{j=1}^{m} S_{b_j}} \sigma_k(Q) G_F(P,Q) dS\end{aligned} \tag{4.3}$$

where $\gamma(P)$ is the source distribution on S_b, which makes the body surface an equipotential surface of potential ϕ_0 (Qiu et al., 2014). The source strength is solved from

$$\begin{aligned}\frac{\partial \phi_k(P)}{\partial n_P} = &-\sigma_k(P) \\ &+ \int_{S_{b_i}} \left[\sigma_k(Q)\frac{\partial G_0(P,Q)}{\partial n_P} - \sigma_k(P)\frac{\partial G_0(P,Q)}{\partial n_Q}\right] dS \\ &+ \int_{\sum_{j=1,j\neq i}^{m} S_{b_j}} \frac{\partial G_0(P,Q)}{\partial n_P}\sigma_k(Q) dS \\ &+ \int_{\sum_{j=1}^{m} S_{b_j}} \frac{\partial G_F(P,Q)}{\partial n_P}\sigma_k(Q) dS\end{aligned} \tag{4.4}$$

In the equations above,

$$G(P,Q) = G_0(P,Q) + G_F(P,Q) \tag{4.5}$$

with

$$G_0(P,Q) = -\frac{1}{4\pi}(\frac{1}{r} + \frac{1}{r_1}) \tag{4.6}$$

and G_F is the wave term of the Green function for deepwater.

The desingularized integral equations (4.3) and (4.4) allow for the discretization by Gauss-Legendre quadrature over the exact geometry. The exact geometry can be represented by a NURBS surface. After the velocity potentials are computed, the exciting forces, added mass and damping on the each body can be obtained (Qiu and Hsiung, 2002; Qiu et al., 2014).

4.2 MAPS0 Simulation

Motion Analysis Program Suite(MAPS) is a potential-flow seakeeping program suite developed by Dr. Wei Qiu. It is based on a panel-free method and includes programs for both frequency-domain and time-domain analysis. MAPS0 is a sub-suite of MAPS for wave-body interaction analysis in the frequency domain.

4.2.1 Geometry Representation

MAPS0 uses Non-Uniform Rational B-Spline (NURBS) surfaces to represent the exact geometry of floating or fixed bodies. SRF file created from FastShip is accepted as standard input. The Gaussian points are automatically distributed on the wetted surface of a floating or fixed body for numerical integration. The number of Gaussian points on each patch surfaces and the type of Gaussian distribution are specified in SRFCTR (SRF Control) file (Qiu, 2013).

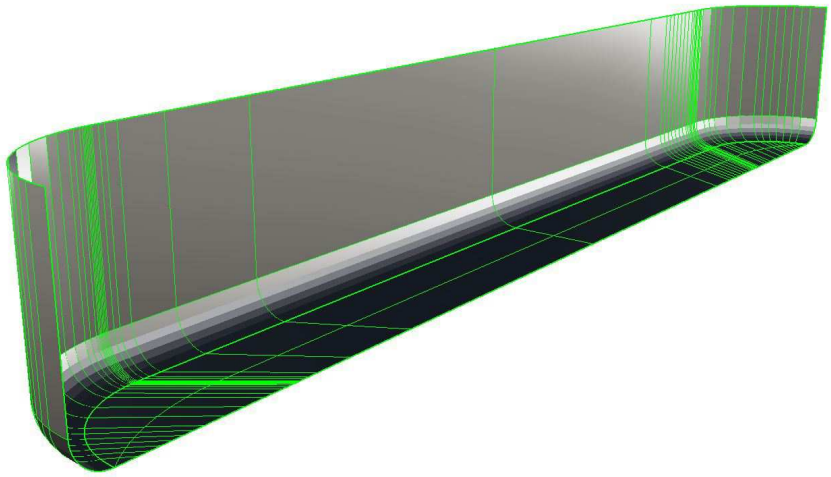

Figure 4.2: NURBS Surface of Model 1

4.2.2 Simulation Cases

In the numerical simulation with MAPS0, tank wall effect and mooring line effect was first studied by performing preliminary simulations for two-body case, to ensure the tank wall and soft restraint mooring line had very small effect on the motions of bodies. Then, the numerical simulation for single body cases and two-body cases were conducted. In the simulation, the wave heading was set as 180 degrees. In the simulation of two-body cases, 3 different gap widths were studied. All numerical simulations were conducted in full scale. The details of the settings are presented in Tables 4.1 and 4.2.

Convergence study was conducted in MAPS0 simulation for two-body cases by using different numbers of Gaussian points. 4 different numbers of Gaussian points (1968, 2624, 3280, 5248, defined as $GP\#1$ to $GP\#4$, respectively) were applied in the simulation. The comparison results are presented in Figures. 4.3 to 4.6. From the figures, it can be seen that the curves agree well with each other, which proves the simulation results are insensitive to the number of Gaussian points used.

Table 4.1: Single Body Simulation Cases

Parameter	Settings
Wave heading	180 degree
Wave frequency	Total number: 100
	Minimum: 0.25 rad/s
	Maximum: 2.23 rad/s
	Increment: 0.02 rad/s

Table 4.2: Two-Body Simulation Cases

Parameter	Settings
Gap width	24 m, 27 m, 33 m
Number of Gaussian points	1968, 2624, 3280, 5248
Wave heading	180 degree
Wave frequency	Total number: 100
	Minimum: 0.25 rad/s
	Maximum: 2.23 rad/s
	Increment: 0.02 rad/s

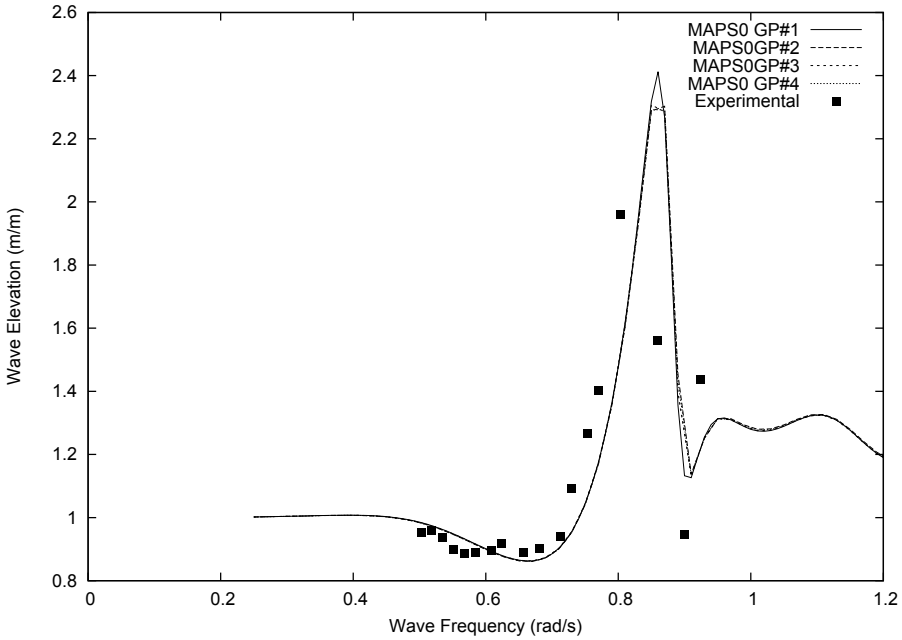

Figure 4.3: Convergence study of wave elevation at wave probe 3 (gap 0.55m)

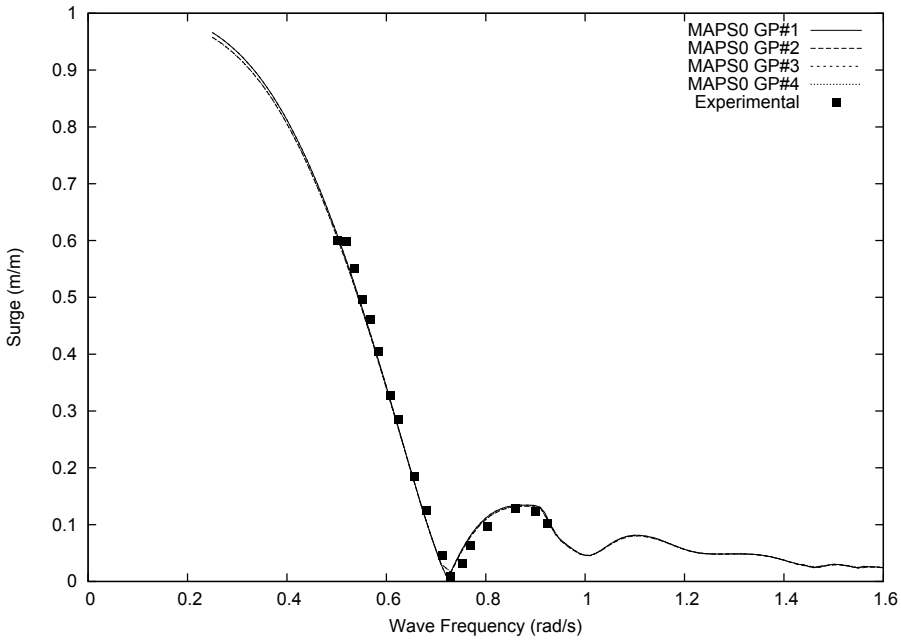

Figure 4.4: Convergence study of surge RAOs for two-body (gap 0.55m) cases

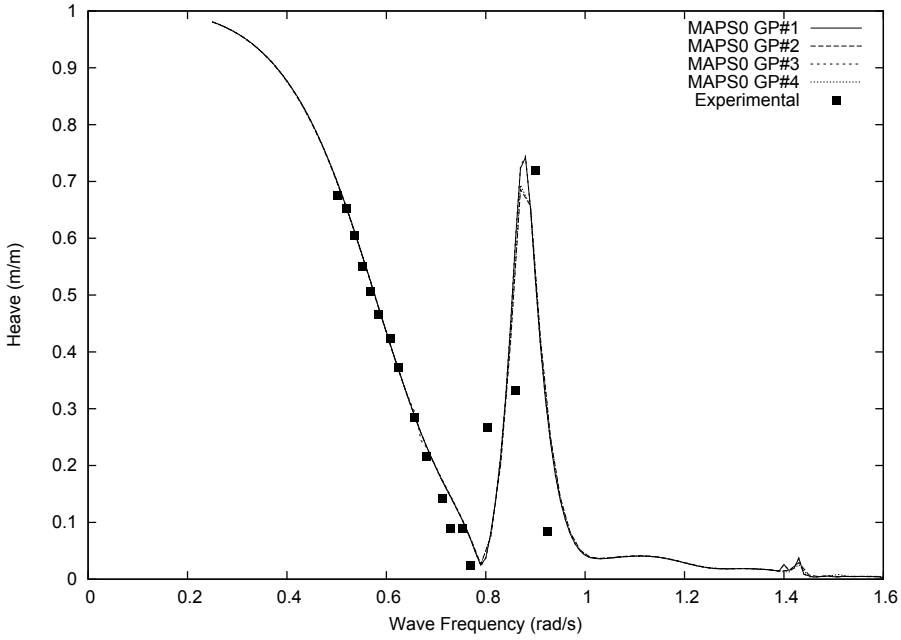

Figure 4.5: Convergence study of heave RAOs for two-body (gap 0.55m) cases

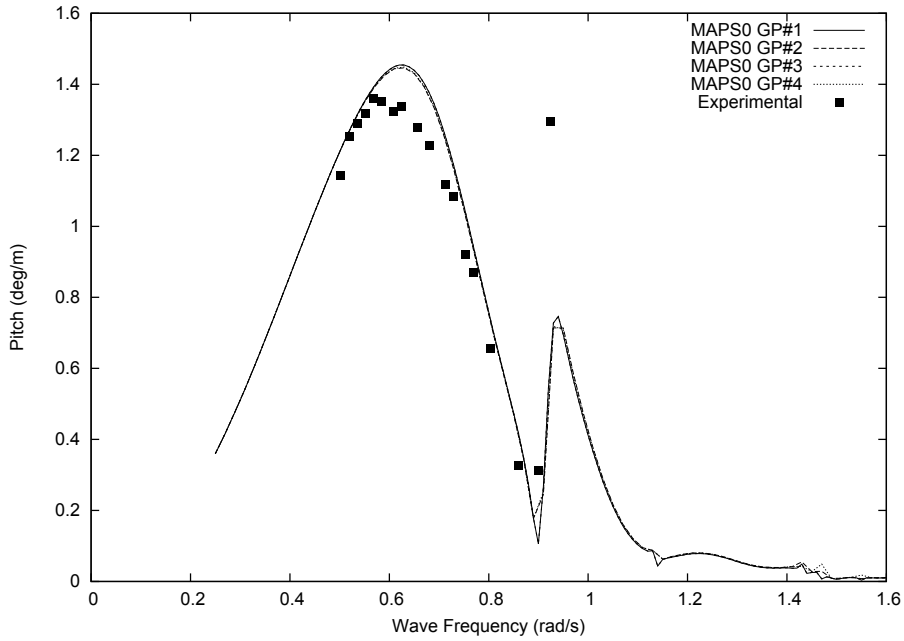

Figure 4.6: Convergence study of pitch RAOs for two-body (gap 0.55m) cases

Chapter 5

Results and Validation Studies

5.1 Tank Wall Effect and Mooring Line Effect

Preliminary numerical simulation was performed with MAPS0 to investigate the effect of tank wall and soft restraint mooring line to ensure they have very small effect on the six degrees of freedom body motion and free surface elevation in head sea condition. In the simulation of tank wall effect with MAPS0, two huge boxes were added in the simulation domain and placed at the tank wall positions. The motions of the boxes were fixed in six degrees of freedom and the main dimensions of the boxes were large enough (over 10 times of body dimensions) to ensure they can work as tank walls in the simulations. In the simulation of mooring line effect with MAPS0, an external restoring matrix was derived and applied on each body. The derivation of the external restoring matrix was based on the set-up of the mooring lines and the stiffness of the springs. Comparison results of the body motion and free surface elevation for two-body cases with/without tank wall/mooring line are presented in Figures 5.1 to Figure 5.14.

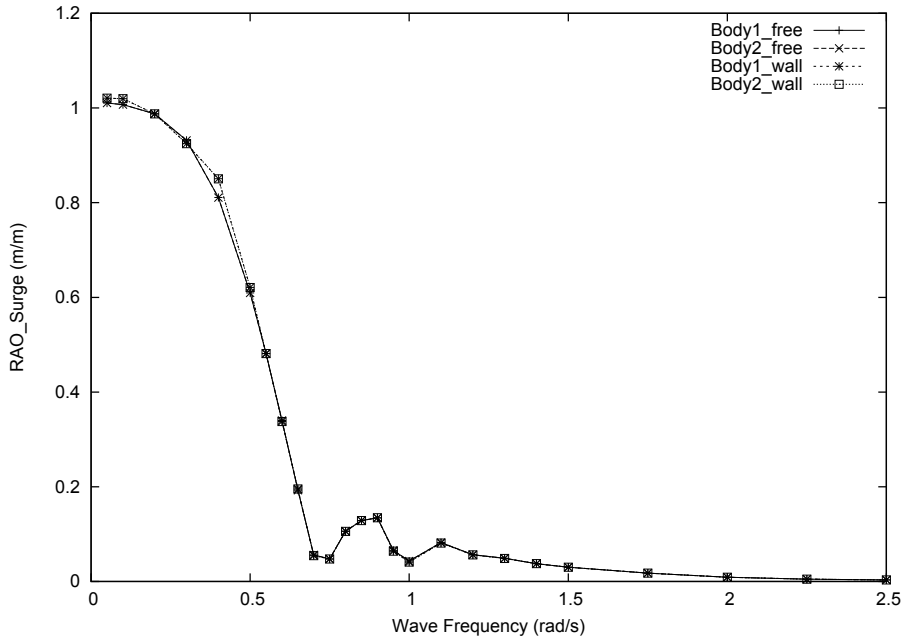

Figure 5.1: Tank wall effect on surge

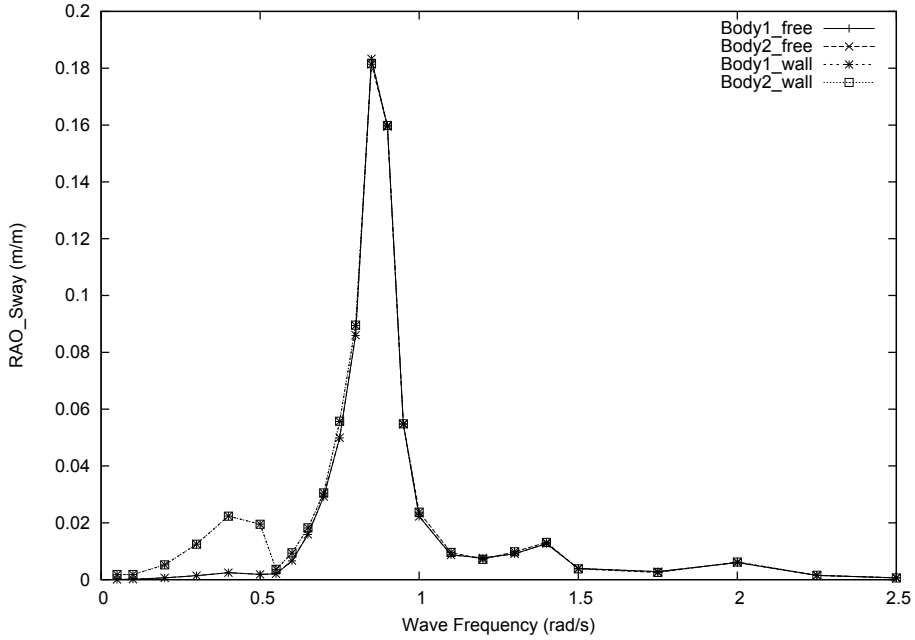

Figure 5.2: Tank wall effect on sway

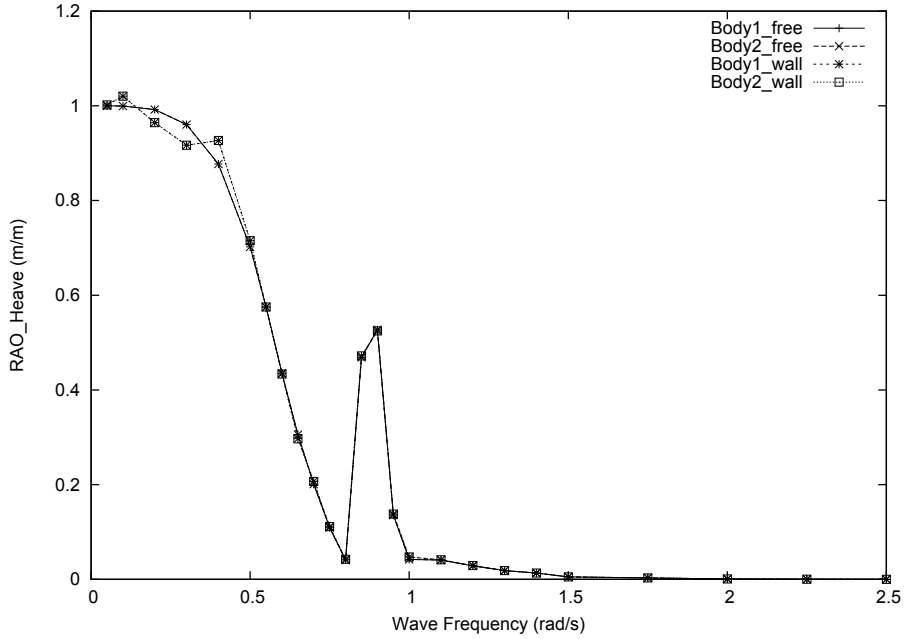

Figure 5.3: Tank wall effect on heave

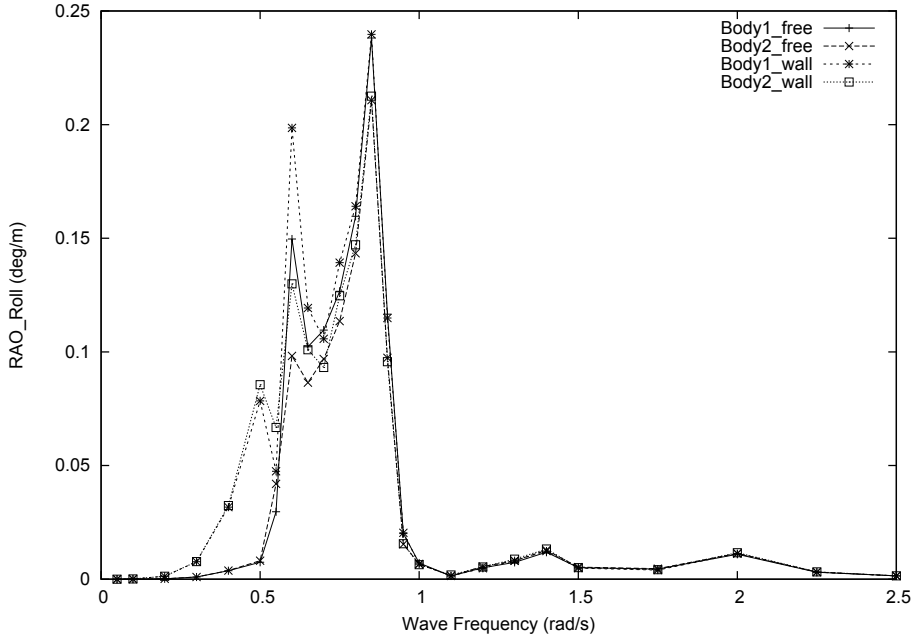

Figure 5.4: Tank wall effect on roll

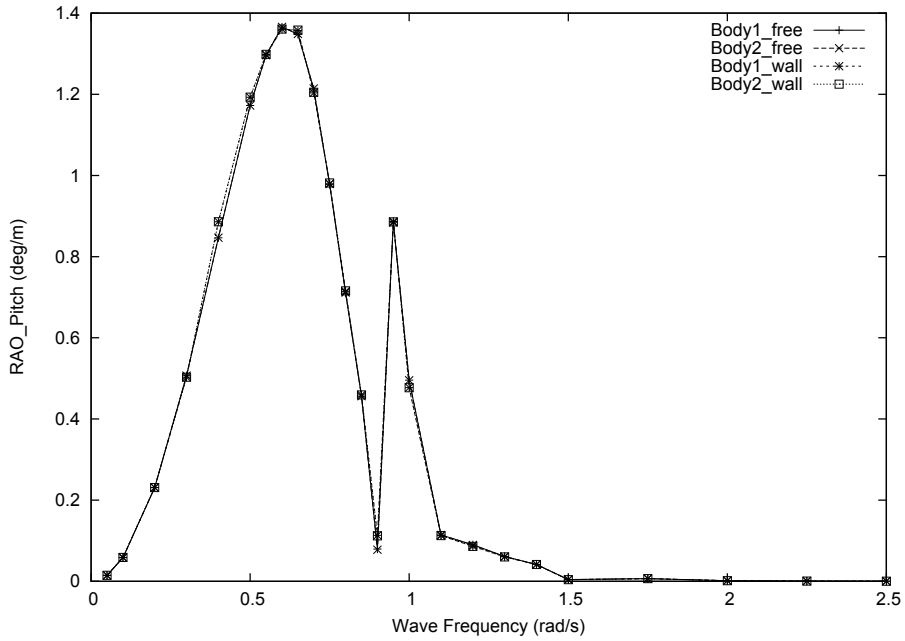

Figure 5.5: Tank wall effect on pitch

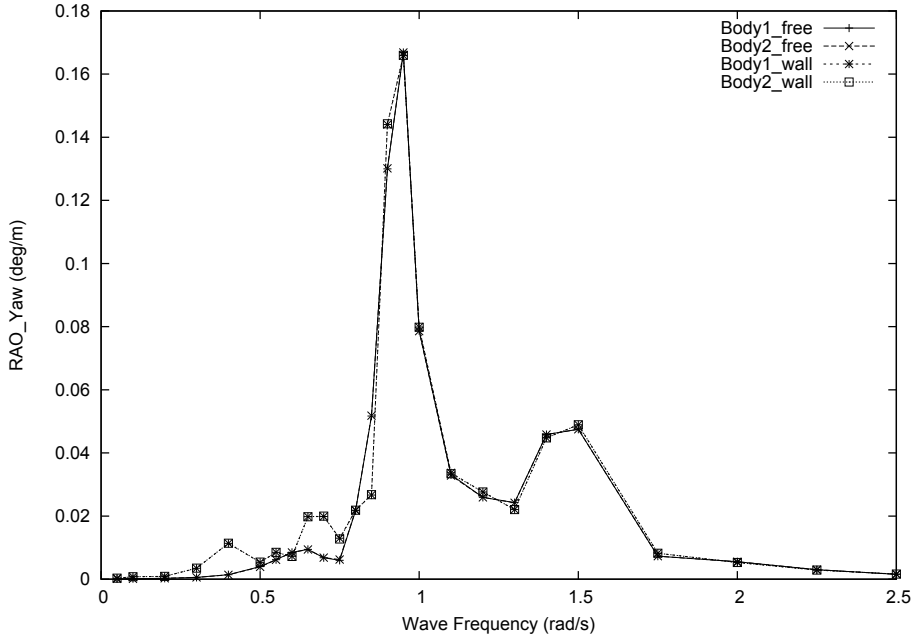

Figure 5.6: Tank wall effect on yaw

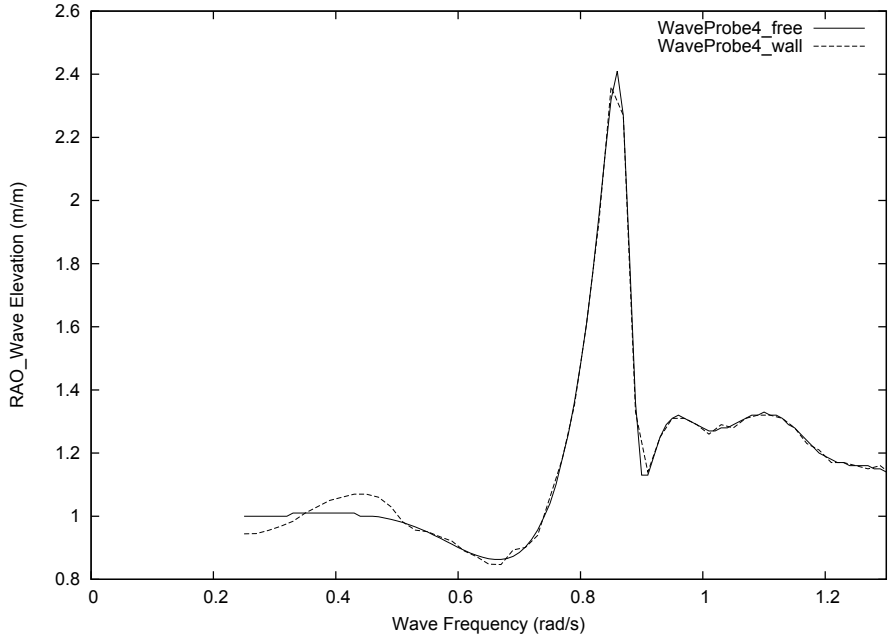

Figure 5.7: Tank wall effect on wave elevation at wave probe 4

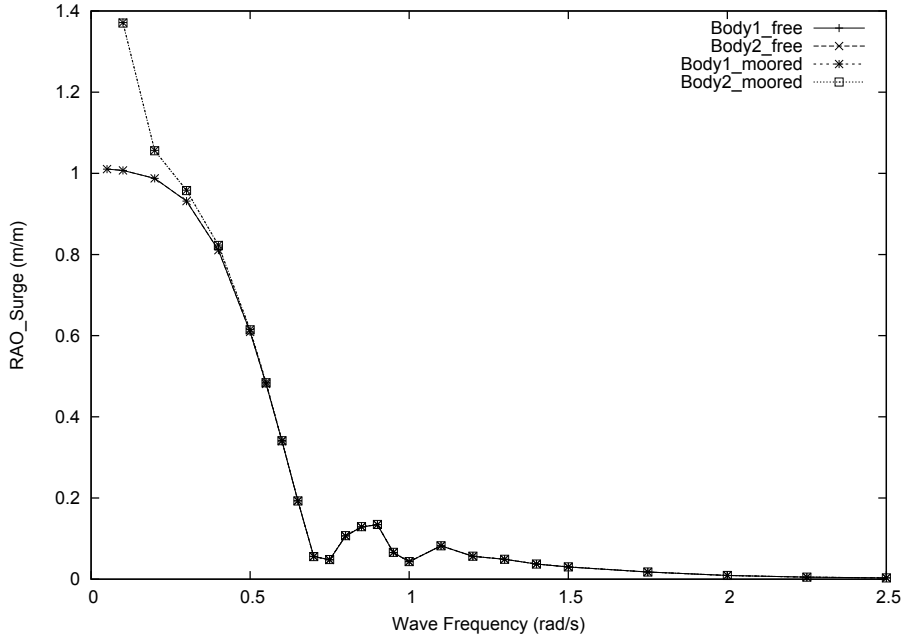

Figure 5.8: Mooring line effect on surge

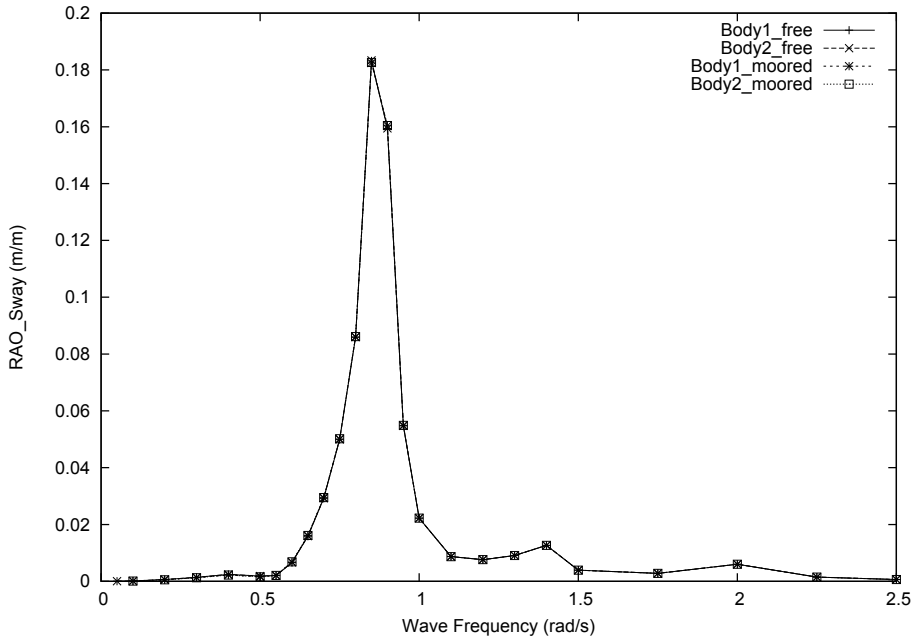

Figure 5.9: Mooring line effect on sway

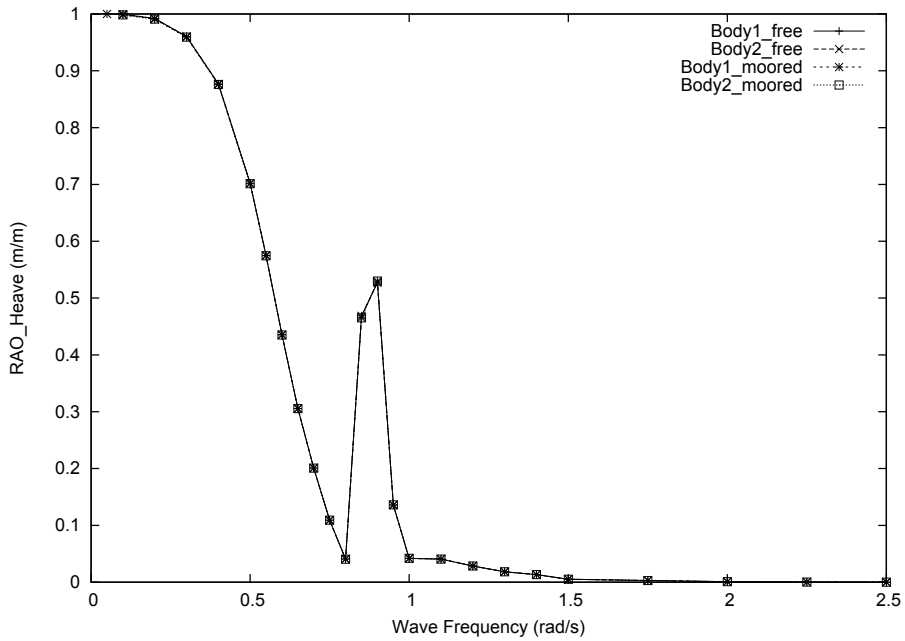

Figure 5.10: Mooring line effect on heave

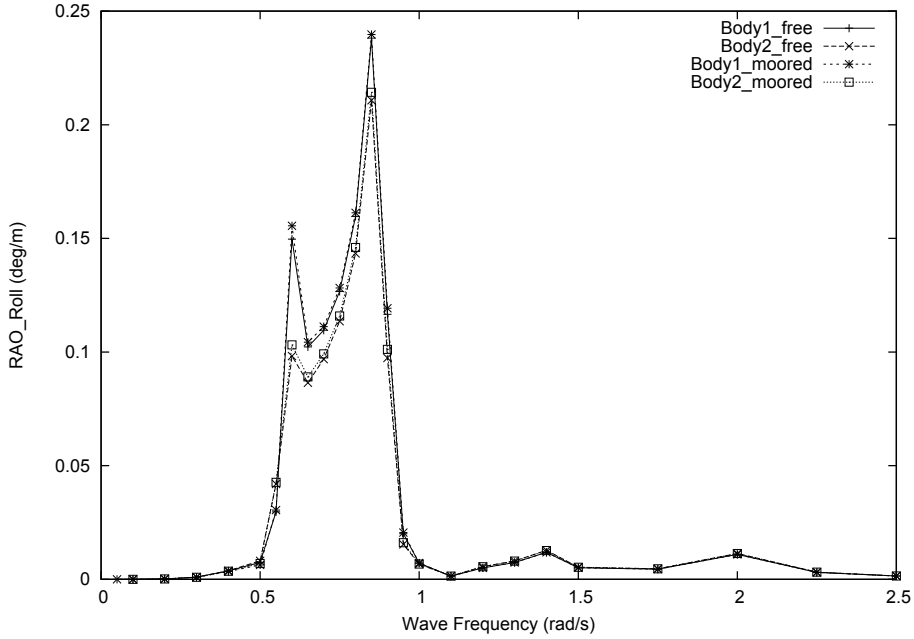

Figure 5.11: Mooring line effect on roll

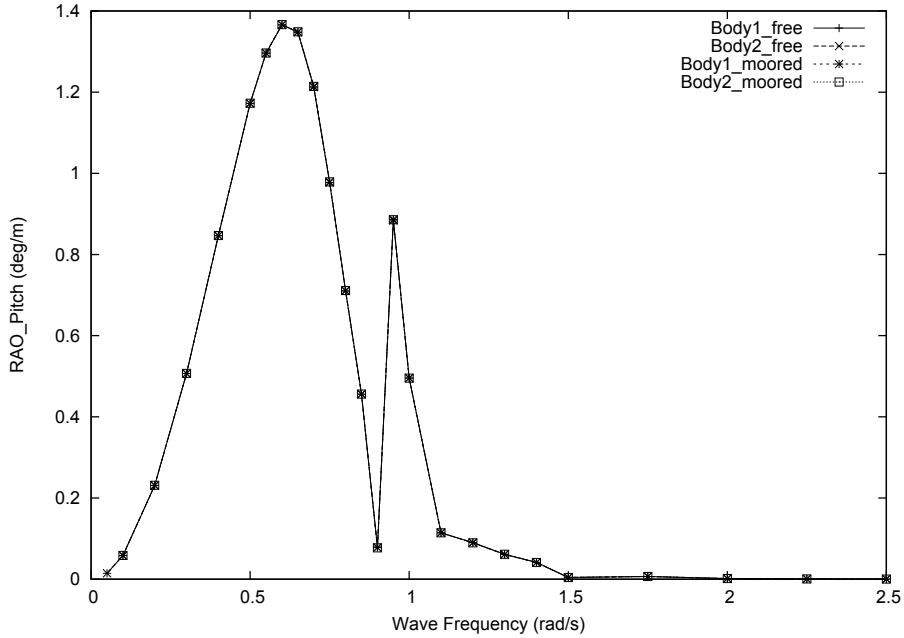

Figure 5.12: Mooring line effect on pitch

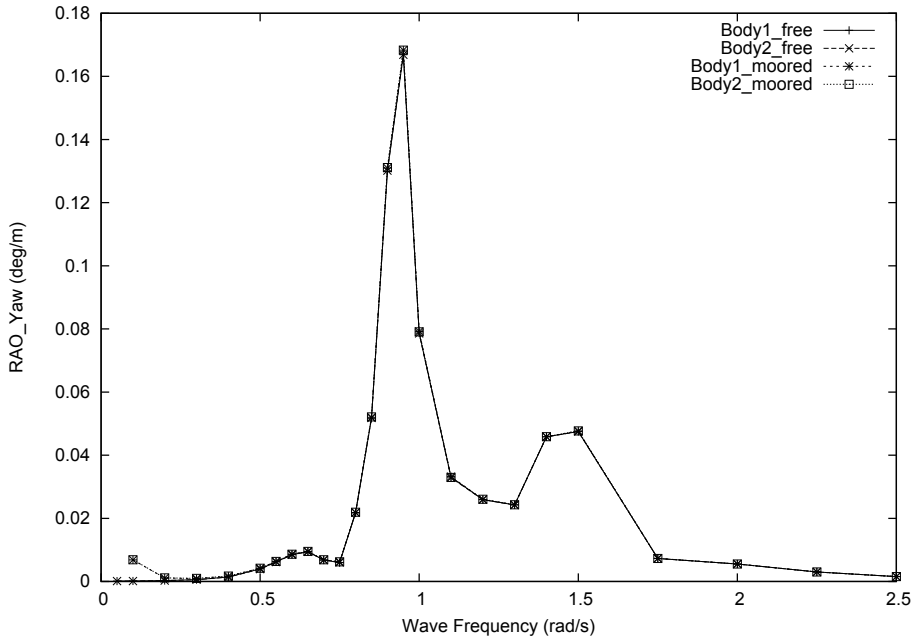

Figure 5.13: Mooring line effect on yaw

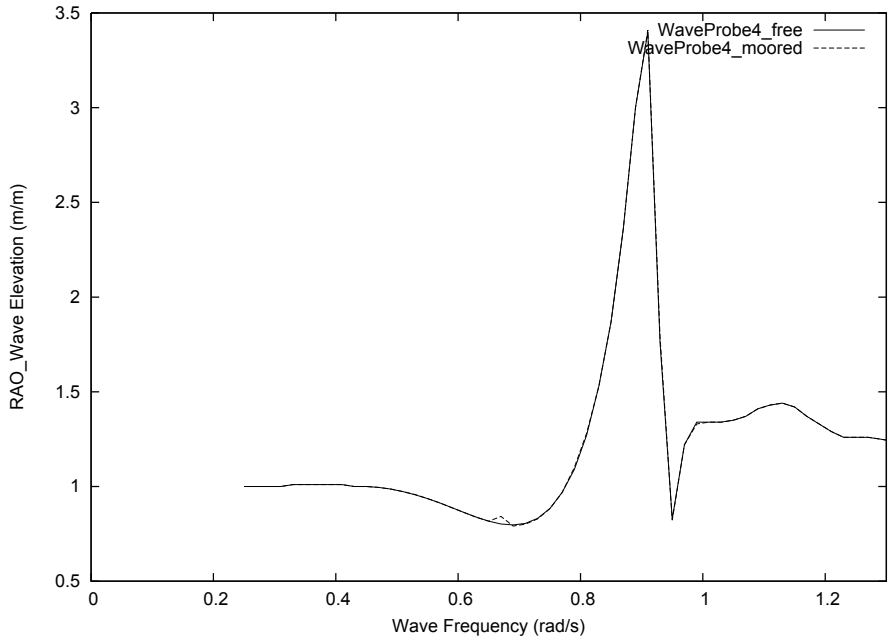

Figure 5.14: Mooring line effect on wave elevation at wave probe 4

From the comparison results, it suggests that the soft mooring line has very small effect on the six degrees of freedom body motion and free surface elevation. Although

the tank wall has very small effect on surge, heave and pitch motions of the bodies, tank wall effect may exist, which would influence measured body roll motion. The tank wall effect should be investigated and removed from the measured roll motions by using numerical methods.

5.2 Single Body Case

5.2.1 Experimental Data

Time series of six degrees of freedom body motions were obtained from single body model tests. A spectra analysis was then applied to the body motion time series throughout Fast Fourier Transform (FFT) and body motion RAOs of single body tests were eventually calculated.

Figures 5.15 and 5.16 present samples of surge and heave time series of single body at the wave frequency of 0.81 Hz and the FFT analysis results. From figure 5.15, it can be seen that a low frequency behaviour existed in the body surge motion. That is because the model was drifting in waves but restrained by soft mooring lines. The low frequency components were eliminated by applying Discrete Fourier Transform and the motion amplitude of desired wave frequency was then obtained. From figure 5.16, it can be found that the body heave motion became stable in the test process. In the FFT analysis results, there was only one spike at 0.81 Hz and the amplitude of heave motion was 8.9 mm.

When FFT analysis for all test cases was completed, six degrees of freedom body motion experimental data were obtained, which are presented in Table 5.1. In the table, f and H stands for incoming wave frequency and wave height. The data is in model scale.

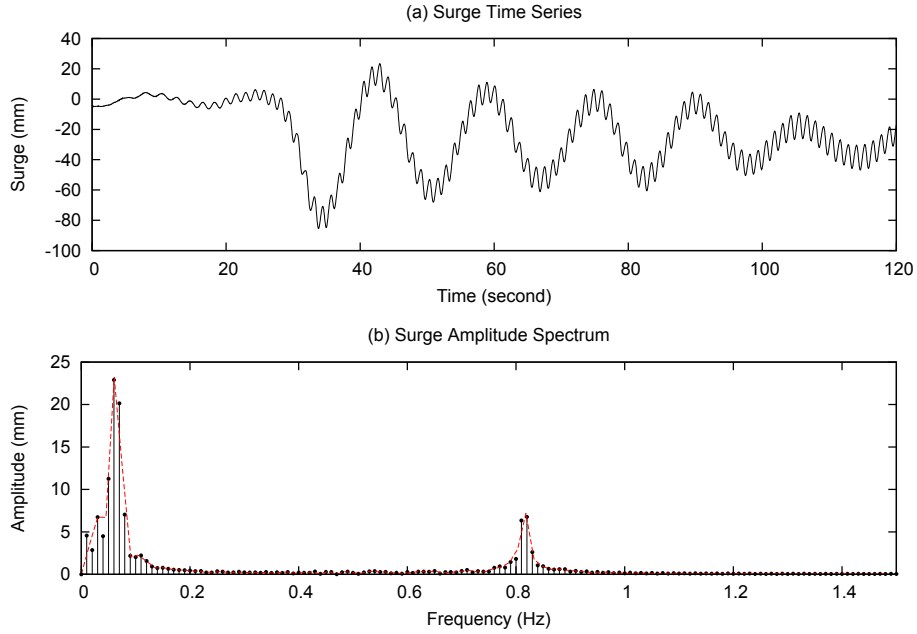

Figure 5.15: Single body surge time series and FFT analysis results (0.81 Hz)

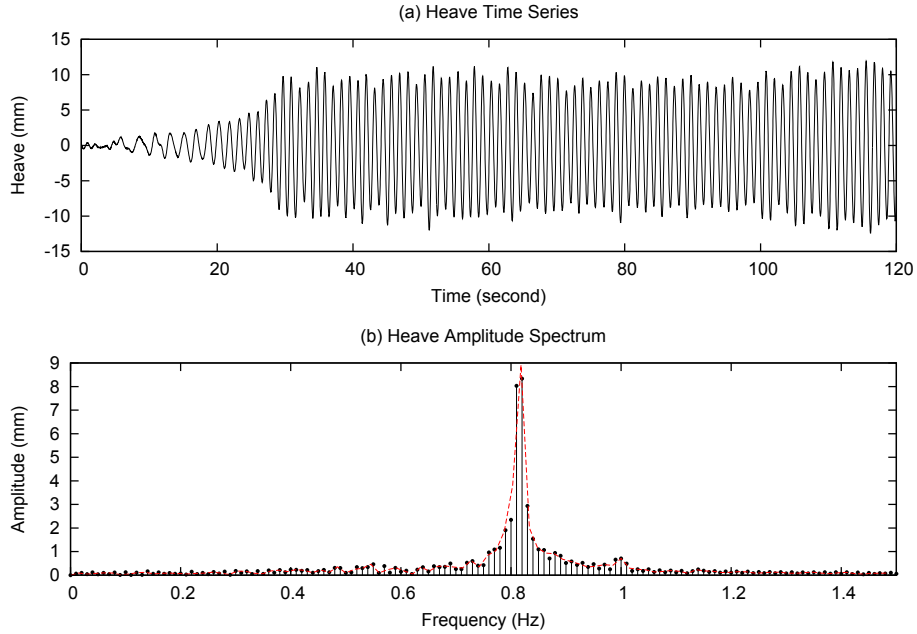

Figure 5.16: Single body heave time series and FFT analysis results (0.81 Hz)

Table 5.1: Body motion data in single body case

f(Hz)	H(mm)	Surge(mm)	Sway(mm)	Heave(mm)	Roll(deg)	Pitch(deg)	Yaw(deg)
1.14	39.06	3.20	0.27	6.13	0.11	1.48	0.06
1.06	43.13	5.53	0.24	9.50	0.06	0.91	0.01
0.99	49.37	4.01	0.31	29.05	0.12	1.88	0.03
0.95	55.90	3.42	0.45	6.03	0.30	2.67	0.09
0.93	57.42	1.81	1.44	6.54	0.72	3.09	0.09
0.90	58.80	0.45	0.48	6.05	0.27	3.70	0.04
0.88	62.55	2.66	0.45	6.54	0.57	4.17	0.06
0.84	68.82	8.80	0.54	11.74	2.00	5.19	0.09
0.81	76.40	13.87	3.05	17.97	5.94	5.92	0.10
0.77	82.34	24.24	1.51	29.08	2.13	6.75	0.16
0.75	87.20	28.95	2.54	35.26	2.02	7.10	0.04
0.72	95.77	38.69	2.09	45.13	1.33	7.74	0.09
0.70	100.28	44.54	1.15	54.87	0.79	7.90	0.05
0.66	116.41	65.25	1.15	70.90	0.59	9.18	0.08
0.62	128.01	76.34	0.70	89.04	0.41	8.85	0.03

5.2.2 Comparison Results

Comparison results of body surge, heave and pitch motions for single body cases are presented in Figures 5.17 to 5.19. In the figures, all data are in full scale. By comparison, it can be seen that the potential-flow prediction results agree well with experimental results for single body case. In Figure 5.18, experimental body heave motion at the wave frequency of 0.99 Hz is much bigger than numerical predictions. This is due to the uncertain factors in the model test process and more repetition tests at this wave frequency are desired.

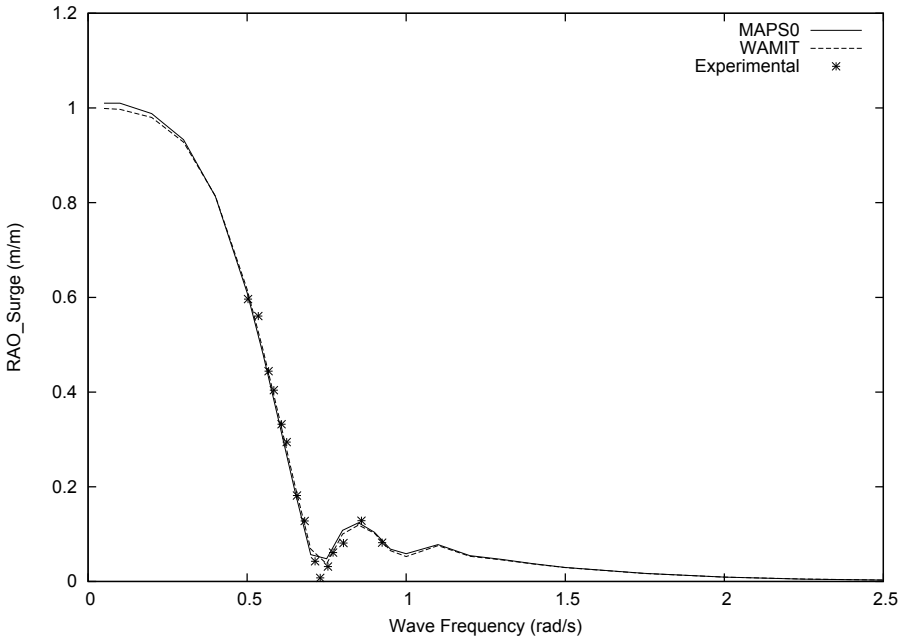

Figure 5.17: Single body surge RAO

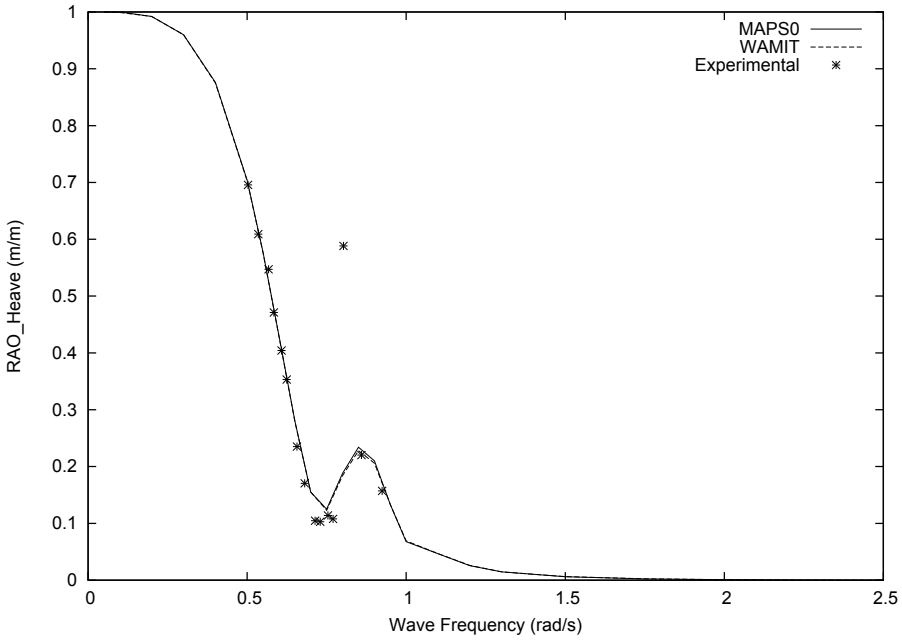

Figure 5.18: Single body heave RAO

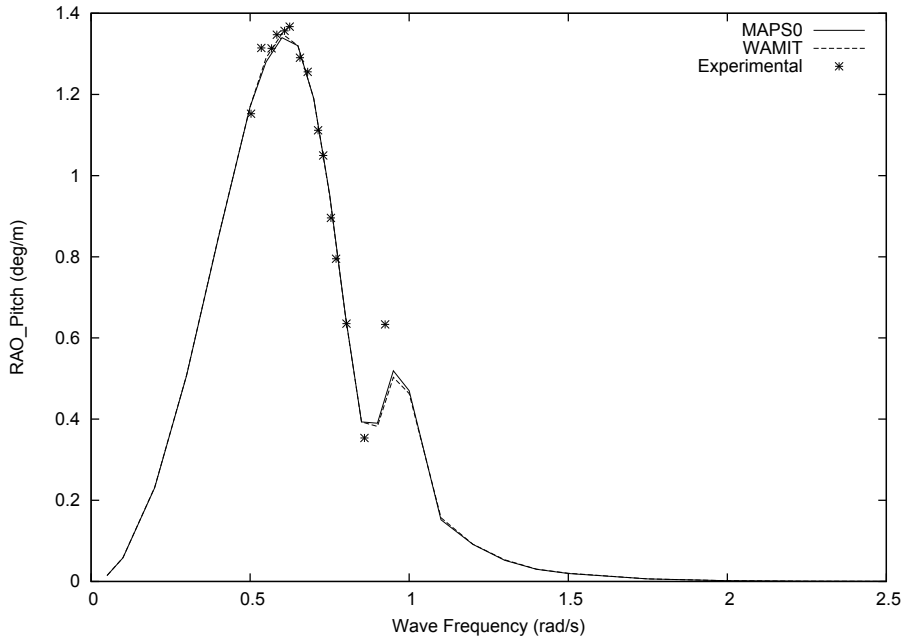

Figure 5.19: Single body pitch RAO

5.3 Two-Body Cases

5.3.1 Experimental Data

Figures 5.20 and 5.29 present samples of time series of six degrees of freedom body motion of two-body cases at the wave frequency of 0.68 Hz (gap width 0.4 m) and the FFT analysis results. From Figures 5.20, 5.21, 5.23 and 5.25, it can be seen that low frequency components existed in the surge, sway, roll and yaw motion of the body. That is because the model was restrained by soft mooring lines. The low frequency components were eliminated by applying Discrete Fourier Transform and the motion amplitude of desired wave frequency was then obtained. From Figures 5.22 and 5.24, it can be found that the heave and pitch motion of the body became stable quickly in the test process. In the FFT analysis results, there was only one spike at 0.68 Hz. From Figures 5.26 to 5.29, it can be seen that the wave elevations became stable

quickly in the test process and the amplitudes can be obtained directly from FFT analysis results.

However, when the wave frequency became bigger, the time series curves of roll motion and yaw motion were very unstable during the test run time of 120 seconds. In those cases, the FFT results of roll motion and yaw motion can not be adopted, which indicated the experimental data of roll and yaw motion of the bodies were not available. Thus, in this thesis, only the body motion data of surge, sway, heave and pitch were presented and compared with numerical simulation results for two-body cases. To obtain the reliable experimental data of roll and yaw motion, a longer test run time would be needed.

The roll motion experimental data, which is with problems, is presented in Appendix D.

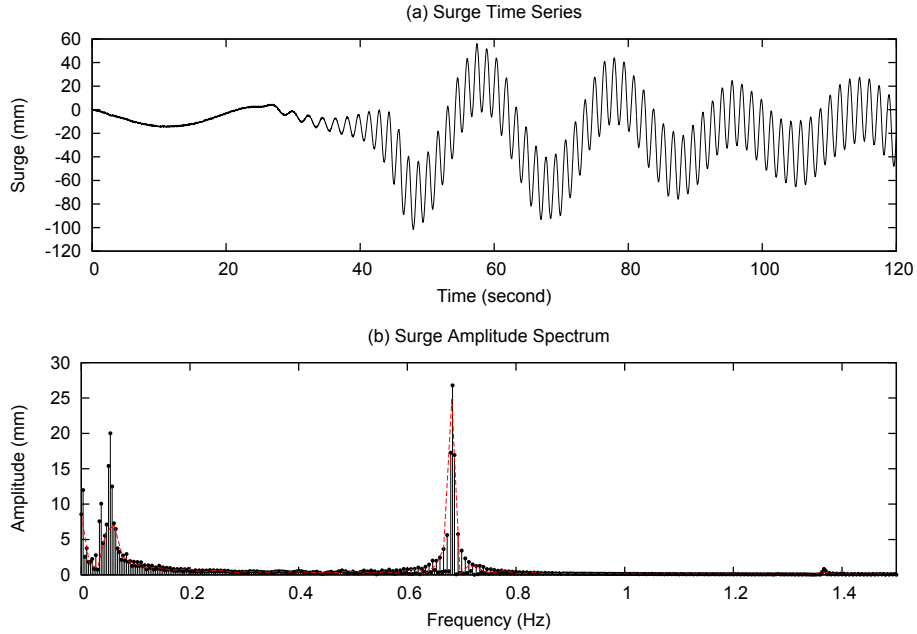

Figure 5.20: Two-body surge time series and FFT analysis results (wave frequency 0.68 Hz, gap width 0.4 m)

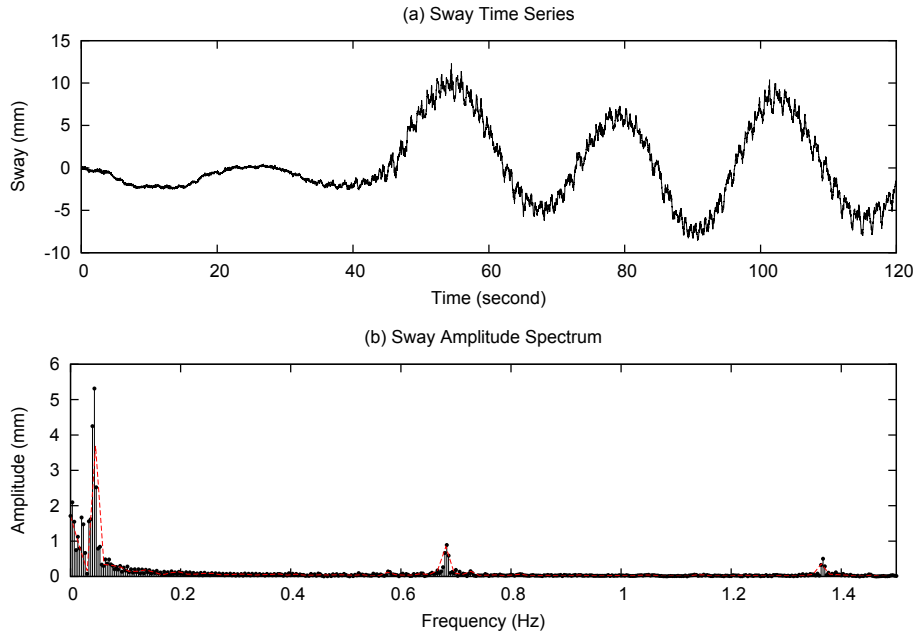

Figure 5.21: Two-body sway time series and FFT analysis results (wave frequency 0.68 Hz, gap width 0.4 m)

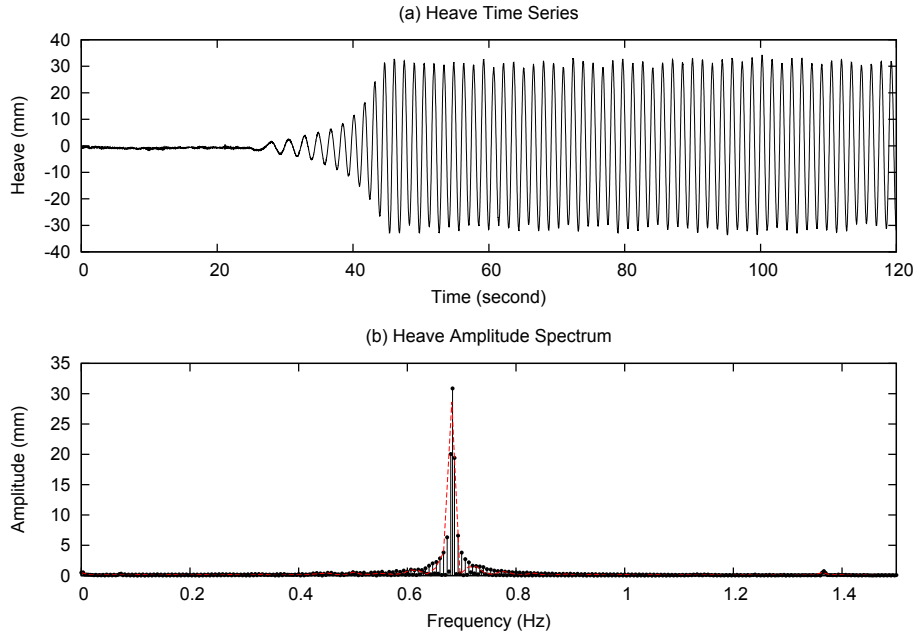

Figure 5.22: Two-body heave time series and FFT analysis results (wave frequency 0.68 Hz, gap width 0.4 m)

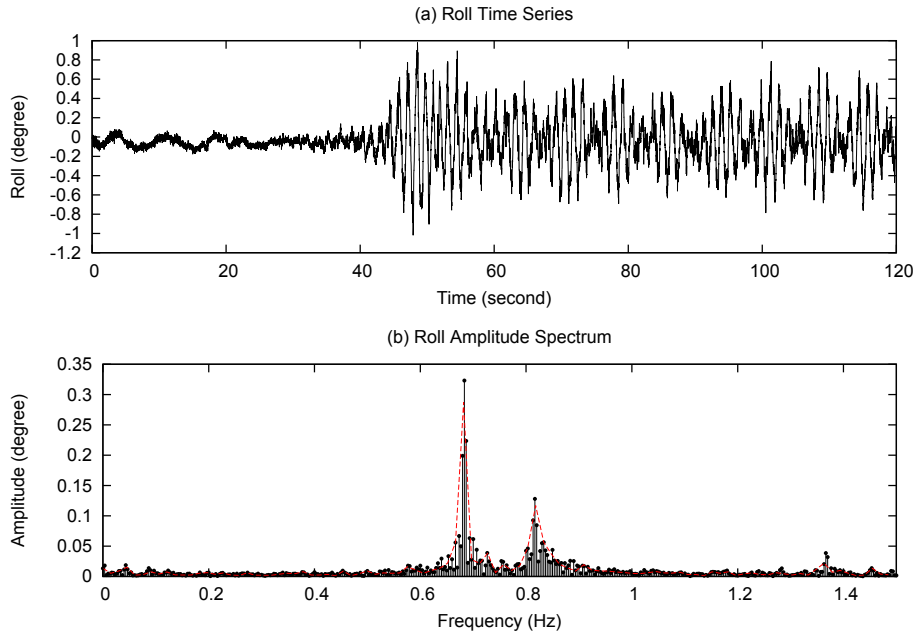

Figure 5.23: Two-body roll time series and FFT analysis results (wave frequency 0.68 Hz, gap width 0.4 m)

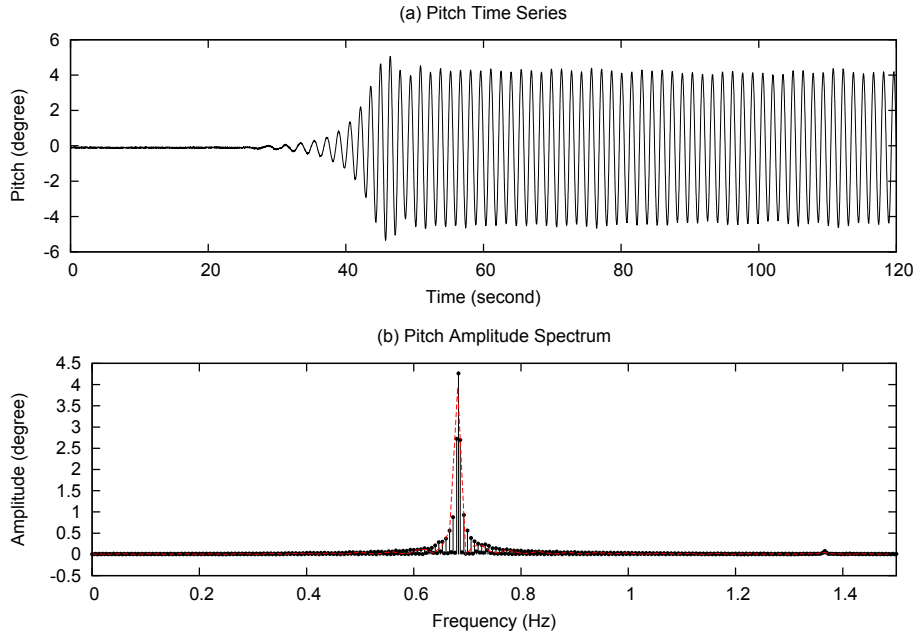

Figure 5.24: Two-body pitch time series and FFT analysis results (wave frequency 0.68 Hz, gap width 0.4 m)

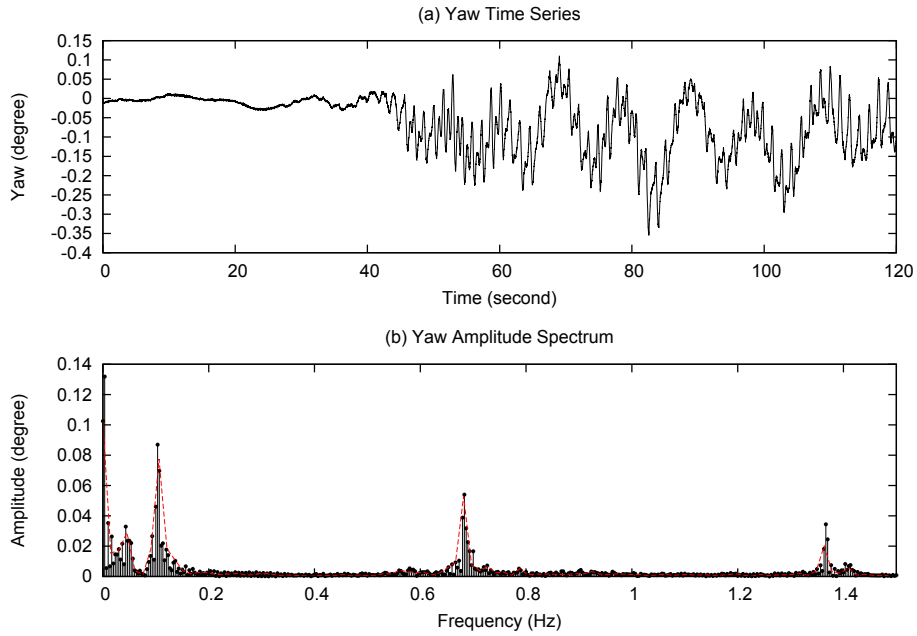

Figure 5.25: Two-body yaw time series and FFT analysis results (wave frequency 0.68 Hz, gap width 0.4 m)

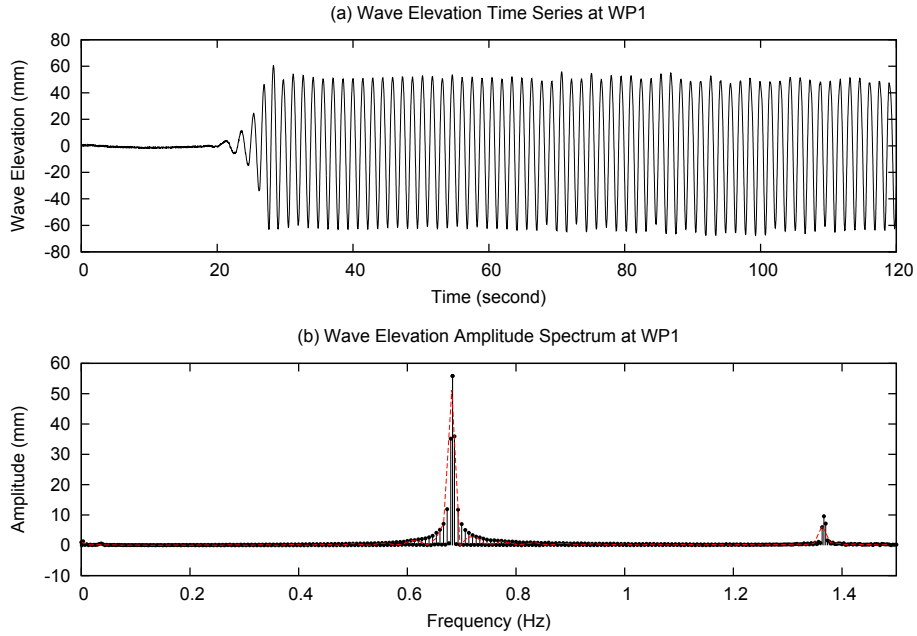

Figure 5.26: Two-body wave elevation time series and FFT analysis results at WP1 (wave frequency 0.68 Hz, gap width 0.4 m)

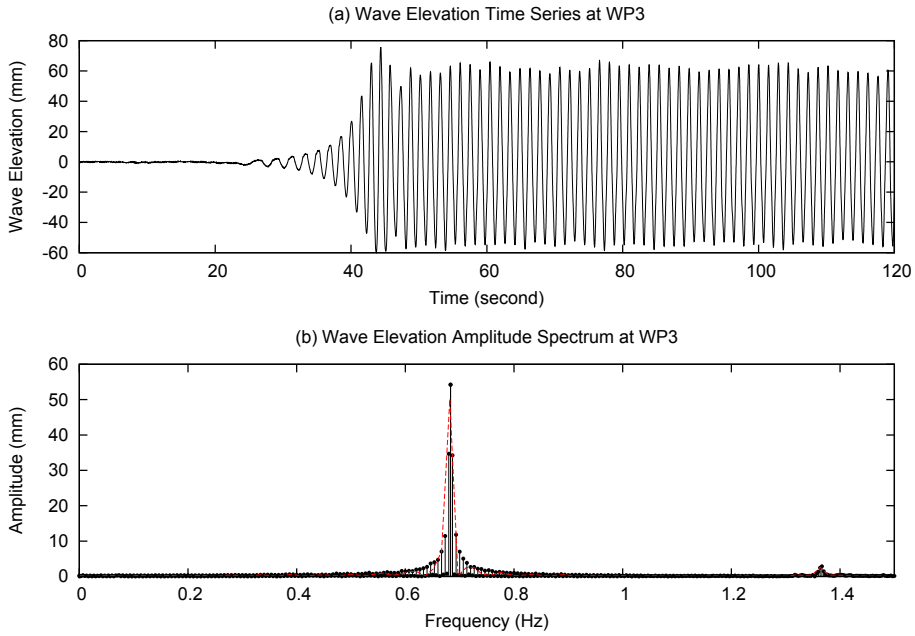

Figure 5.27: Two-body wave elevation time series and FFT analysis results at WP3 (wave frequency 0.68 Hz, gap width 0.4 m)

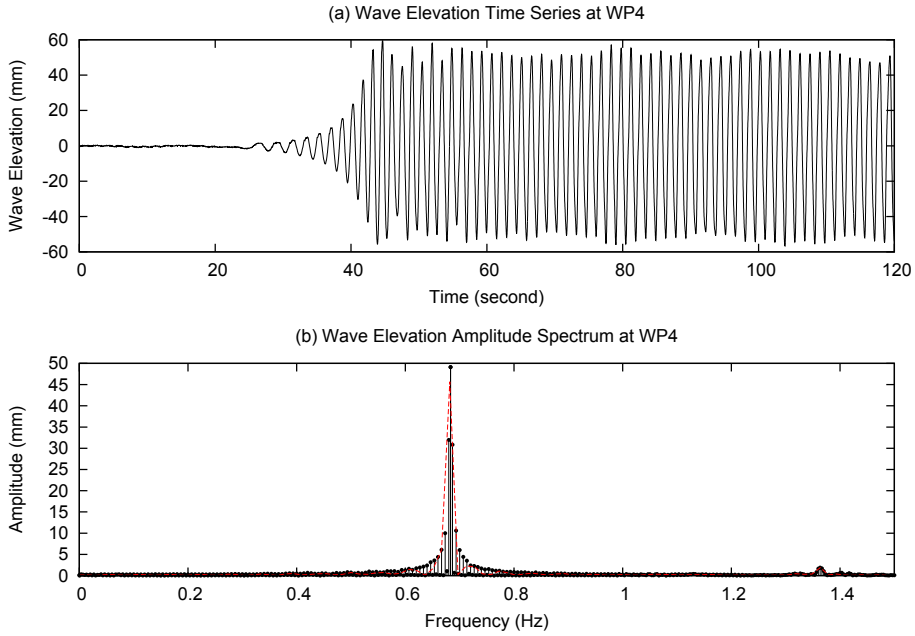

Figure 5.28: Two-body wave elevation time series and FFT analysis results at WP4 (wave frequency 0.68 Hz, gap width 0.4 m)

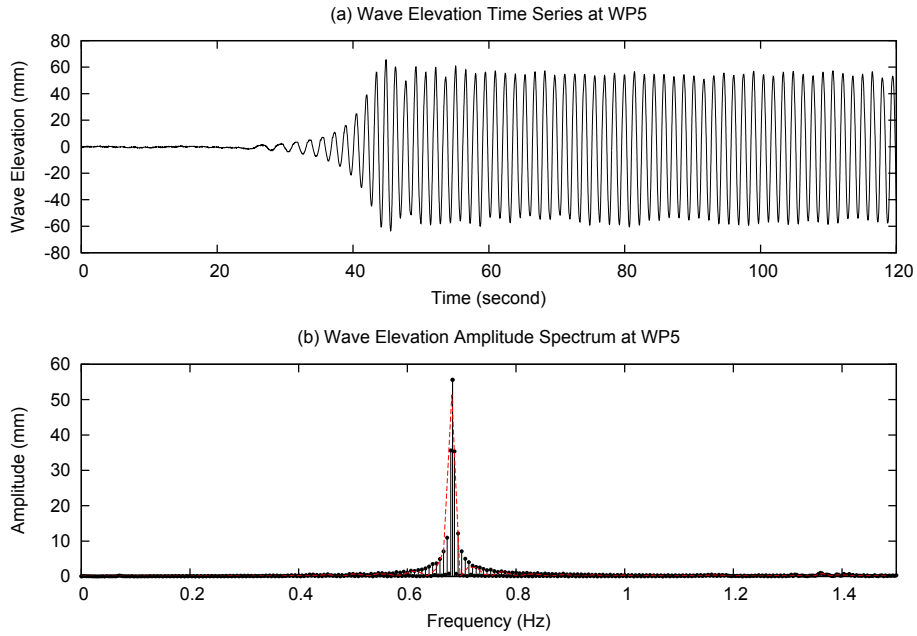

Figure 5.29: Two-body wave elevation time series and FFT analysis results at WP5 (wave frequency 0.68 Hz, gap width 0.4 m)

When FFT analysis for all test cases was completed, body motion and free surface elevation in gap experimental data for two-body case were obtained, which are presented in Tables 5.2 to 5.19. In the table, f and H stands for incoming wave frequency and wave height. The data is in model scale.

Three different gap widths were tested in the test process. All cases were repeated twice. Round 1 and 2 stand for the two repetitions.

Table 5.2: Motion data of model 1 in two-body case, round 1, gap width 0.4 m

f(Hz)	H(mm)	Surge(mm)	Sway(mm)	Heave(mm)	Pitch(deg)
1.14	37.25	4.53	3.83	4.77	2.36
1.11	39.10	4.66	9.20	31.04	0.60
1.06	41.92	4.46	6.88	13.28	0.97
0.99	42.53	4.95	2.47	1.45	1.84
0.95	54.48	2.85	2.63	4.86	2.87
0.93	56.74	1.48	1.83	6.18	3.33
0.90	58.44	1.40	1.93	10.98	3.84
0.88	63.31	3.56	1.96	9.42	4.40
0.84	68.21	8.76	2.51	14.41	5.13
0.81	77.17	14.69	4.33	21.60	5.94
0.77	83.80	24.26	2.30	31.09	6.81
0.75	87.16	30.07	1.85	34.67	7.30
0.72	97.12	40.47	1.73	45.10	8.14
0.70	101.01	46.87	0.57	53.56	8.34
0.68	110.96	57.23	0.48	61.60	9.06
0.66	117.82	64.91	0.57	72.94	9.24
0.64	120.36	72.41	0.83	79.54	9.15
0.62	129.10	78.21	1.02	90.30	9.05

Table 5.3: Motion data of model 2 in two-body case, round 1, gap width 0.4 m

f(Hz)	H(mm)	Surge(mm)	Sway(mm)	Heave(mm)	Pitch(deg)
1.14	37.25	4.52	3.76	5.54	2.37
1.11	39.10	4.72	8.94	31.41	0.62
1.06	41.92	4.35	7.00	13.23	0.99
0.99	42.53	4.82	2.61	1.56	1.98
0.95	54.48	3.37	2.41	4.79	2.72
0.93	56.74	1.87	2.59	8.16	3.20
0.90	58.44	1.30	2.93	6.85	3.84
0.88	63.31	3.42	1.12	9.74	4.35
0.84	68.21	9.01	0.47	13.96	5.24
0.81	77.17	14.84	2.10	22.33	5.93
0.77	83.80	23.93	0.29	31.13	6.75
0.75	87.16	28.81	1.01	36.76	7.05
0.72	97.12	39.71	1.11	45.16	7.95
0.70	101.01	46.17	1.84	52.27	8.17
0.68	110.96	56.36	1.21	61.00	8.87
0.66	117.82	64.23	2.37	71.46	9.12
0.64	120.36	72.12	1.89	78.67	9.09
0.62	129.10	77.83	2.29	88.71	8.95

Table 5.4: Wave elevation data in two-body case, round 1, gap width 0.4 m

f(Hz)	H(mm)	Wave Probe 3(mm)	Wave Probe 4(mm)	Wave Probe 5(mm)
1.14	37.25	48.63	57.29	78.40
1.11	39.10	29.45	62.06	85.92
1.06	41.92	31.34	79.64	46.46
0.99	42.53	32.77	72.31	34.43
0.95	54.48	45.29	70.73	39.47
0.93	56.74	52.92	61.26	39.94
0.90	58.44	63.92	54.74	45.22
0.88	63.31	69.03	54.15	51.82
0.84	68.21	75.36	56.59	63.12
0.81	77.17	83.41	64.42	71.45
0.77	83.80	93.90	73.67	80.99
0.75	87.16	96.35	76.91	87.11
0.72	97.12	103.19	84.14	99.34
0.70	101.01	103.01	89.26	106.81
0.68	110.96	113.95	98.41	113.99
0.66	117.82	124.66	108.31	118.18
0.64	120.36	128.45	114.15	120.84
0.62	129.10	127.04	124.78	132.94

Table 5.5: Motion data of model 1 in two-body case, round 2, gap width 0.4 m

f(Hz)	H(mm)	Surge(mm)	Sway(mm)	Heave(mm)	Pitch(deg)
1.14	37.68	4.72	2.83	5.59	2.24
1.11	39.93	4.54	7.98	30.74	0.57
1.06	41.42	4.64	7.79	12.40	0.98
0.99	48.35	4.41	2.30	1.51	1.97
0.95	54.51	3.64	2.25	3.95	2.70
0.93	56.99	1.57	1.98	6.30	3.32
0.90	57.85	1.18	1.89	10.81	3.83
0.88	67.46	3.82	0.97	10.94	4.60
0.84	72.36	8.93	0.54	14.29	5.44
0.81	78.74	14.53	4.92	22.04	5.93
0.77	85.08	24.54	2.27	30.99	6.83
0.75	88.19	29.67	1.46	34.29	7.18
0.72	98.13	41.43	1.46	45.88	8.24
0.70	101.73	47.35	0.43	53.86	8.46
0.68	111.50	57.45	0.60	62.31	9.13
0.66	118.59	66.52	0.75	72.63	9.36
0.64	120.97	72.68	0.85	79.45	9.17
0.62	129.66	78.12	0.99	90.37	8.99

Table 5.6: Motion data of model 2 in two-body case, round 2, gap width 0.4 m

f(Hz)	H(mm)	Surge(mm)	Sway(mm)	Heave(mm)	Pitch(deg)
1.14	37.68	4.70	2.98	4.88	2.25
1.11	39.93	4.66	8.00	30.81	0.56
1.06	41.42	4.67	7.62	12.51	0.97
0.99	48.35	4.56	2.31	0.98	1.82
0.95	54.51	2.96	2.40	3.88	2.86
0.93	56.99	1.85	2.74	8.18	3.18
0.90	57.85	1.06	2.77	6.77	3.82
0.88	67.46	3.68	2.10	10.35	4.54
0.84	72.36	8.74	3.17	14.69	5.31
0.81	78.74	14.64	2.16	22.41	5.88
0.77	85.08	24.22	0.58	30.68	6.76
0.75	88.19	28.36	1.06	36.20	6.92
0.72	98.13	40.62	1.34	45.99	8.03
0.70	101.73	46.71	1.94	52.44	8.29
0.68	111.50	56.51	0.90	61.67	8.94
0.66	118.59	65.78	2.15	71.13	9.22
0.64	120.97	72.40	1.31	78.38	9.10
0.62	129.66	77.69	2.35	88.73	8.89

Table 5.7: Wave elevation data in two-body case, round 2, gap width 0.4 m

f(Hz)	H(mm)	Wave Probe 3(mm)	Wave Probe 4(mm)	Wave Probe 5(mm)
1.14	37.68	50.47	55.75	79.34
1.11	39.93	30.55	57.91	85.07
1.06	41.42	34.24	68.65	50.97
0.99	48.35	32.06	72.51	33.88
0.95	54.51	45.26	70.91	40.04
0.93	56.99	53.56	60.15	40.73
0.90	57.85	63.47	53.95	45.17
0.88	67.46	70.38	57.24	52.75
0.84	72.36	77.60	58.98	64.38
0.81	78.74	83.78	66.49	70.33
0.77	85.08	94.46	73.66	81.16
0.75	88.19	93.20	76.42	85.74
0.72	98.13	104.62	85.35	100.76
0.70	101.73	103.56	91.03	108.76
0.68	111.50	114.13	99.28	115.83
0.66	118.59	125.46	110.23	119.82
0.64	120.97	128.44	113.57	120.22
0.62	129.66	127.06	123.95	131.77

Table 5.8: Motion data of model 1 in two-body case, round 1, gap width 0.45 m

f(Hz)	H(mm)	Surge(mm)	Sway(mm)	Heave(mm)	Pitch(deg)
1.14	38.30	4.66	3.94	4.31	2.68
1.11	40.00	4.53	12.39	31.56	0.63
1.06	42.10	5.11	7.69	11.56	0.90
0.99	48.70	4.14	2.79	1.66	1.99
0.95	54.70	5.13	2.41	4.11	2.66
0.93	57.00	2.89	2.45	5.04	3.22
0.90	58.90	2.66	2.49	9.94	3.82
0.88	64.60	3.13	1.62	9.62	4.29
0.84	70.50	8.72	0.40	14.02	5.14
0.81	76.60	13.87	3.51	20.94	5.83
0.77	84.30	23.77	3.22	30.70	6.78
0.75	87.00	29.41	2.11	33.69	7.24
0.72	97.70	40.38	2.14	45.13	8.03
0.70	101.60	46.90	1.79	52.72	8.37
0.68	111.50	56.83	0.94	60.82	8.98
0.66	118.70	64.65	1.40	72.16	9.12
0.64	122.10	70.83	1.99	78.94	9.02
0.62	130.10	78.45	1.29	88.26	8.97

Table 5.9: Motion data of model 2 in two-body case, round 1, gap width 0.45 m

f(Hz)	H(mm)	Surge(mm)	Sway(mm)	Heave(mm)	Pitch(deg)
1.14	38.30	4.51	4.01	3.59	2.64
1.11	40.00	4.49	10.39	33.21	0.63
1.06	42.10	5.09	7.92	11.72	0.93
0.99	48.70	4.42	2.85	2.80	1.84
0.95	54.70	4.53	2.66	4.01	2.86
0.93	57.00	2.60	2.81	6.56	3.21
0.90	58.90	1.90	3.25	7.17	3.85
0.88	64.60	2.98	2.29	9.40	4.37
0.84	70.50	8.81	2.54	14.27	5.06
0.81	76.60	13.90	2.88	21.71	5.80
0.77	84.30	23.76	0.44	31.14	6.71
0.75	87.00	28.13	1.31	36.65	6.99
0.72	97.70	39.74	0.95	44.39	7.82
0.70	101.60	46.20	1.39	50.44	8.14
0.68	111.50	56.01	0.68	59.97	8.75
0.66	118.70	64.10	1.96	70.82	8.99
0.64	122.10	70.76	1.61	77.89	8.94
0.62	130.10	77.12	1.75	85.64	8.74

Table 5.10: Wave elevation data in two-body case, round 1, gap width 0.45 m

f(Hz)	H(mm)	Wave Probe 3(mm)	Wave Probe 4(mm)	Wave Probe 5(mm)
1.14	38.30	42.62	57.26	75.66
1.11	40.00	45.80	43.79	91.76
1.06	42.10	39.71	73.74	55.37
0.99	48.70	32.12	76.99	35.41
0.95	54.70	44.66	71.03	39.67
0.93	57.00	53.08	66.22	42.72
0.90	58.90	63.87	57.05	45.94
0.88	64.60	67.43	55.38	51.23
0.84	70.50	74.10	57.65	62.26
0.81	76.60	82.24	66.03	71.20
0.77	84.30	94.02	74.14	80.89
0.75	87.00	95.02	77.46	87.56
0.72	97.70	102.30	84.93	98.10
0.70	101.60	102.78	89.21	106.83
0.68	111.50	113.19	97.89	113.96
0.66	118.70	124.13	109.35	117.96
0.64	122.10	127.97	115.58	120.36
0.62	130.10	126.34	123.09	130.36

Table 5.11: Motion data of model 1 in two-body case, round 2, gap width 0.45 m

f(Hz)	H(mm)	Surge(mm)	Sway(mm)	Heave(mm)	Pitch(deg)
1.14	38.40	4.93	2.45	3.78	2.64
1.11	40.10	4.39	11.18	33.90	0.70
1.06	42.40	5.17	7.30	10.83	0.97
0.99	48.20	4.77	3.06	1.31	1.97
0.95	54.30	3.27	2.31	4.37	2.68
0.93	57.70	1.85	2.60	5.42	3.27
0.90	59.10	0.73	2.05	10.09	3.80
0.88	64.80	2.62	1.55	9.81	4.29
0.84	69.50	8.78	0.46	14.54	5.25
0.81	76.40	14.08	3.87	21.45	5.88
0.77	84.00	23.81	2.95	30.77	6.77
0.75	87.30	29.27	2.03	33.73	7.21
0.72	97.80	40.04	1.94	44.36	8.02
0.70	100.40	47.13	0.97	52.48	8.35
0.68	110.00	56.56	0.80	60.18	8.90
0.66	117.60	64.51	1.48	71.55	9.15
0.64	122.00	71.04	1.88	78.40	9.01
0.62	130.20	77.66	0.85	89.01	8.95

Table 5.12: Motion data of model 2 in two-body case, round 2, gap width 0.45 m

f(Hz)	H(mm)	Surge(mm)	Sway(mm)	Heave(mm)	Pitch(deg)
1.14	38.40	4.74	2.90	3.42	2.59
1.11	40.10	4.19	9.35	33.37	0.70
1.06	42.40	5.15	7.52	10.88	0.98
0.99	48.20	5.01	2.95	2.47	1.82
0.95	54.30	2.74	2.60	4.09	2.85
0.93	57.70	1.90	2.89	6.75	3.22
0.90	59.10	0.72	2.65	7.00	3.83
0.88	64.80	2.87	2.15	9.56	4.37
0.84	69.50	8.62	2.27	14.56	5.13
0.81	76.40	13.97	3.23	22.12	5.82
0.77	84.00	23.72	0.49	31.12	6.69
0.75	87.30	28.11	1.04	36.29	6.94
0.72	97.80	39.31	1.36	44.77	7.79
0.70	100.40	46.39	1.62	50.90	8.14
0.68	110.00	55.79	0.61	59.44	8.69
0.66	117.60	64.11	1.80	70.28	9.03
0.64	122.00	70.99	1.13	77.19	8.92
0.62	130.20	77.10	1.89	87.29	8.81

Table 5.13: Wave elevation data in two-body case, round 2, gap width 0.45 m

f(Hz)	H(mm)	Wave Probe 3(mm)	Wave Probe 4(mm)	Wave Probe 5(mm)
1.14	38.40	42.97	56.36	74.95
1.11	40.10	44.48	42.32	92.26
1.06	42.40	37.13	75.62	50.77
0.99	48.20	32.09	76.64	35.46
0.95	54.30	44.88	71.46	39.67
0.93	57.70	52.45	66.81	43.12
0.90	59.10	63.11	56.52	45.86
0.88	64.80	67.88	56.19	51.80
0.84	69.50	74.96	58.21	63.41
0.81	76.40	82.12	66.04	71.64
0.77	84.00	93.25	73.48	81.34
0.75	87.30	95.55	76.92	88.03
0.72	97.80	102.80	84.68	98.10
0.70	100.40	101.98	89.83	107.20
0.68	110.00	111.91	97.29	112.37
0.66	117.60	123.03	108.95	119.12
0.64	122.00	127.90	115.20	120.59
0.62	130.20	126.10	123.71	131.72

Table 5.14: Motion data of model 1 in two-body case, round 1, gap width 0.55 m

f(Hz)	H(mm)	Surge(mm)	Sway(mm)	Heave(mm)	Pitch(deg)
1.14	37.50	3.82	2.28	3.15	2.92
1.11	40.10	4.93	3.56	28.84	0.75
1.06	42.40	5.45	6.65	14.11	0.83
0.99	49.20	4.74	5.78	13.16	1.94
0.95	55.20	3.47	2.93	1.28	2.88
0.93	57.40	1.84	2.89	5.14	3.17
0.90	58.30	0.49	2.33	5.19	3.79
0.88	63.50	2.87	1.69	9.05	4.26
0.84	68.60	8.59	1.55	14.86	5.05
0.81	75.60	14.01	3.18	21.53	5.79
0.77	83.50	23.80	0.30	31.06	6.70
0.75	87.30	28.57	0.83	36.95	6.93
0.72	96.90	39.31	0.99	45.16	7.85
0.70	101.10	46.66	1.67	51.18	8.26
0.68	111.00	55.16	1.58	61.01	8.77
0.66	117.60	64.73	2.45	71.09	9.09
0.64	119.90	71.65	0.89	78.22	9.01
0.62	129.00	77.35	1.80	87.11	8.84

Table 5.15: Motion data of model 2 in two-body case, round 1, gap width 0.55 m

f(Hz)	H(mm)	Surge(mm)	Sway(mm)	Heave(mm)	Pitch(deg)
1.14	37.50	3.95	2.21	3.81	2.94
1.11	40.10	5.20	3.45	28.65	0.60
1.06	42.40	5.44	6.74	14.15	0.88
0.99	49.20	4.71	6.09	11.46	1.99
0.95	55.20	4.20	2.72	1.60	2.67
0.93	57.40	1.80	2.45	3.68	3.19
0.90	58.30	0.60	2.22	9.59	3.76
0.88	63.50	2.55	1.10	9.01	4.19
0.84	68.60	8.65	0.60	14.45	5.16
0.81	75.60	14.01	2.97	20.87	5.82
0.77	83.50	23.93	2.42	30.66	6.78
0.75	87.30	29.75	2.00	33.66	7.19
0.72	96.90	40.01	1.50	45.15	8.08
0.70	101.10	47.32	1.31	52.66	8.46
0.68	111.00	56.30	0.51	61.87	9.00
0.66	117.60	65.32	0.65	72.66	9.21
0.64	119.90	71.90	0.97	79.45	9.09
0.62	129.00	77.90	1.19	88.87	8.95

Table 5.16: Wave elevation data in two-body case, round 1, gap width 0.55 m

f(Hz)	H(mm)	Wave Probe 3(mm)	Wave Probe 4(mm)	Wave Probe 5(mm)
1.14	37.50	36.68	53.90	64.98
1.11	40.10	65.90	37.97	80.33
1.06	42.40	40.11	66.17	58.91
0.99	49.20	36.28	96.42	39.92
0.95	55.20	44.96	77.39	42.80
0.93	57.40	52.99	72.65	45.07
0.90	58.30	62.78	63.67	48.25
0.88	63.50	66.74	59.69	52.18
0.84	68.60	74.70	61.92	63.13
0.81	75.60	81.35	67.27	71.22
0.77	83.50	93.44	76.77	82.09
0.75	87.30	94.30	78.20	86.19
0.72	96.90	102.89	86.27	98.53
0.70	101.10	102.60	89.44	106.79
0.68	111.00	113.76	99.88	113.88
0.66	117.60	122.34	110.04	119.24
0.64	119.90	127.18	115.13	119.24
0.62	129.00	124.47	122.77	130.89

Table 5.17: Motion data of model 1 in two-body case, round 2, gap width 0.55 m

f(Hz)	H(mm)	Surge(mm)	Sway(mm)	Heave(mm)	Pitch(deg)
1.14	37.50	4.23	1.75	3.69	2.96
1.11	39.70	5.21	3.50	30.57	0.61
1.06	41.80	5.14	5.74	13.77	0.87
0.99	48.80	4.25	7.37	15.40	1.97
0.95	54.10	3.89	2.69	1.72	2.71
0.93	56.60	2.14	2.56	3.84	3.20
0.90	58.30	0.73	2.18	9.53	3.80
0.88	63.80	2.63	1.38	9.27	4.29
0.84	69.70	8.70	0.42	15.02	5.23
0.81	76.30	14.53	3.73	21.07	5.89
0.77	84.30	23.82	2.72	31.22	6.84
0.75	87.20	29.92	1.64	34.30	7.27
0.70	100.70	46.55	0.83	53.16	8.33
0.68	110.20	56.18	0.44	61.62	8.96
0.66	118.00	65.17	0.96	72.37	9.28
0.64	119.00	71.59	0.77	79.77	9.03
0.62	129.00	78.46	1.61	87.87	8.94

Table 5.18: Motion data of model 2 in two-body case, round 2, gap width 0.55 m

f(Hz)	H(mm)	Surge(mm)	Sway(mm)	Heave(mm)	Pitch(deg)
1.14	37.50	4.11	1.81	3.39	2.94
1.11	39.70	5.17	4.37	30.34	0.73
1.06	41.80	5.29	5.48	13.58	0.83
0.99	48.80	4.21	7.15	17.17	1.94
0.95	54.10	3.15	2.92	1.45	2.86
0.93	56.60	1.97	3.00	5.49	3.20
0.90	58.30	0.69	2.40	5.55	3.80
0.88	63.80	2.72	1.84	9.28	4.36
0.84	69.70	8.46	1.75	15.53	5.10
0.81	76.30	14.79	3.09	21.75	5.85
0.77	84.30	23.61	0.66	31.01	6.75
0.75	87.20	28.51	0.86	36.68	6.98
0.70	100.70	45.72	1.76	51.32	8.13
0.68	110.20	55.12	0.95	60.96	8.76
0.66	118.00	64.58	2.43	70.90	9.16
0.64	119.00	71.45	1.37	78.65	8.97
0.62	129.00	78.86	1.03	89.52	9.03

Table 5.19: Wave elevation data in two-body case, round 2, gap width 0.55 m

f(Hz)	H(mm)	Wave Probe 3(mm)	Wave Probe 4(mm)	Wave Probe 5(mm)
1.14	37.50	36.34	54.16	66.15
1.11	39.70	65.63	36.84	81.03
1.06	41.80	40.05	64.26	59.21
0.99	48.80	39.49	100.44	38.73
0.95	54.10	44.72	76.34	42.52
0.93	56.60	52.45	70.39	44.44
0.90	58.30	62.53	61.96	47.80
0.88	63.80	66.42	59.78	52.51
0.84	69.70	74.91	62.03	62.93
0.81	76.30	81.86	67.75	71.43
0.77	84.30	93.79	75.92	81.52
0.75	87.20	94.74	78.49	85.97
0.72	97.60	103.88	86.13	98.73
0.70	100.70	101.36	89.94	106.25
0.68	110.20	113.70	99.37	113.82
0.66	118.00	123.36	111.63	119.18
0.64	119.00	126.77	114.07	118.83
0.62	129.00	126.48	124.39	130.92

5.3.2 Comparison Results

5.3.2.1 Comparison Results of MAPS0, WAMIT and Experimental Data

Comparison results of body motions and free surface elevations in gap for two-body cases with different gap widths are presented in Figures 5.30 to 5.50. In the figures, all data are in full scale.

By comparison, it can be seen that numerical simulation results with potential-flow method basically agree well with experimental data. The experimental data of four of six degrees of freedom body motion and wave elevation in gap can be used as benchmark data in the future research on multi-body interaction problems in waves. Also, it can be found that MAPS0 obtained better predictions of free surface elevation in gap than WAMIT at high wave frequency conditions.

For the predictions of free surface elevations in gap, it can also be found that both MAPS0 and WAMIT over-predicted the free surface elevations in gap near gap resonant frequency. At low wave frequency conditions, their predictions agreed well with experimental results.

From the comparison results, it proves that the numerical simulations based on potential-flow theory over-predicted the gap resonant problem when two vessels are in close proximity as the viscous damping was not considered in the simulations. Experimental data obtained from model tests are significant as they can help to determine the viscous damping factor, which can be applied in the numerical simulation to obtain better predictions.

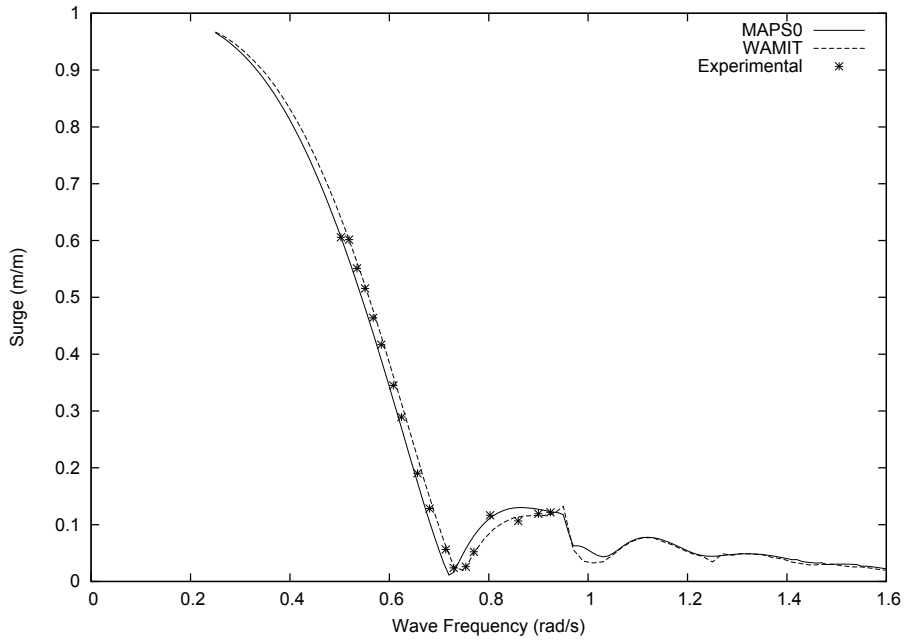

Figure 5.30: Surge RAO of body 1 in two-body case, gap width 0.4m

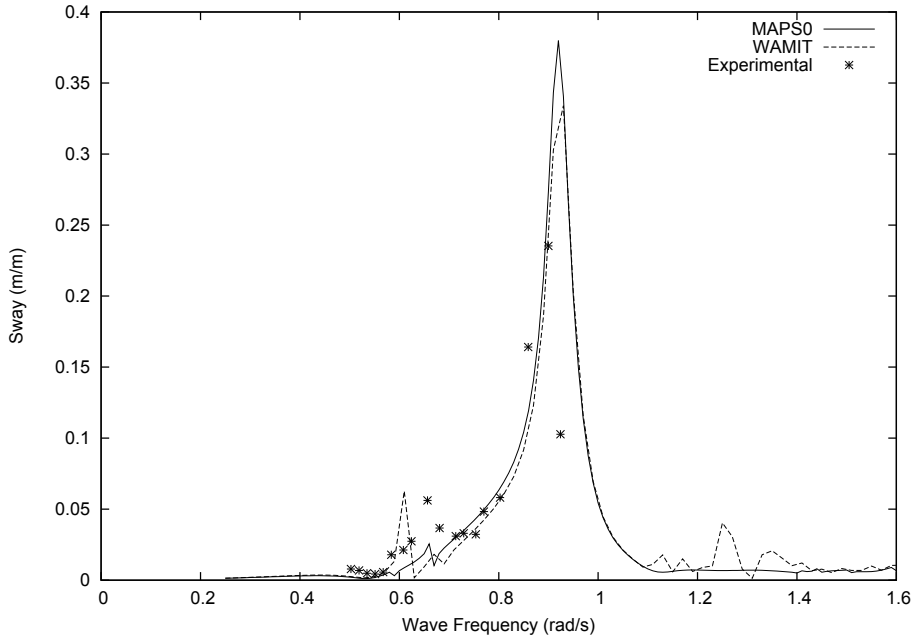

Figure 5.31: Sway RAO of body 1 in two-body case, gap width 0.4m

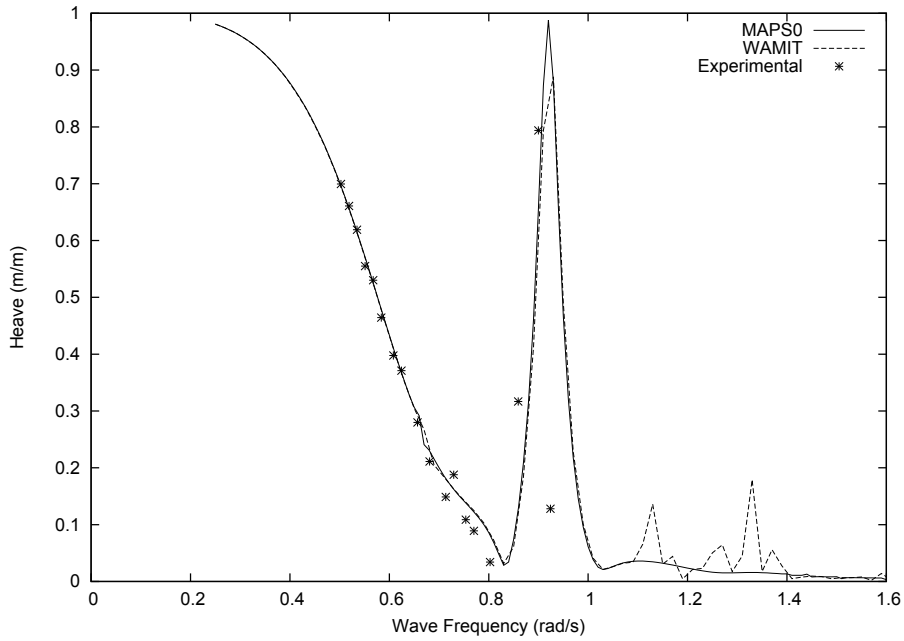

Figure 5.32: Heave RAO of body 1 in two-body case, gap width 0.4m

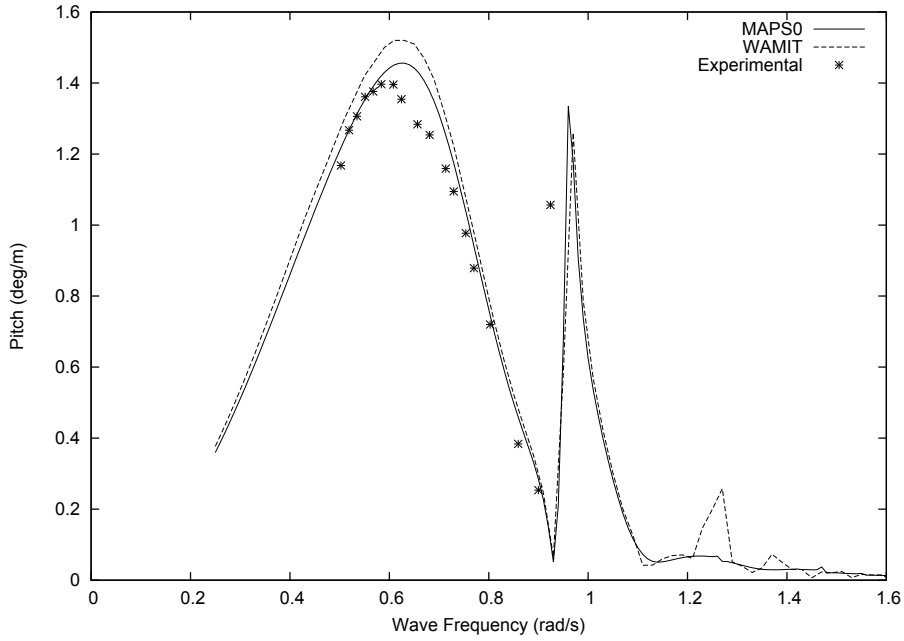

Figure 5.33: Pitch RAO of body 1 in two-body case, gap width 0.4m

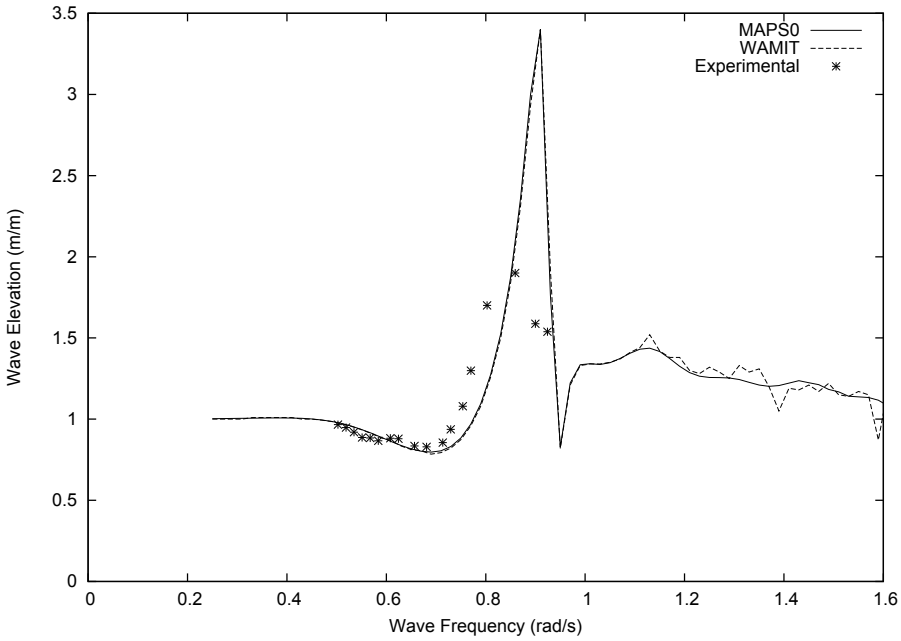

Figure 5.34: Wave elevation at wave probe 3 in two-body case, gap width 0.4m

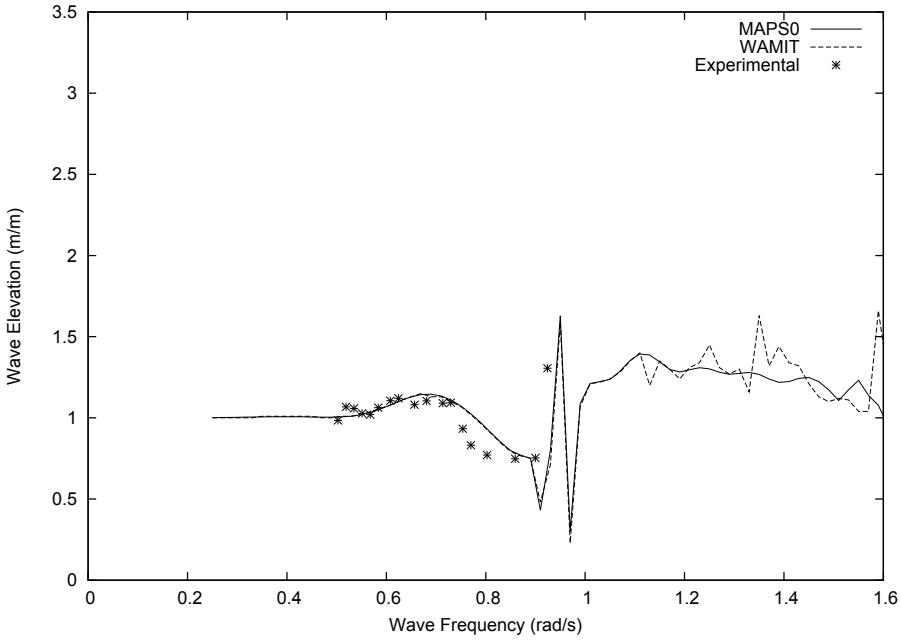

Figure 5.35: Wave elevation at wave probe 4 in two-body case, gap width 0.4m

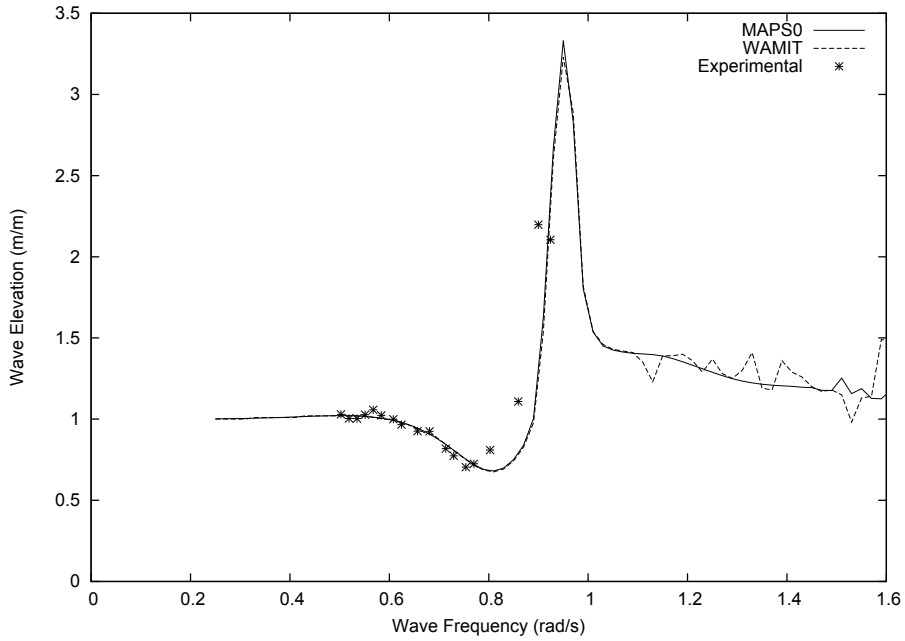

Figure 5.36: Wave elevation at wave probe 5 in two-body case, gap width 0.4m

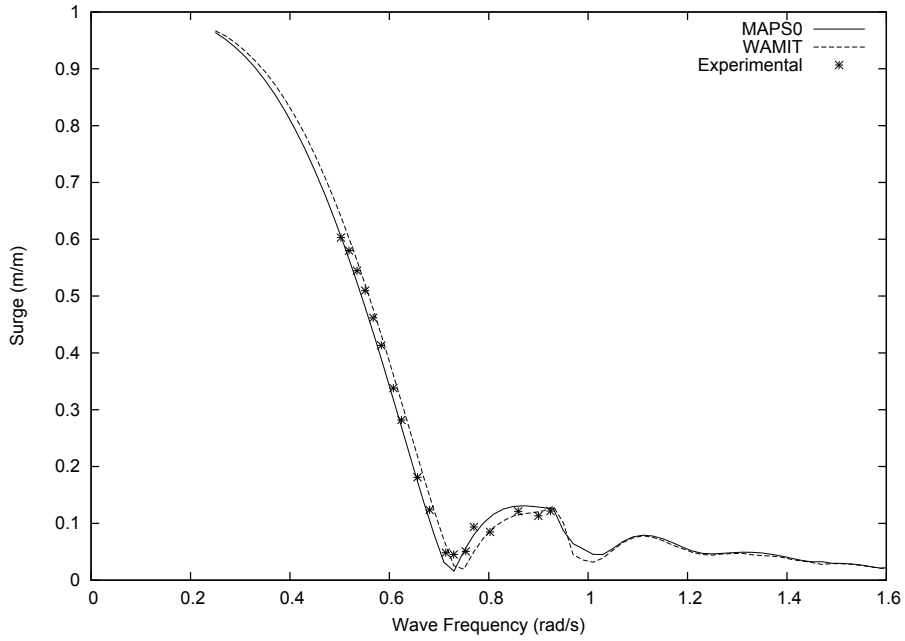

Figure 5.37: Surge RAO of body 1 in two-body case, gap width 0.45m

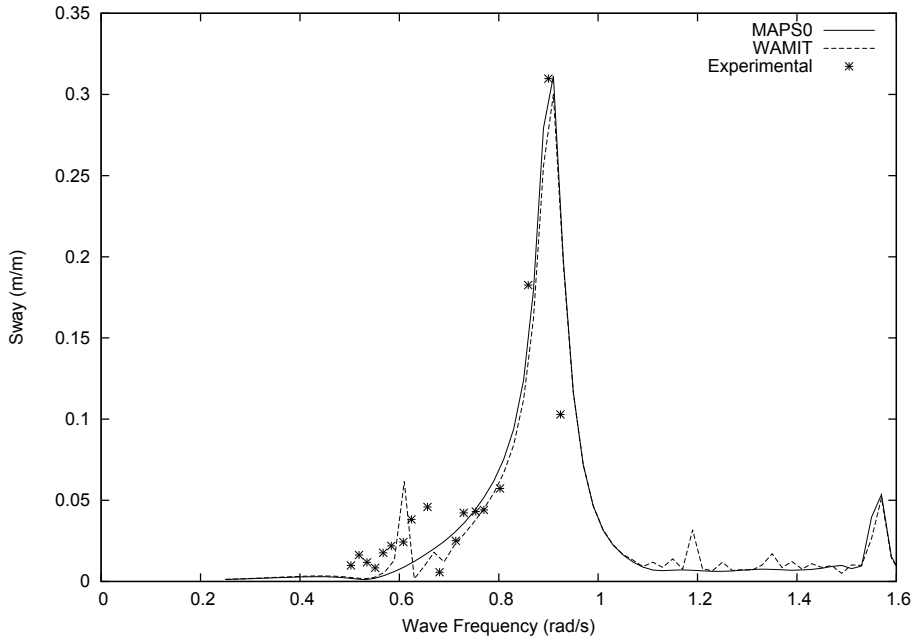

Figure 5.38: Sway RAO of body 1 in two-body case, gap width 0.45m

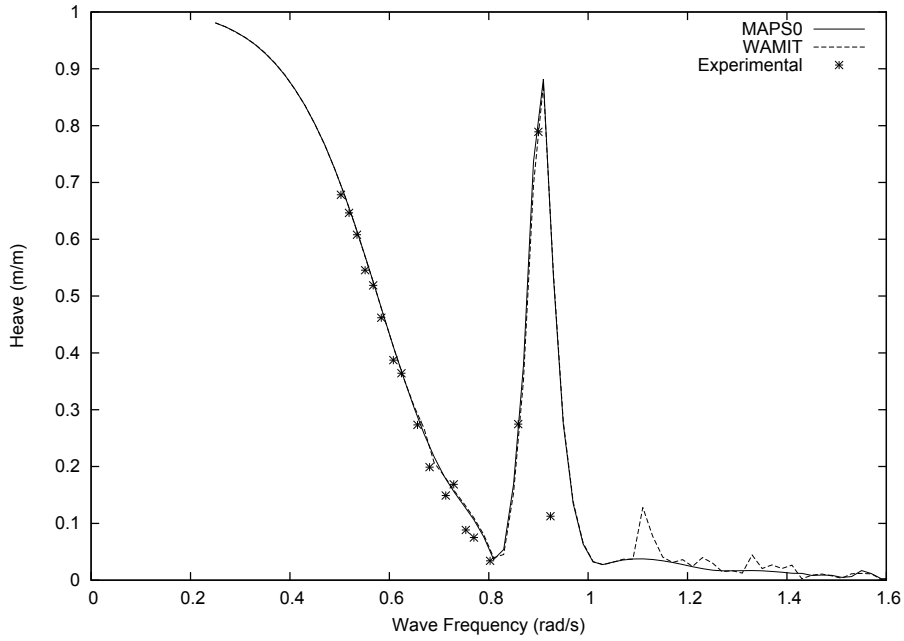

Figure 5.39: Heave RAO of body 1 in two-body case, gap width 0.45m

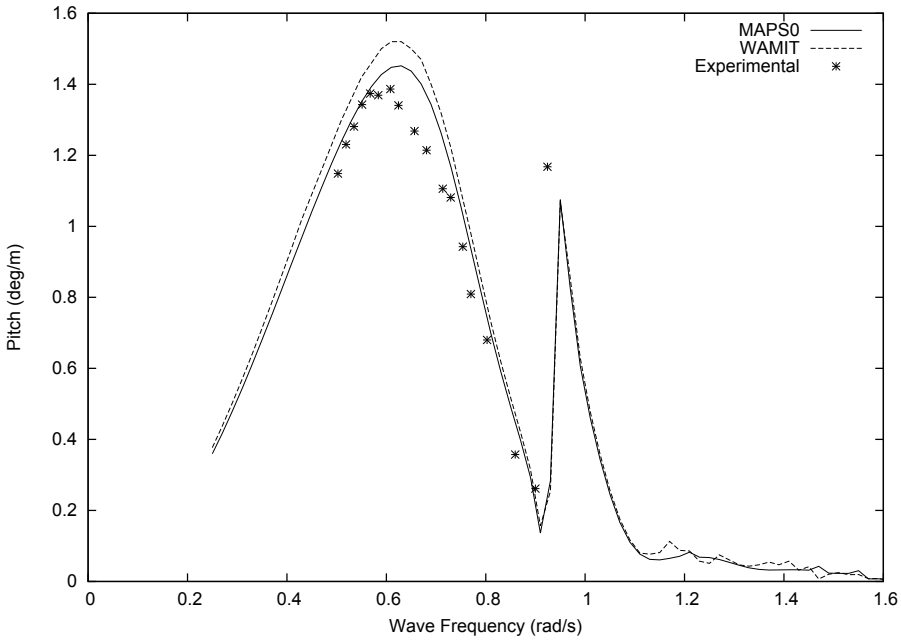

Figure 5.40: Pitch RAO of body 1 in two-body case, gap width 0.45m

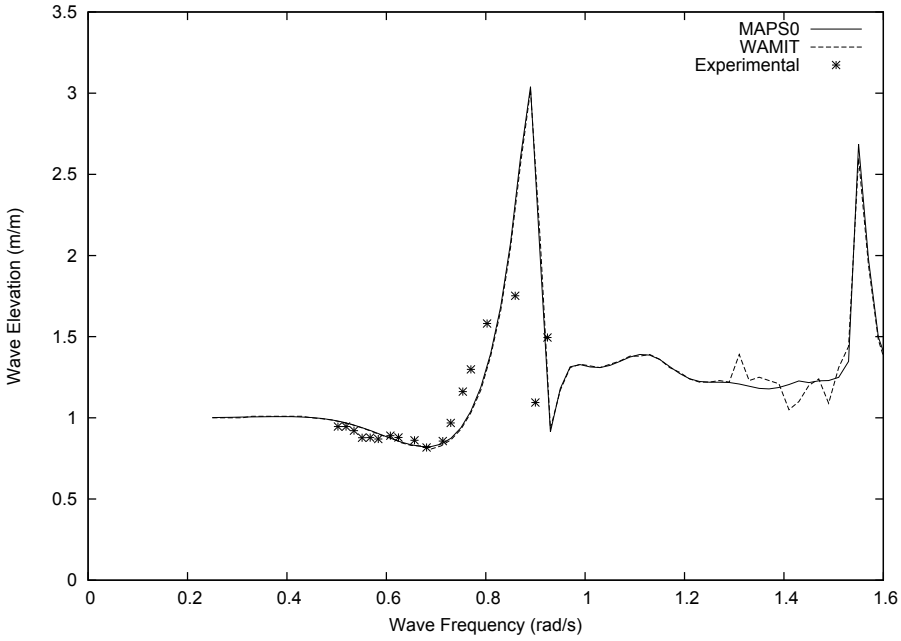

Figure 5.41: Wave elevation at wave probe 3 in two-body case, gap width 0.45m

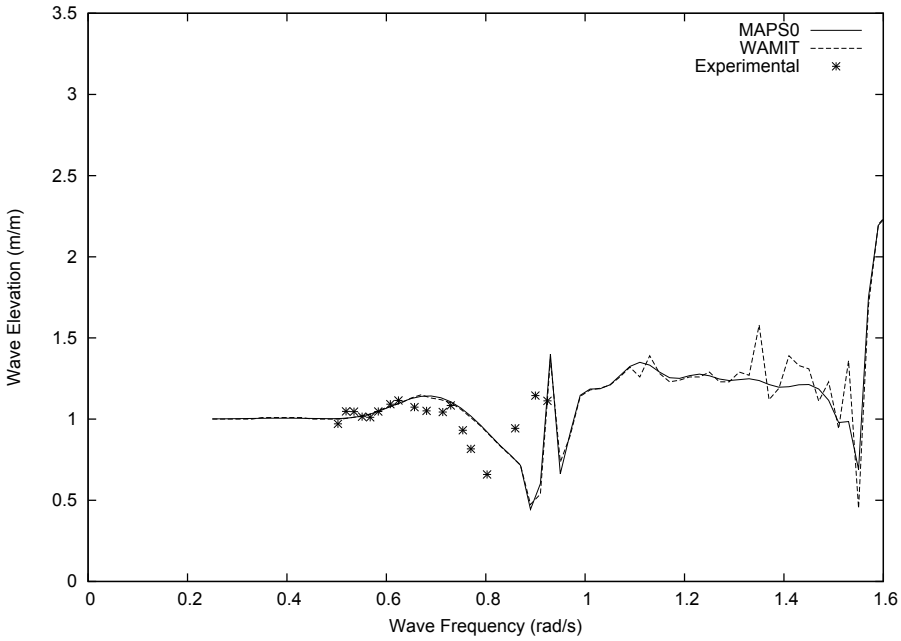

Figure 5.42: Wave elevation at wave probe 4 in two-body case, gap width 0.45m

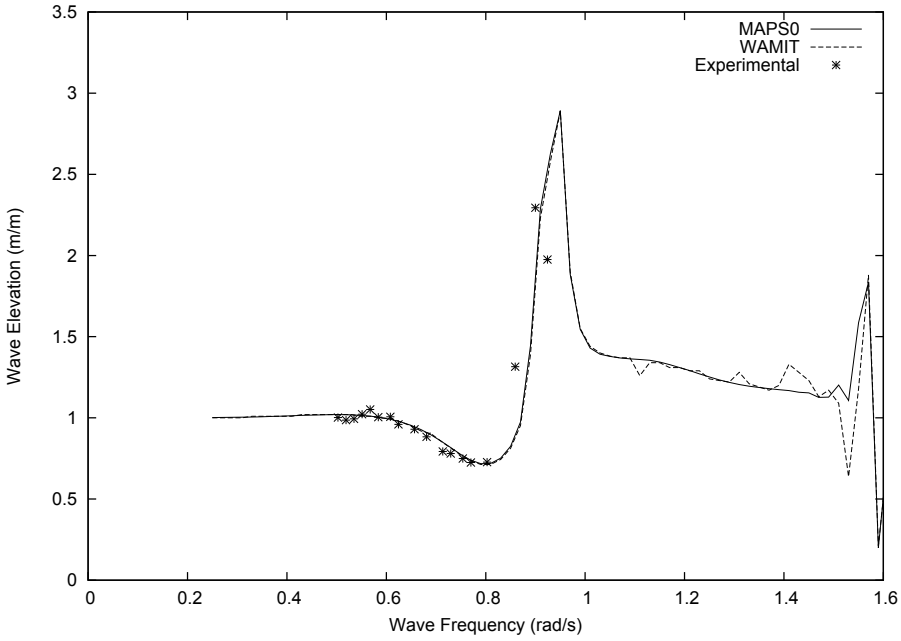

Figure 5.43: Wave elevation at wave probe 5 in two-body case, gap width 0.45m

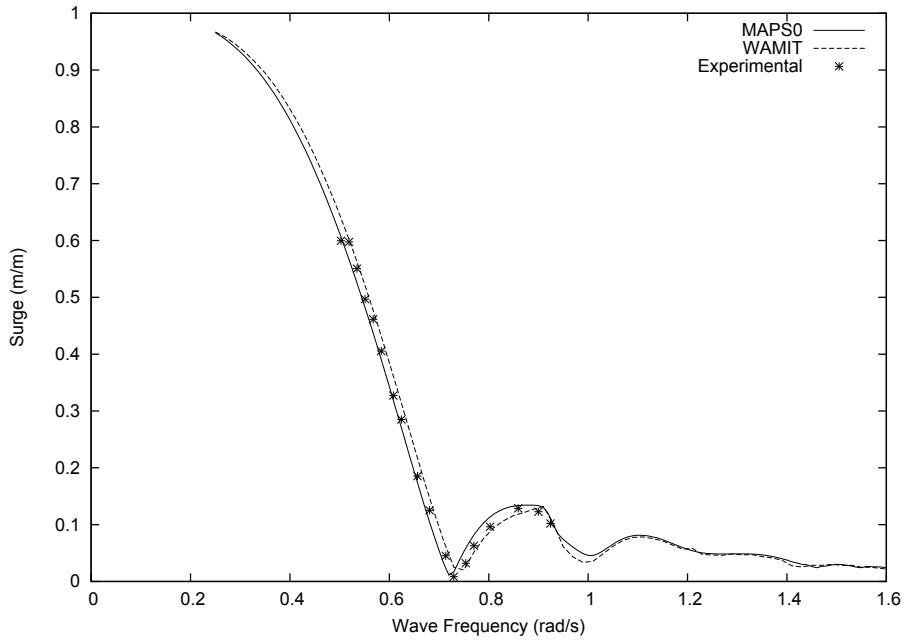

Figure 5.44: Surge RAO of body 1 in two-body case, gap width 0.55m

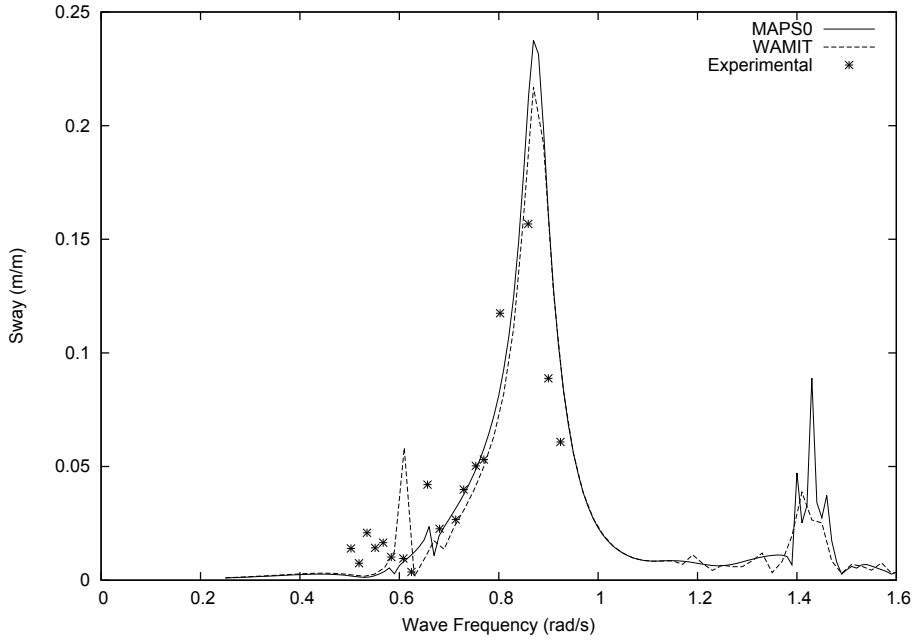

Figure 5.45: Sway RAO of body 1 in two-body case, gap width 0.55m

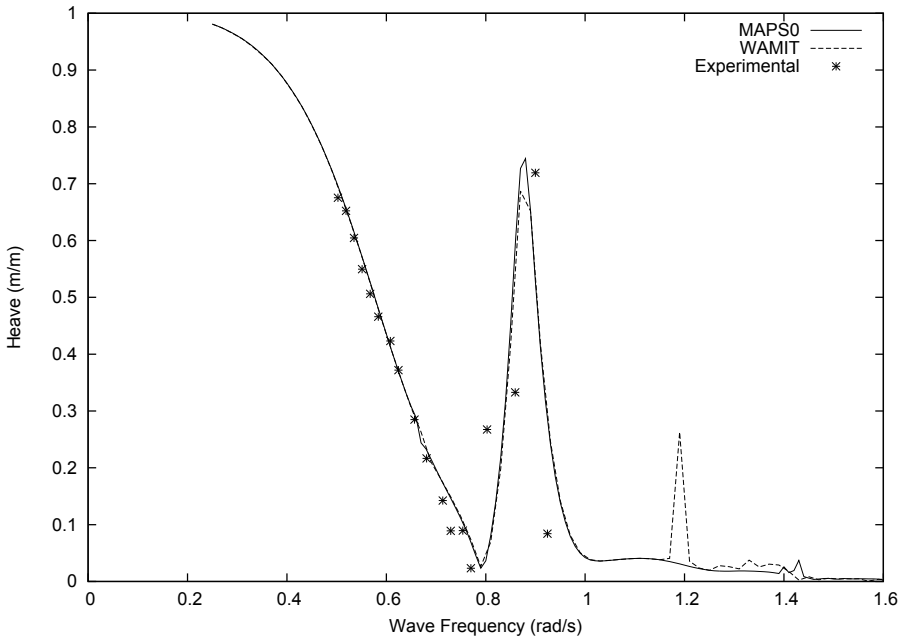

Figure 5.46: Heave RAO of body 1 in two-body case, gap width 0.55m

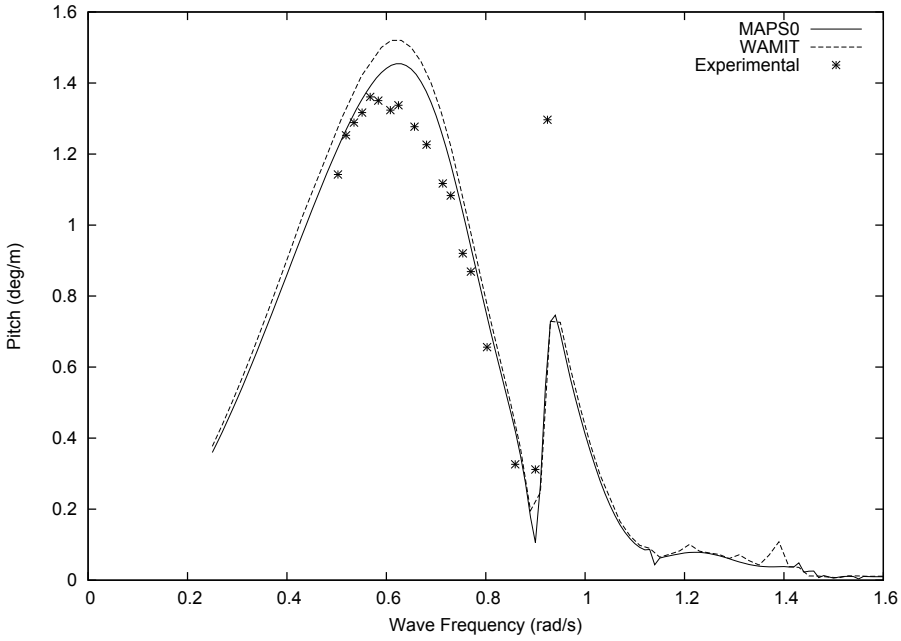

Figure 5.47: Pitch RAO of body 1 in two-body case, gap width 0.55m

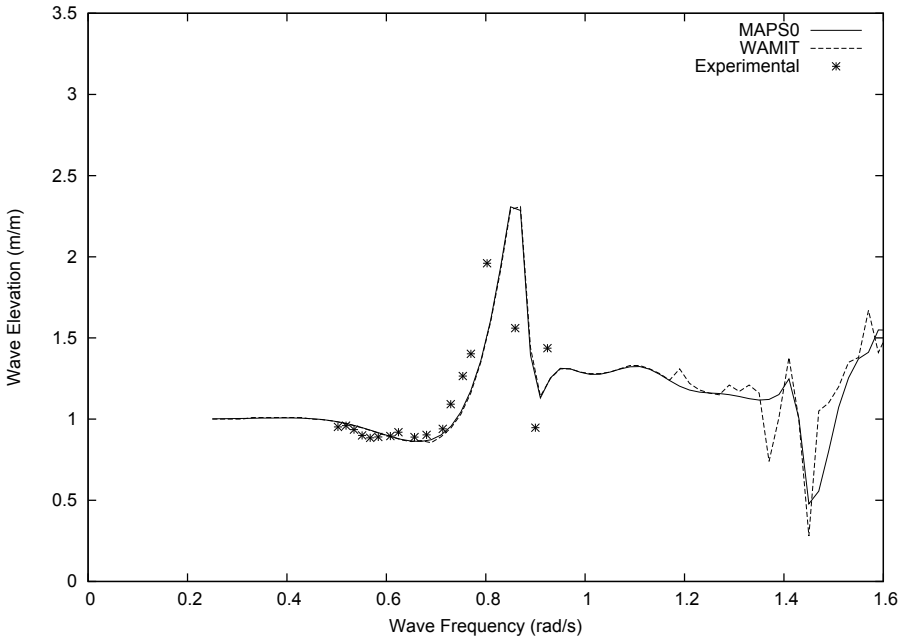

Figure 5.48: Wave elevation at wave probe 3 in two-body case, gap width 0.55m

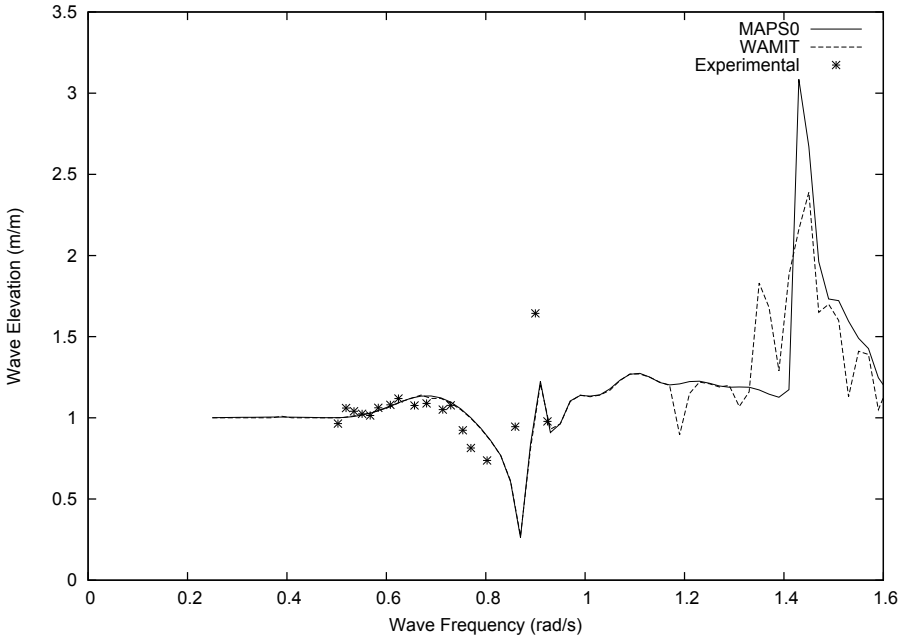

Figure 5.49: Wave elevation at wave probe 4 in two-body case, gap width 0.55m

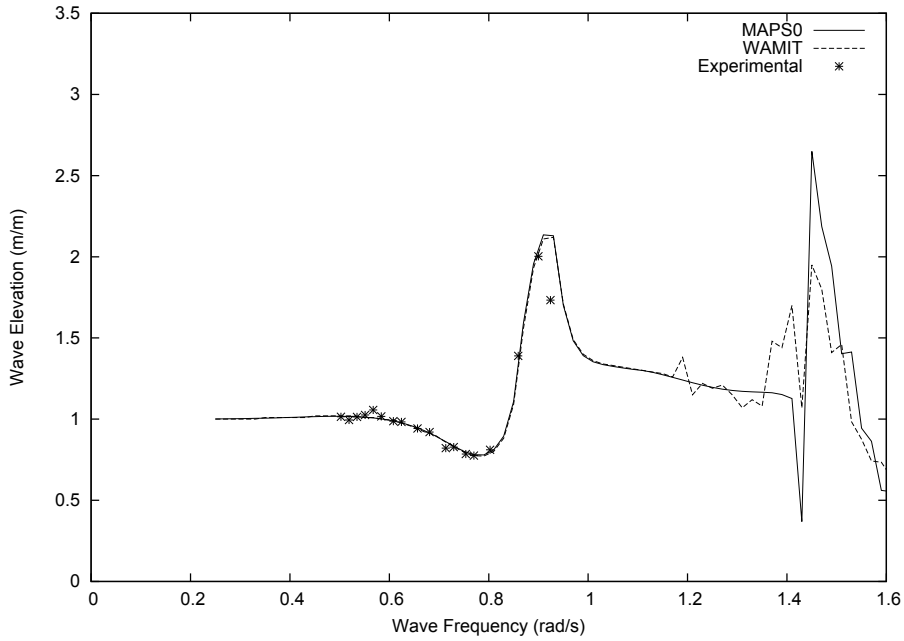

Figure 5.50: Wave elevation at wave probe 5 in two-body case, gap width 0.55m

5.3.2.2 Comparison Results of Different Gap Widths

Free surface elevation results at three wave probes in the gap for different gap widths are presented in Figures 5.51 to 5.53. In the figures, gap 1 stands for the gap with 0.4 m gap width in model scale, which is the smallest gap width. Gap 3 is with the biggest gap width. From the figures, it can be found that a larger resonant wave elevation would occur in the gap as the gap width becomes smaller. Also, With the increase of gap width, the resonant frequency moves towards lower frequency.

This phenomenon can be explained with the theory proposed by Molin et al. (2002). In the gap resonant phenomenon, resonant modes and their frequencies can be estimated on the assumptions of infinite water depth and infinite beams of motionless barges. An equation of gap resonant frequencies was given:

$$\omega_n^2 \simeq g\lambda_n \frac{1 + J_n tanh\lambda_n h}{J_n + tanh\lambda_n h} \tag{5.1}$$

where

$$J_n(r) = \frac{2}{n\pi^2 r}\{\int_0^1 \frac{r^2}{u^2\sqrt{u^2+r^2}}[1+2u+(u-1)cos(n\pi u) - \frac{3}{n\pi}sin(n\pi u)]du - \frac{1}{sin\theta_0} + 1 + 2rln\frac{1+cos\theta_0}{1-cos\theta_0}\} \tag{5.2}$$

where $\lambda_n = n\pi/l$, $r = b/l$, $tan\theta_0 = r^{-1}$, l is the length of the gap, b is the width and h is the draft.

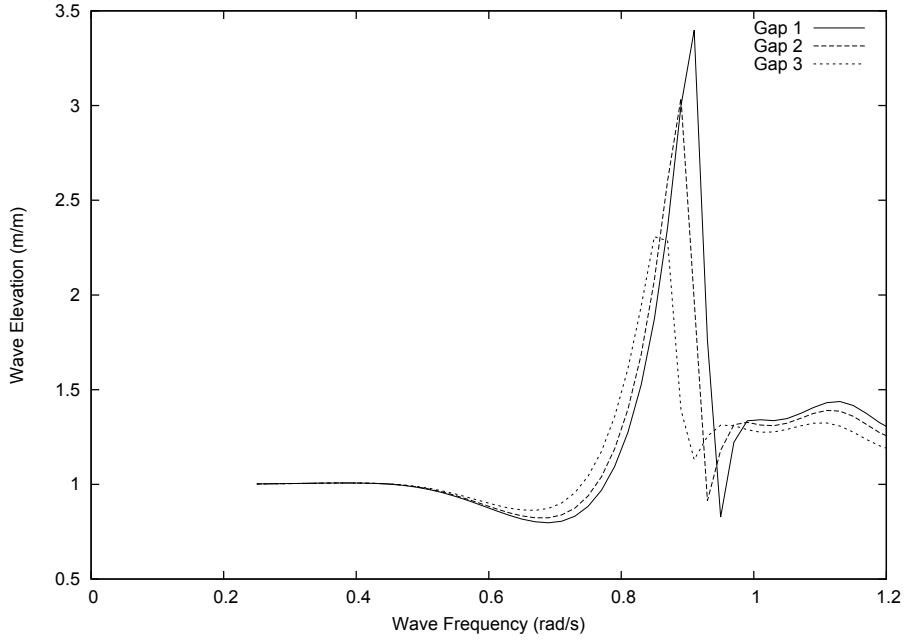

Figure 5.51: Wave elevation at wave probe 3 with 3 gap widths

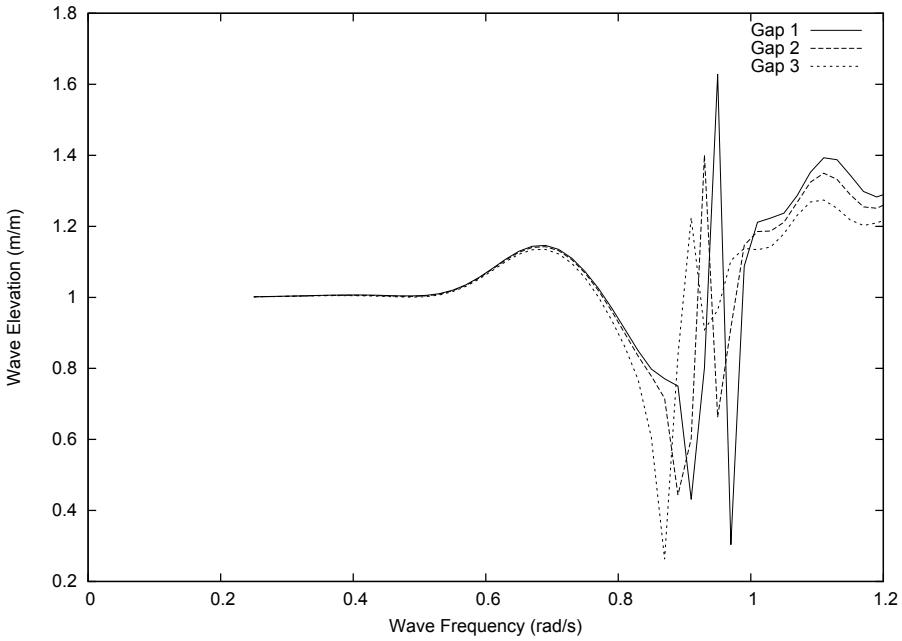

Figure 5.52: Wave elevation at wave probe 4 with 3 gap widths

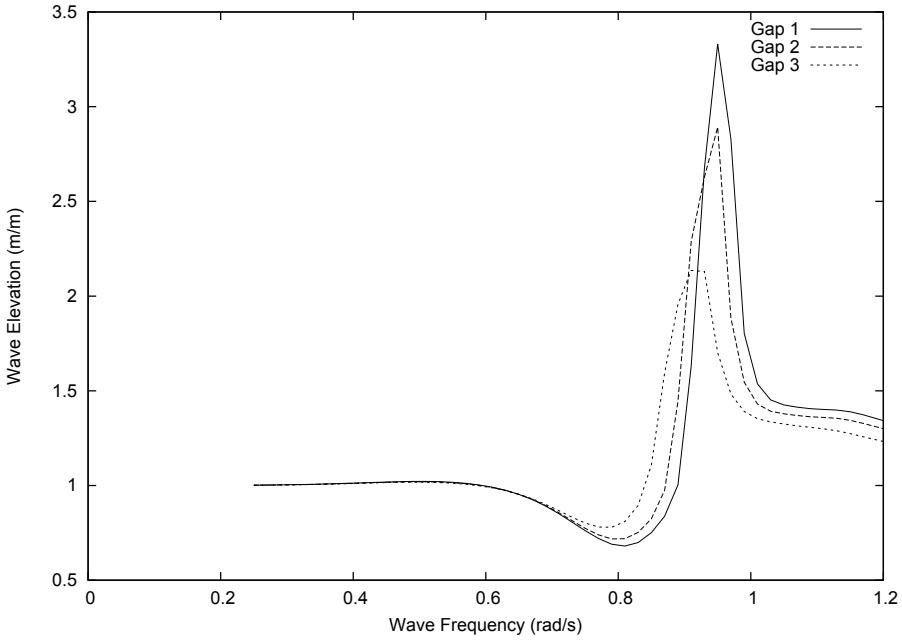

Figure 5.53: Wave elevation at wave probe 5 with 3 gap widths

5.4 Comparison Results of Single Body/Two-body Cases

Comparison results of body surge, heave and pitch motions between single body cases and two-body cases are presented in Figure 5.54 to Figure 5.62. In the figures, all data are in full scale. From the comparison results, it is obvious to see the effect of gap resonance phenomenon on the body motions.

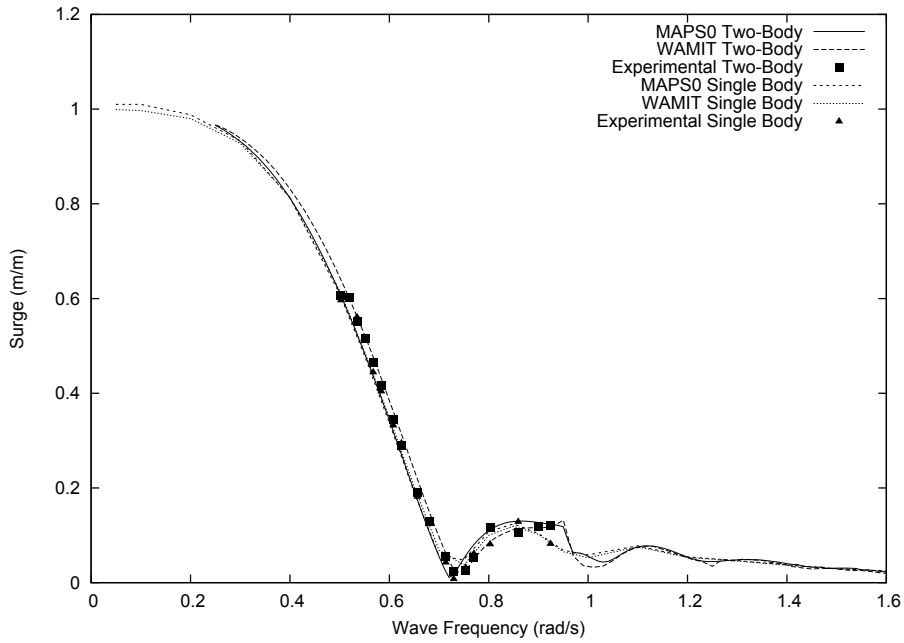

Figure 5.54: Surge RAOs of single body and two-body (gap 0.4m) cases

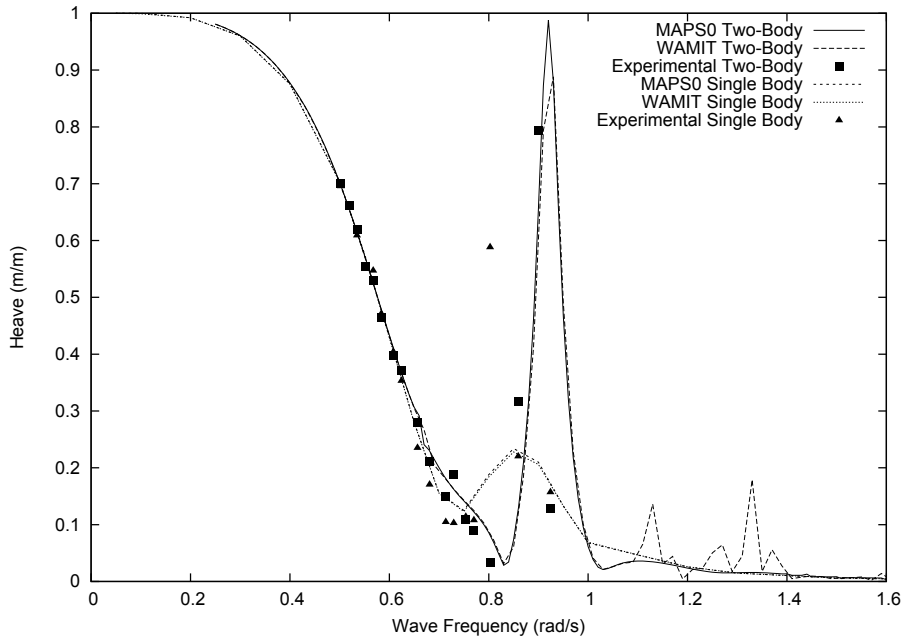

Figure 5.55: Heave RAOs of single body and two-body (gap 0.4m) cases

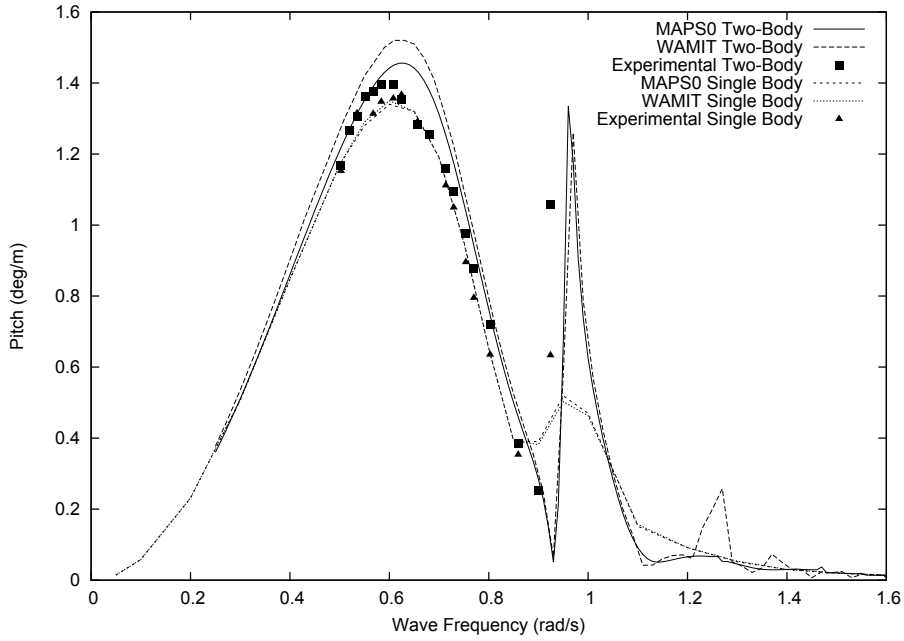

Figure 5.56: Pitch RAOs of single body and two-body (gap 0.4m) cases

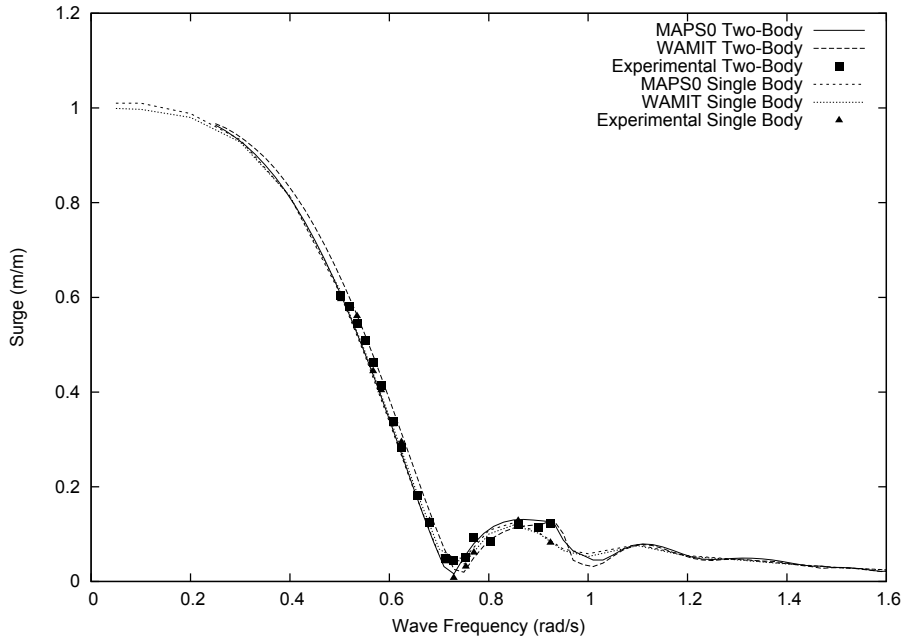

Figure 5.57: Surge RAOs of single body and two-body (gap 0.45m) cases

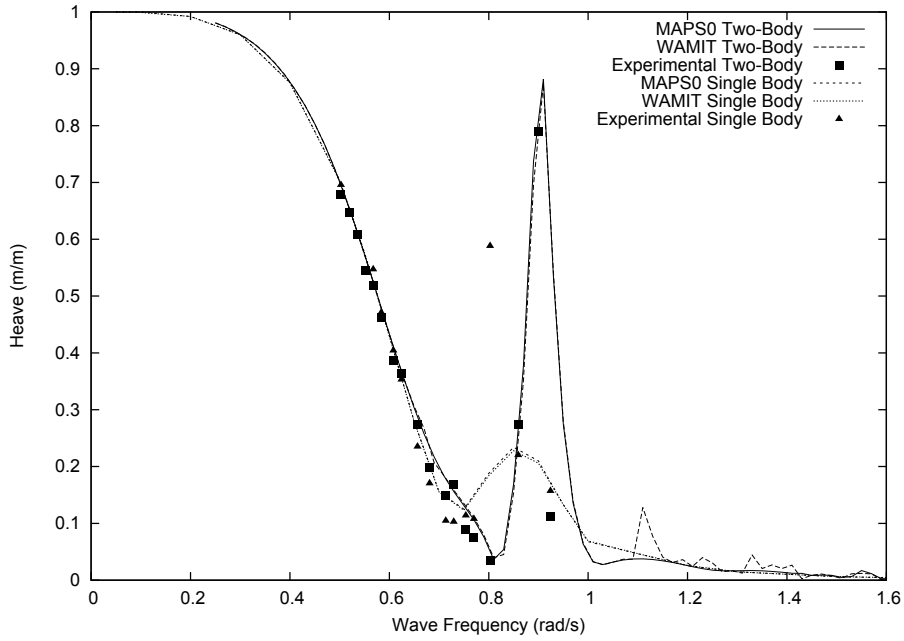

Figure 5.58: Heave RAOs of single body and two-body (gap 0.45m) cases

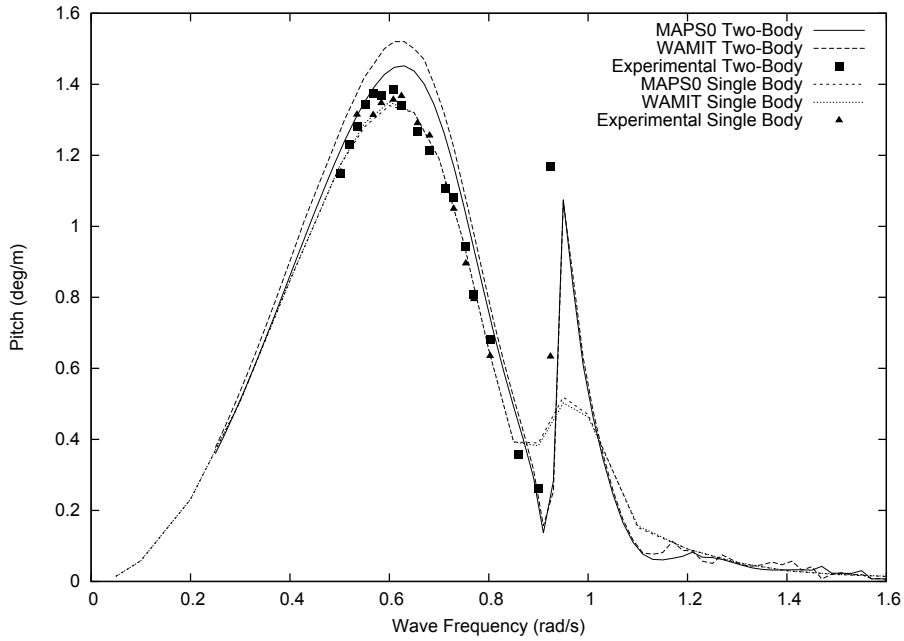

Figure 5.59: Pitch RAOs of single body and two-body (gap 0.45m) cases

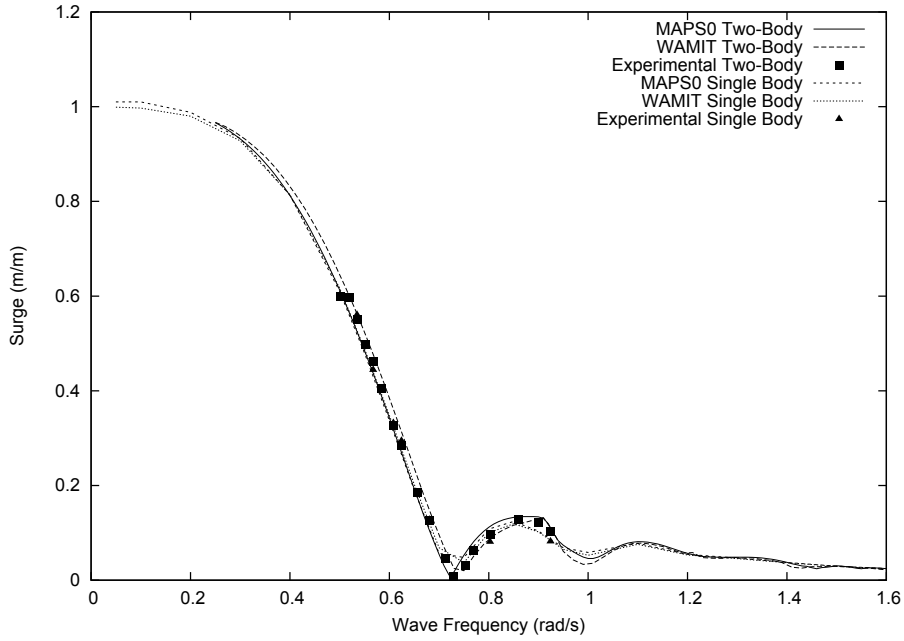

Figure 5.60: Surge RAOs of single body and two-body (gap 0.55m) cases

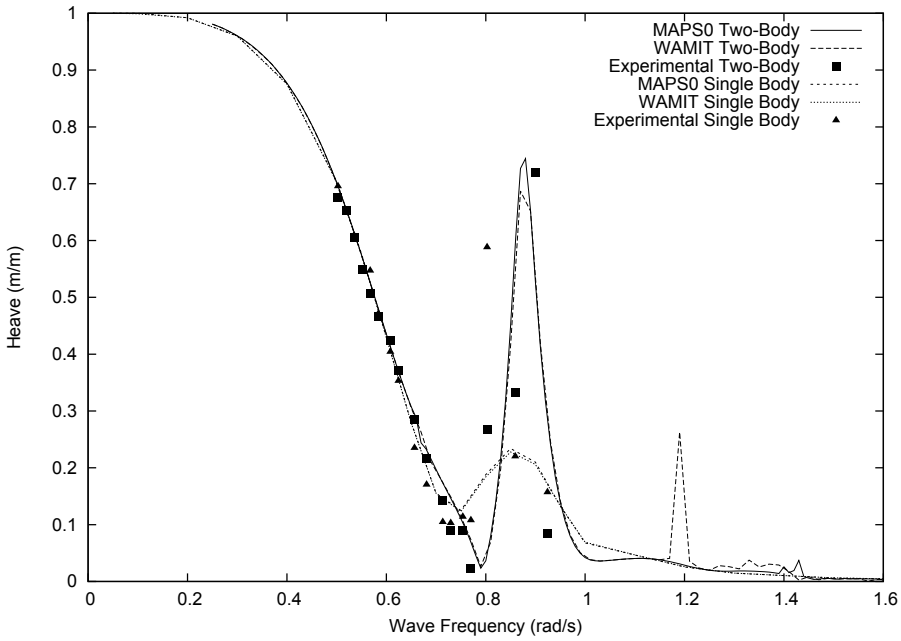

Figure 5.61: Heave RAOs of single body and two-body (gap 0.55m) cases

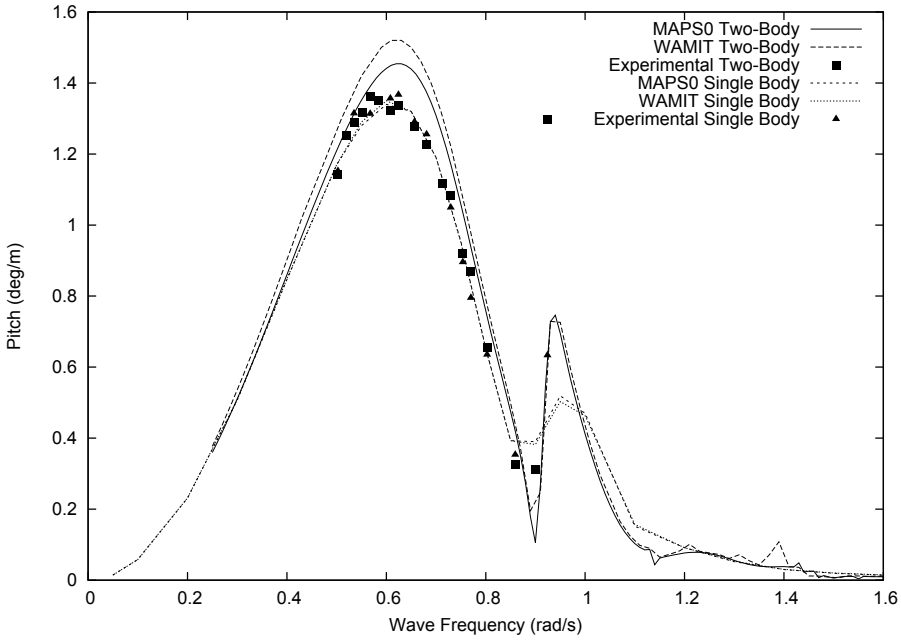

Figure 5.62: Pitch RAOs of single body and two-body (gap 0.55m) cases

Chapter 6

Conclusions and Recommendations

6.1 Conclusions

The study investigated the two-body interaction problem in waves with both experimental method and numerical method based on potential-flow theory.

Model tests of two-body interaction in waves were designed and conducted in head sea conditions. Two identical 1:60 scaled box-like FPSO models were designed and used in the tests. The model tests aim to provide benchmark data of body motion and wave elevation in gap for future numerical studies on two-body interaction problem in waves. In the tests, the tank wall effect and mooring line effect were considered and studied to ensure that they had small effect on the body motion and wave elevation in gap. Different initial gap widths were also investigated in the tests.

Numerical simulations with two potential-flow based programs, MAPS0 and WAMIT, were performed and the simulation results were compared with the experimental data obtained from the model tests.

By comparing the results of experimental tests and numerical simulations, it can be found that the numerical results agree well with the experimental data, which proves

the experimental data obtained from the model tests can be appropriately adopted and employed in future numerical studies. By comparing the results of single body and two-body cases, it is obvious to see the gap resonant effect on the body motions when two bodies are in close proximity in waves. By comparing the results of cases with different gap widths, it can be found that a larger resonant wave elevation and a bigger resonant wave frequency would occur in the gap as the gap width decreases. The comparison results also show that numerical simulations based on potential-flow theory over-predict the gap resonant problem when two vessels are in close proximity as the viscous damping was not considered in the simulations. Experimental data obtained from model tests are significant as they can help to determine the viscous damping factor, which can be applied in the numerical simulation to obtain better predictions.

6.2 Recommandations

With the restictions from the towing tank size, wave maker capacity and limited experiment schedule, the work in this thesis is just a small step toward the ultimate goal in the study of two-body interaction problem in waves. Improvements needs to be made for future work.

Future effort can be made to the following aspects:

- To eliminate the tank wall effect, the model tests should be conducted in a tank with bigger width than a towing tank, such as a wave basin.
- Model tests with a wider range of wave frequency, especially in the resonance region, are recommended. Also, more wave headings and gap widths should be tested in the experiment if experiment schedule permits.

- A longer run time of the tests are recommended to obtain the stable body motions, especially for roll and yaw motion.
- More repetitions are recommended and uncertainty analysis should be conducted.
- Numerical simulation with CFD methods are also recommended to investigate the contribution of viscosity to the free surface elevation between two bodies in close proximity.

Bibliography

Bunnick, T., Pauw, W., and Voogt, A. (2009). Hydrodynamic analysis for side-by-side offloading. In *Proc. ISOPE2009*.

Cheetham, P., Du, S., May, R., and Smith, S. (2007). Hydrodynamic analysis of ships side-by-side in waves. In *In International Aerospace CFD Conference*.

Chen, X. (2004). Hydrodynamics in offshore and naval applications - part i. In *Keynote Lecture of 6th Intl. Conf. Hydrodynamics*.

Cho, S., Sung, H., Hong, S., Hong, S., Ha, M., Choi, Y., Yu, B., Jang, R., and Choi, H. (2011). Experimental study on the effect of sloshing on side-by-side moored fsru and lngc. In *Proc. ISOPE2011*.

Clauss, G., Dudek, M., and Testa, D. (2013). Gap effects at side-by-side lng-transfer operations. In *Proc. OMAE2013*.

Hong, D., Hong, S., Nam, B., and Hong, S. (2013). Comparative numerical study of repulsive drift forces and gap resonances between two vessels floating side-by-side in proximity in head seas using a discontinuous hobem and a constant bem with boundary matching formulation. *Ocean Engineering*, 72.

Huijsmans, R., Pinkster, J., and Wilde, J. (2001). Diffraction and radiation of waves around side by side moored vessels. In *Proc. ISOPE2001*.

ITTC (2002). Ittc recommended procedures and guidelines 7.5-02-07-03.2 (analysis procedure for model tests in regular wave).

ITTC (2005). Ittc recommended procedures and guidelines 7.5-02-07-03.1 (floating offshore platform experiments).

Kashiwagi, M. and Shi, Q. (2010). Pressure distribution computed by wave-interaction theory for adjacent multiple bodies. 22(5):526–531.

Kim, M., Jeong, H., Kwak, H., Kim, B., and Eom, J. (2012). Improvement method on offloading operability of side-by-side moored flng. In *Proc. ISOPE2012*.

Kodan, N. (1984). The motions of adjacent floating structures in oblique waves. *Journal of Energy Resources Technology*, 106:199–205.

Li, X., Yang, J., and Xiao, L. (2003). Motion analysis on a large fpso in shallow water. In *Proc. ISOPE2003*.

Lu, L. and Chen, X. (2012). Dissipation in the gap resonance between two bodies. In *Proc. IWWWFB2012*.

Lu, L., Cheng, L., Teng, B., and Sun, L. (2010a). Comparison of potential flow and viscous fluid models in gap resonance. In *Proc. IWWWFB2010*.

Lu, L., Cheng, L., Teng, B., and Sun, L. (2010b). Numerical simulation and comparison of potential flow and viscous fluid models in near trapping of narrow gaps. *J. Hydrodynamics*, 22:120–125.

Lu, L., Teng, B., Cheng, L., Sun, L., and Chen, X. (2011). Modelling of multi-bodies in close proximity under water waves - fluid resonance in narrow gaps. *Science China Physics, Mechanics & Astronomy*, 54:16–25.

Ma, Q., Yan, S., and Zhou, J. (2013). Fully nonlinear simulation of resonant wave motion in gap between two structures. In *Proc. ISOPE2013*.

McTaggart, K., Cumming, D., Hsiung, C., and Li, L. (2003). Seakeeping of two ships in close proximity. *Ocean Engineering*, 30:1051–1063.

Miao, G., Saitoh, T., and Ishida, H. (2001). Water wave interaction of twin large scale caissons with a small gap between. *Coastal Engineering Journal*, 43:39–58.

Molin, B. (2001). On the piston and sloshing modes in moonpools. *Journal of Fluid Mechanics*, 430:27–50.

Molin, B., Remy, F., Camhi, A., and Ledoux, A. (2009). Experimental and numerical study of the gap resonances in-between two rectangular barges. In *Proc. IMAM2009*.

Molin, B., Remy, F., Kimmoun, O., and Stassen, Y. (2002). Experimental study of the wave propagation and decay in a channel through a rigid ice sheet. *Applied Ocean Research*, 24:247–260.

Newman, J. (2003). Application of generalized modes for the simulation of free surface patches in multi body hydrodynamics. In *WAMIT Consortium Report*.

Pauw, W., Huijsmans, R., and Voogt, A. (2007). Advances in the hydrodynamics of side-by-side moored vessels. In *Proc. OMAE2007*.

Qiu, W. (2013). *User's Manual of Motion Analysis Program Suite*.

Qiu, W. and Hsiung, C. (2002). A panel-free method for time-domain analysis of the radiation problem. *Ocean Engineering*, 29:1555–1567.

Qiu, W., Peng, H., and Chuang, J. (2006). Computation of wave-body interactions using the panel-free method and exact geometry. *Journal of Offshore Mechanics and Arctic Engineering*, 128:31–38.

Qiu, W., Wen, P., Liu, M., and Peng, H. (2014). Numerical studies of hydrodynamic interactions of two bodies in waves. In *Proc. NuTTS 2014*.

Qualisys (2013). *User's Manual of Qualisys*.

Smith, D. (2014). Seakeeping experiment of two side-by-side floating bodies. Master's thesis, Memorial Univerisity of Newfoundland, St. John's, Canada.

Wang, C., G, W., and Khoo, B. (2011). Fully nonlinear simulation of resonant motion of liquid confined between floating structures. *J. Computers & Fluids*, 44(1):89–101.

Xiang, X. and Faltinsen, O. (2011). Time domain simulation of two interacting ships advancing parallel in waves. In *Proc. OMAE2011*.

Xu, X., Yang, J., Li, X., and Lu, H. (2013). Wave drift forces on three barges arranged side by side in floatover installation. In *Proc. OMAE2013*.

Zhang, Z., Sun, L., Ma, Q., and Xu, G. (2013). A numerical investigation on hydrodynamics of two floating bodies of arbitrary arrangements in regular waves. In *Proc. ISOPE2013*.

Zhou, Q., Liu, M., Peng, H., and Qiu, W. (2015). Experimental studies of hydrodynamic interactions of two bodies in waves. In *Proc. OMAE2015*.

Zhu, H., Zhu, R., and Miao, G. (2008). A time domain investigation on the hydrodynamic resonance phenomena of 3-d multiple floating structures. *J. Hydrodynamics*, 20:611–616.

Zou, L. and Larsson, L. (2013). Numerical predictions of ship-to-ship interaction in shallow water. *Ocean Engineering*, 72:386–402.

Appendices

Appendix A

Theory of Inclining Test

In Figure A.1, M is the metacentre, G is the center of gravity, B is the center of buoyancy and K is the keel. KG is the distance from the keel to the center of gravity. KM is the distance from the keel to the metacentre. KB is the distance from the keel to the centre of buoyancy. BM is the distance from the centre of buoyancy to the metacentre. GM is the metacentric height.

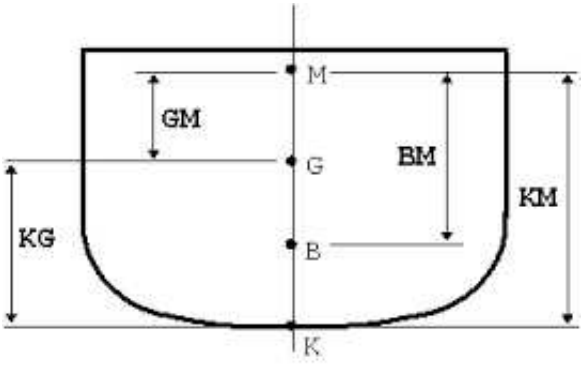

Figure A.1: Metacentric height

The following equation can be established to obtained the vertical center of gravity.

$$KG = KB + BM - GM \tag{A.1}$$

KB can be easily obtained based on the ship geometry. B is located at the centre of the submerged volume, which can be determined with common used design software, such as Rhinoceros.

BM can be calculated by the following equations.

$$BM = I_T/\nabla \tag{A.2}$$

Where I_T is the static moment and ∇ is the submerged volume.

$$I_T = \int_{-2/L}^{2/L} y^3 dx \tag{A.3}$$

GM is found by carrying out the inclining test.

$$GM = \frac{pl}{\triangle \ tan\theta} \tag{A.4}$$

where p is the weight being moved, l is the distance the weight is moved, $\triangle$ is the weight of the ship and θ is the roll angle.

Appendix B

Theory and Procedure of Swing Test

The purpose of a swing test is to find the vertical center of gravity and moments of inertia. The vertical center of gravity found using this method is not as accurate as the inclining test and should be used only to confirm that the results obtained from the inclining test were reasonable. The swing frame is shown in Figure B.1.

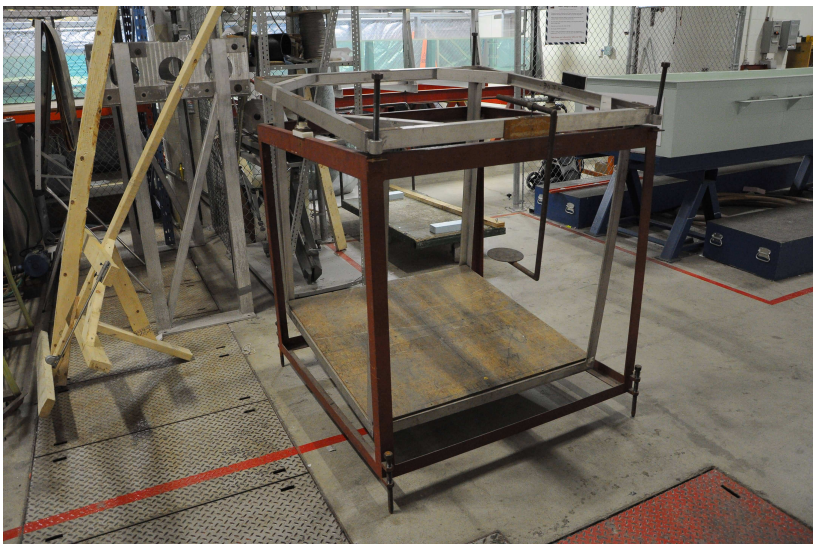

Figure B.1: Swing frame

The restoring moment Gb is given by

$$Gb = P(z + \frac{L}{tan\theta}) \tag{B.1}$$

where G is the center of gravity, b is the horizontal distance G moves when a weight is added and an angle is created, P is the weight of the pan and the added weights, z is the vertical distance from the knife edge to the position of the pan and added weights, L is the horizontal distance from the knife edge to the position of the pan and added weights and θ is the angle of the swing frame in degrees. L, z and θ are presented in Figure B.2.

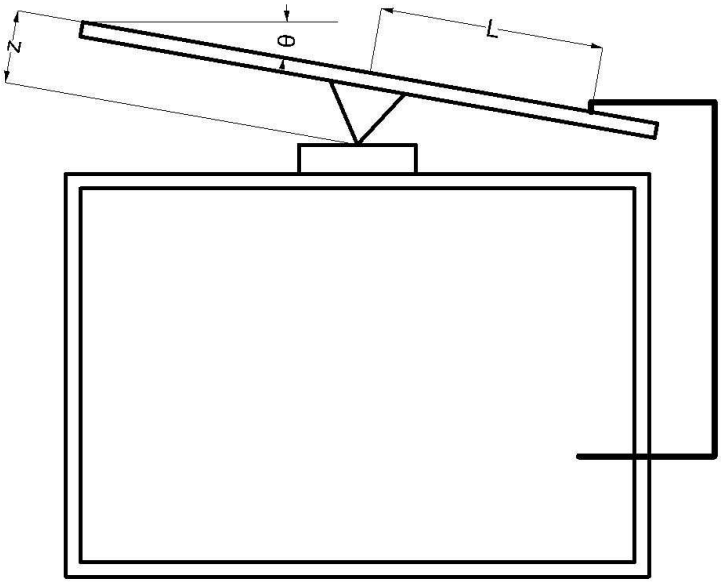

Figure B.2: Variables in swing test

First, the restoring moment of just the swing frame G_0b_0 is calculated. Second, the restoring moment of the swing frame and ship model G_1b_1 is calculated.

$$G_2b_2 = G_1b_1 - G_0b_0 \tag{B.2}$$

where G_2b_2 is the restoring moment of the ship model alone.

$$G_2 = m_2 g \tag{B.3}$$

where m_2 is the mass of the ballasted ship model and g is $9.81 m/s^2$.

$$b_2 = x tan\theta \tag{B.4}$$

where, x is the vertical distance from G_2 to the knife-edge.

$$VCG = d - z - x \tag{B.5}$$

where VCG is the distance from the keel to the center of gravity and d is the distance from the top of the swing frame to the bottom of the swing frame. The moment of inertia of swing frame about the knife-edge J_0 is calculated by

$$J_0 = (T_0/2\pi)^2(G_0b_0) \tag{B.6}$$

where, T_0 is the period of the swing frame. The moment of inertia of the model and frame about the knife-edge J_1 is calculated by

$$J_1 = (T_1/2\pi)^2(G_1b_1) \tag{B.7}$$

where, T_1 is the period of the swing frame and the ship model. The moment of inertia of the ship model J_2 is calculated by

$$J_2 = J_1 - J_0 \tag{B.8}$$

To get the moment of inertia of the ballasted model about its center of gravity J' the parallel axis theorem is used.

$$J' = J_2 - m_2 x^2 \tag{B.9}$$

The procedure of the swing test is listed below.

- Level the swing frame with an inclinometer by adjusting the lifting bolts on each corner of the frame.
- Attach a pan on one side of the swing frame and add weights on it to obtain an appropriate swing angle, which is approximately four degrees.
- Record the mass of the pan and the mass of the added weights.
- Measure and record the values of θ, z, and L.
- Attach the pan and added weights to one side of the swing frame and let the motion of the frame come to a complete stop.
- Once the frame was stabilized, quickly remove the weight and using a stopwatch and the inertial sensor record ten cycles then divide by ten to achieve the period.
- Repeat the procedure, for the same test case, four times, twice on each side of the swing frame.
- Once the period was obtained for each the average was taken and that value was then used in the equations to calculate the vertical center of gravity and the moments of inertia.
- All procedures listed above should be completed for three cases; for the swing frame alone, roll motion and pitch motion. When doing the swing test for the swing frame alone, nothing should be placed on the frame but the inclinometer

and its weight should be added to the total mass of the frame. When doing the swing test for roll motion, the ballasted ship model should be placed on the swing frame with its centerline parallel to the line connecting the two knife-edges. When doing the swing test for pitch motion, the ballasted ship model should be placed on the swing frame with its midship parallel to the line connecting the two knife-edges.

Appendix C

Theory of Decay Test

The purpose of carrying out a decay test is to find the period and the damping coefficient of the model's roll motion.

The dynamic equation for roll is

$$(I_{xx} + A_{xx})\ddot{\theta}(t) + B_{44}\dot{\theta}(t) + D\theta(t) = 0 \tag{C.1}$$

where I_{xx} is the moment of inertia for roll, A_{xx} is the added moment of inertia, B_{44} is the roll damping coefficient, D is the restoring coefficient and θ is the roll angle.

Assuming $2\zeta\omega_n = B_{44}/(I_{xx} + A_{xx})$ and $\omega_n^2 = D/(I_{xx} + A_{xx})$, the dynamic equation for roll can be written as

$$\ddot{\theta}(t) + 2\zeta\omega_n\dot{\theta} + \omega_n^2\theta(t) = 0 \tag{C.2}$$

where ζ is the damping ratio and ω_n is the natural frequency.

The solution of the equation yields the following format.

$$\theta(t) = \theta_0 e^{-\zeta\omega_n t} cos(\omega_d t + \alpha) \tag{C.3}$$

where α is the phase angle and ω_d is the damped frequency.

$$\omega_d = \omega_n \sqrt{1 - \zeta^2} \tag{C.4}$$

$\theta(t)$ can be obtained as it is the motion time series from the decay test. The peak values in the graph of the time series can be fitted with a curve with an equation in the form $y = a * e^{bt}$, where a is the initial roll angle and $b = \zeta\omega_n$. The damping is equal to $2\zeta\omega_n$

Appendix D

Experimental Data of Roll Motion in Two-Body Cases

Experimental data of body roll motion for three different gap widths in two-body cases is presented in Tables D.1 to D.3. In the table, f and H stands for incoming wave frequency and wave height. The data is in model scale. In the tests, the cases were repeated twice. Round 1 and 2 stand for the two repetitions.

The data was obtained by analyzing the time series of body roll motion with Fast Fourier Transform. Due to the effect of tank wall and the short run time of the test, the roll motion data need to be further processed by employing numerical methods.

The comparison results of the questionable experimental data and the numerical data for body roll motion in two-body cases are presented in Figures D.1 to D.3. From the figures, it can be seen that the curves agree not as well as the agreements in other degrees of body motions. The reason was that a longer run time of the tests and the elimination of the tank wall effect are needed to obtain better experimental data for body roll motion. Also, as no viscous roll damping was considered in the numerical simulation, MAPS0 and WAMIT both over-predicted the body roll motion near gap

Table D.1: Roll motion data of two models in two-body case, gap width 0.4 m

f(Hz)	H(mm)	Round 1		Round 2	
		Model 1 (deg)	Model 2 (deg)	Model 1 (deg)	Model 2 (deg)
1.14	37.25	0.31	0.56	0.56	0.27
1.11	39.10	3.62	3.83	3.16	3.32
1.06	41.92	1.67	1.60	1.76	1.85
0.99	42.53	0.70	0.77	0.77	0.68
0.95	54.48	0.91	1.18	1.21	0.97
0.93	56.74	1.45	0.80	1.50	0.85
0.90	58.44	1.77	1.12	1.74	1.11
0.88	63.31	1.23	1.97	2.01	1.21
0.84	68.21	6.60	3.16	3.99	8.29
0.81	77.17	6.42	4.55	7.47	3.92
0.77	83.80	2.77	0.93	2.77	0.75
0.75	87.16	1.85	0.84	1.68	0.95
0.72	97.12	1.32	0.90	1.23	1.01
0.70	101.01	0.82	0.88	0.73	0.91
0.68	110.96	0.55	0.63	0.57	0.61
0.66	117.82	0.50	0.63	0.55	0.59
0.64	120.36	0.58	0.22	0.56	0.22
0.62	129.10	0.37	0.42	0.38	0.42

Table D.2: Roll motion data of two models in two-body case, gap width 0.45 m

f(Hz)	H(mm)	Round 1		Round 2	
		Model 1 (deg)	Model 2 (deg)	Model 1 (deg)	Model 2 (deg)
1.14	38.30	0.51	0.81	0.51	0.33
1.11	40.00	3.51	3.86	3.58	3.67
1.06	42.10	1.90	2.08	2.03	2.24
0.99	48.70	0.86	0.78	0.91	0.87
0.95	54.70	1.08	0.83	1.11	0.87
0.93	57.00	1.41	0.99	1.41	1.00
0.90	58.90	1.83	1.09	1.76	1.04
0.88	64.60	1.94	1.11	1.94	1.01
0.84	70.50	3.14	6.24	3.23	5.72
0.81	76.60	5.57	6.04	5.82	6.20
0.77	84.30	3.45	0.77	3.23	0.86
0.75	87.00	1.99	0.79	2.01	0.74
0.72	97.70	1.44	0.84	1.38	0.99
0.70	101.60	1.06	0.84	0.92	0.83
0.68	111.50	0.71	0.54	0.68	0.57
0.66	118.70	0.69	0.62	0.68	0.63
0.64	122.10	0.82	0.15	0.74	0.18
0.62	130.10	0.42	0.43	0.38	0.44

Table D.3: Roll motion data of two models in two-body case, gap width 0.55 m

f(Hz)	H(mm)	Round 1		Round 2	
		Model 1 (deg)	Model 2 (deg)	Model 1 (deg)	Model 2 (deg)
1.14	37.50	0.19	0.45	0.41	0.16
1.11	40.10	1.20	1.07	1.18	1.41
1.06	42.40	1.84	1.72	1.36	1.42
0.99	49.20	1.90	1.91	2.29	2.27
0.95	55.20	1.02	1.21	1.22	1.04
0.93	57.40	1.09	1.37	1.37	1.13
0.90	58.30	0.93	1.80	1.81	0.96
0.88	63.50	0.58	1.77	1.75	0.61
0.84	68.60	3.47	2.68	2.85	4.01
0.81	75.60	6.67	5.08	5.56	6.40
0.77	83.50	0.97	2.85	2.96	0.93
0.75	87.30	0.88	1.84	1.71	0.73
0.70	101.10	0.89	0.87	0.71	0.95
0.68	111.00	0.72	0.49	0.48	0.61
0.66	117.60	0.80	0.43	0.50	0.70
0.64	119.90	0.18	0.62	0.54	0.14
0.62	129.00	0.62	0.34	0.61	0.34

resonant frequency. For better predictions of roll motion, viscous roll damping factors should be added in the numerical simulations. The viscous roll damping factors can be determined by analyzing the results of roll decay tests.

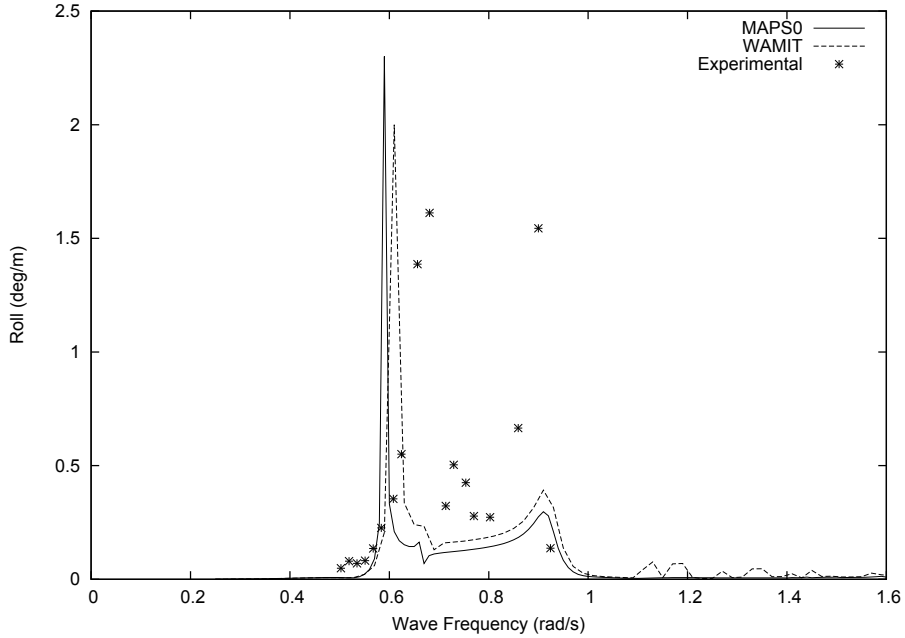

Figure D.1: Roll RAO of body 1 in two-body case, gap width 0.4m

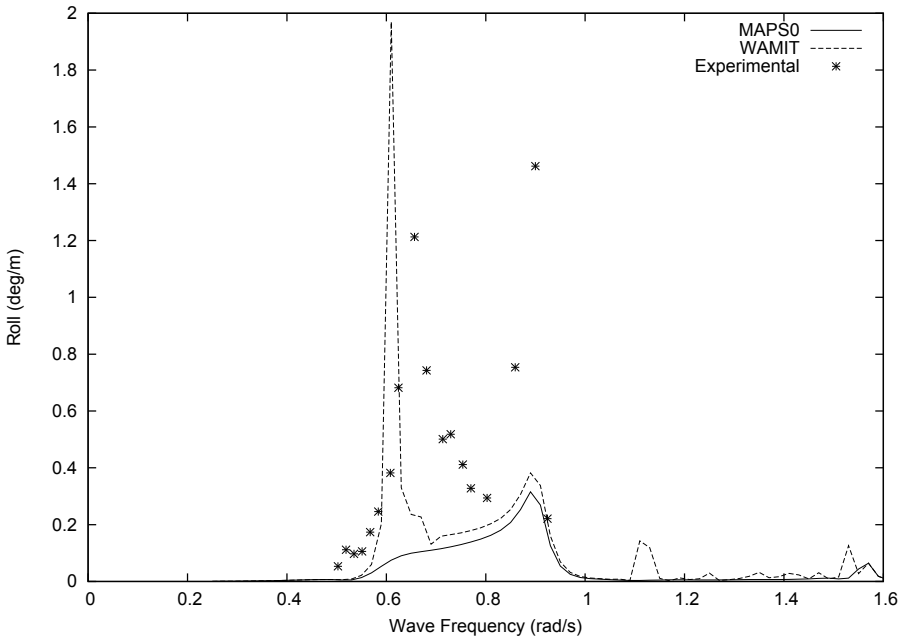

Figure D.2: Roll RAO of body 1 in two-body case, gap width 0.45m

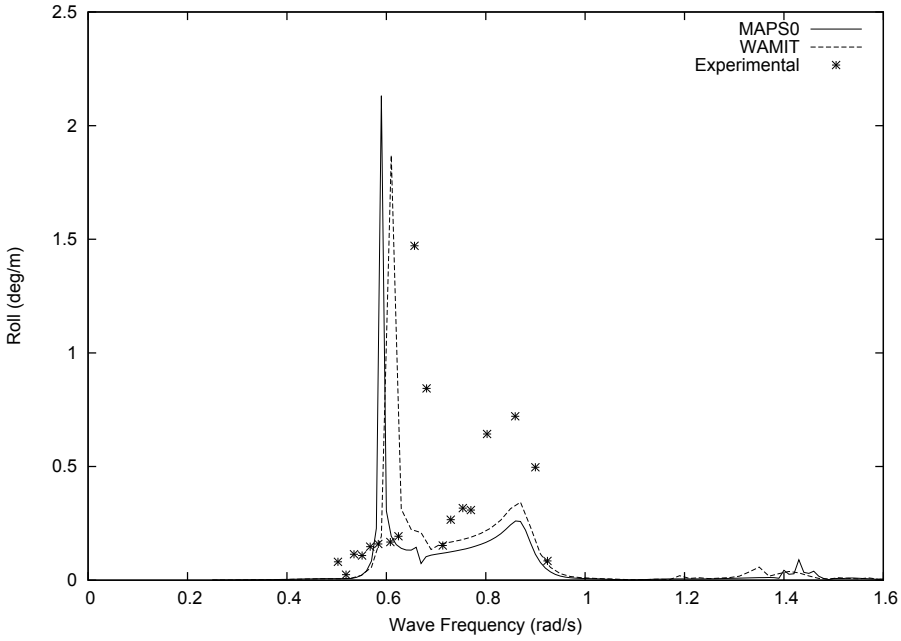

Figure D.3: Roll RAO of body 1 in two-body case, gap width 0.55m